THE EFFECTS OF IRON(II) ON ARSENIC(III) OXIDATION AND ARSENIC SORPTION/DESORPTION ON MANGANESE OXIDES

by

Yun Wu

A dissertation submitted to the Faculty of the University of Delaware in partial fulfillment of the requirements for the degree of Doctor of Philosophy in Plant and Soil Sciences

Summer 2014

THE EFFECTS OF IRON(II) ON ARSENIC(III) OXIDATION AND ARSENIC SORPTION/DESORPTION ON MANGANESE OXIDES

by

Yun Wu

Approved: _____
Blake C. Meyers, Ph.D.
Chair of the Department of Plant and Soil Sciences

Approved: _____
Mark W. Rieger, Ph.D.
Dean of the College of Agriculture and Natural Resources

Approved: _____
James G. Richards, Ph.D.
Vice Provost for Graduate and Professional Education

I certify that I have read this dissertation and that in my opinion it meets the academic and professional standard required by the University as a dissertation for the degree of Doctor of Philosophy.

Signed: _____

Donald L. Sparks, Ph.D.
Professor in charge of dissertation

I certify that I have read this dissertation and that in my opinion it meets the academic and professional standard required by the University as a dissertation for the degree of Doctor of Philosophy.

Signed: _____

Yan Jin, Ph.D.
Member of dissertation committee

I certify that I have read this dissertation and that in my opinion it meets the academic and professional standard required by the University as a dissertation for the degree of Doctor of Philosophy.

Signed: _____

Ravi K. Kukkadapu, Ph.D.
Member of dissertation committee

I certify that I have read this dissertation and that in my opinion it meets the academic and professional standard required by the University as a dissertation for the degree of Doctor of Philosophy.

Signed: _____

Paul Northrup, Ph.D.
Member of dissertation committee

ACKNOWLEDGMENTS

I couldn't be able to finish this dissertation without guidance from my advisor and committee members, support from my parents and help from friends. Because of you all, I have a very valuable, unforgettable and enjoyable five year time at University of Delaware. I am profoundly grateful to all of you.

I would like to express my deepest and sincerely appreciation to my advisor Dr. Donald Sparks, for all his guidance and support on me. He is a great mentor. He gives me the independence and the flexibility to do my research, and provides me a lot of wonderful opportunities to grow as a researcher.

I would also like to acknowledge my committee members, Dr. Yan Jin, Dr. Ravi Kukkadapu and Dr. Paul Northrup, for their assistances and suggestions on my research. Especially, I want to thank Dr. Ravi Kukkadapu, for his help on Mössbauer analysis and insightful discussions.

Gratitude is expressed to Jerry Hendricks, who is an invaluable lab manager and always provides me with promptly help. I appreciate the assistance from Dr. Kenneth Livi on TEM analysis, Caroline Golt on arsenic speciation and UD Soil Test Lab. I thank all current and previous members in Environmental Soil Chemistry group, for your help and company on courses, experiments and beam trips. Special thanks also goes to my friends. The happiest times I have at UD are with you.

I am extremely grateful to my parents, Anyi Wu and Qixia Wang. Without your love, encouragements and supports, I would never come this far. I am very proud of being your daughter and I love you both forever.

TABLE OF CONTENTS

LIST OF TABLES

LIST OF FIGURES

ABSTRACT

Arsenic contamination of groundwater and soils is a major global environmental challenge and poses a significant health risk to millions of people throughout the world. Both As(III) and As(V) are carcinogens, but As(III) is more toxic and more mobile. Thus, oxidation of As(III) to As(V) is an effective way to reduce As toxicity. As(III) oxidation by Mn-oxides has been extensively studied in the laboratory, however, the oxidation/sorption kinetics and mechanisms of As(III) under natural heterogeneous environments remains unclear. As(III) and Fe(II) coexist in many As contaminated environments and the presence of Fe(II) can influence the behavior of As(III) on Mn oxides. In this study, As(III) oxidation by a poorly-crystalline phyllomanganate (δ-MnO_2) in the presence and absence of dissolved Fe(II) was investigated using stirred-flow and batch experiments. The solids after reaction are characterized by X-ray absorption spectroscopy (XAS), Mössbauer spectroscopy and transmission electron microscope coupled with energy-dispersive X-ray spectroscopy (TEM-EDS). Results showed that in the presence of Fe(II), As(III) oxidation was inhibited due to the competitive oxidation of Fe(II) as well as the formation of Fe(III)-(hydr)oxides on the δ-MnO_2 surface. However, the sorption of As(III), As(V) and Mn(II) increased, since the newly formed Fe(III)-(hydr)oxides provided additional sorption sites. XAS analysis revealed that at low Fe(II) concentration, As(V) was the predominant As species on the solid phase, while at high Fe(II) concentration, both As(III) and As(V) were sorbed on the solid phase. As preferred to bind with the newly formed Fe(III)-(hydr)oxides through a bidentate

binuclear corner-sharing complex. Fe(III)-(hydr)oxides formed during Fe(II) oxidation by δ-MnO_2 were predominantly ferrihydrite and goethite as well as a small amount of lepidocrocite. The adsorbed As can be desorbed from the Fe/Mn-oxides surface, to some extent, and more As(III) is desorbed than As(V), due to the weaker binding of As(III) with Fe/Mn-oxides. This study suggests that the oxidation of As(III) by δ-MnO_2 in the presence of Fe(II) is very complex, involving several simultaneous reactions. A comprehensive understanding of the As(III) oxidation and As sorption on Mn-oxides as impacted by Fe(II) is essential and will provide significant information that can be used to better predict the toxicity and mobility of As in the environment as well as to develop strategies for remediation of As-contaminated waters and soils.

Chapter 1

INTRODUCTION

1.1 Arsenic Problem Worldwide

Arsenic (As) is a ubiquitous contaminant in soil and water environments due to natural geologic processes and anthropogenic inputs. It ranks 20th in natural abundance, comprising about 0.00005% of the Earth's crust, 14th in seawater and 12th in the human body (Mandal and Suzuki, 2002; Woolson, 1975). As has been used in medicine, agriculture, electronics, wood processing, livestock, industry and metallurgy (Mandal and Suzuki, 2002; Nriagu, 1990). As contamination of groundwater and soil is a worldwide problem and threatens the health of millions of people. Arsenic pollution has been reported recently in many countries such as the United States, China, Chile, Bangladesh, Taiwan, Mexico, Argentina, Poland, Canada, Hungary, New Zealand, Japan and India (Mohan and Pittman, 2007). One of the most serious instances is in Bangladesh, where people are extensively exposed to drinking water contaminated with high As concentrations. Over the past few decades, the health of humans, farm animals, wildlife, microorganisms, and some plants in the U.S. have been jeopardized by As contaminated soil and water. It is estimated that the "average" human in the U.S., Canada, and the UK consumes between 53 and 63 micrograms of As per day (Abernathy, 2001). Long-term human exposure to As in drinking water can result in bladder, lung, skin, and kidney cancer as well as pigmentation changes, skin thickening (hyperkeratosis), neurological disorders, muscular weakness, loss of appetite, and nausea. This differs from acute poisoning, which typically causes

vomiting, esophageal and abdominal pain, and bloody "rice water" diarrhea (Mohan and Pittman, 2007).

The World Health Organization (WHO) provisional guideline of 10 μg/L (ppb) has been adopted as the drinking water standard. However, many countries have retained the earlier WHO guideline of 50 μg/L as their standard or as an interim target including Bangladesh and China. On October 31, 2001 the United States Environmental Protection Agency (USEPA) announced that it was lowering the maximum contaminant level (MCL) for As in drinking water from 50 μg/L to 10 μg/L, and all water systems must comply by January 2006 (USEPA, 2001). Recent data show there is still an unacceptable level of risk at the EPA's newly adopted 10 μg/L MCL. It has been shown that the consumption of only 3 μg/L of As creates a risk of bladder and lung cancer in 4 to 10 people per 10,000 people, which indicates the new MCL may still be too high (Christen, 2001). This exceeds EPA's maximum acceptable level of risk of 1 in 1,000,000 people by 1000-fold. While the regulations governing As contamination in waters are well defined, the regulatory cleanup goals for remediation of contaminated soils are still under development and may vary greatly among countries, states, and land uses (Miretzky and Cirelli, 2010). For example, the regulatory limits set by the Ministry of Environment in Canada for As contamination in agricultural, industrial, and residential soils are 25, 50, and 25 mg/kg, respectively, whereas the current soil cleanup goals set by the Florida Department of Environmental Protection for As in residential and industrial soils are 0.80 and 3.7 mg/kg, respectively (Miretzky and Cirelli, 2010).

1.2 Sources and Cycles of Arsenic in the Environment

Reducing and controlling As contamination is challenging since it enters the environment through both natural and anthropogenic sources. Rocks can contain high concentrations of As, and thus As can be released into groundwater and soils through the weathering of rocks. Anthropogenic sources of As contribute to As contamination of groundwater, water, soil and atmosphere. Once As enters the environment, it cycles between the groundwater, water, soil and atmosphere, contaminating the earth's resources.

1.2.1 Natural Sources

A portion of As contamination in soil and aqueous environments is due to natural sources, with weathering of As -containing rocks being the main source, releasing 45,000 metric tons per year (Tamaki and Frankenberger, 1992). Arsenic naturally occurs in over 200 different mineral forms, of which approximately 60% are arsenates, 20% sulfides and sulfosalts and the remaining 20% includes arsenides, arsenites, oxides, silicates and elemental As (Mandal and Suzuki, 2002). But only certain of these are commonly encountered in significant amounts (Table 1.1). Mineral distribution depends on the parent rock composition and the extent of weathering that has occurred. The concentration of As in sedimentary and igneous rocks ranges from 0.1 to 2,000 mg/kg (ppm). Sedimentary rocks have a mean As concentration of 13 mg/kg in shales and 25 mg/kg in coal, while igneous rocks have a lower mean concentration of 1.5 mg/kg (Sparks et al., 2007). Metamorphic rocks contain less As, ranging from 0.4 to 18 mg/kg As. While As is mainly released into soil and aqueous environments through the weathering of rocks, it is also deposited into the atmosphere

by volcanic and geyser activities (Smith et al., 1998). Volcanic activity and other natural sources of As contamination account for over half of As's atmospheric flow.

1.2.2 Anthropogenic Sources

Even though As causes serious human health problems, it is used in many sectors, including agriculture, metallurgy, electronic, industry, livestock, and medicine. The major use of As in agriculture is as pesticides, insecticides, herbicides, defoliants, wood preservatives, tree debarking and soil sterilants (Mandal and Suzuki, 2002). Major industrial sources of As include commercial wastes (40%), coal ash (22%) and atmospheric fallout from the production of steel (13%) (Smith et al., 1998). These uses of As greatly contribute to As contamination of soil, groundwater and air. Anthropogenic sources release approximately 24,000 tons of As per year into the atmosphere, while natural sources only release about 8,000 tons of As per year into the atmosphere (Kirk, 2003).

The primary sources of As introduction into the environment in Delaware are pesticides, poultry litter, and historical tanneries. An organic As compound known as Roxarsone is incorporated into poultry feeds to control Coccidiosis, increase growth rate, improve feed utilization, enhance pigmentation, and may be effective in suppressing Salmonella (Alpharma, 1999). Most of the As is excreted by the chicken and is incorporated into poultry litter, a mixture of bedding material and manure. The use of poultry litter as an agricultural soil amendment has been an ongoing process for many years on the Delmarva Peninsula, and can cause an increased level of As in soil.

Table 1.1 Major arsenic minerals occurring in nature (WHO, 2001).

Mineral	Composition	Occurrence
Native arsenic	As	Hydrothermal veins
Proustite	Ag_3AsS_3	Generally one of the late Ag minerals in the sequence of primary deposition
Rammelsbergite	$NiAs_2$	Commonly in mesothermal vein deposits
Safflorite	$(Co,Fe)As_2$	Generally in mesothermal vein deposits
Seligmannite	$PbCuAsS_3$	Occurs in hydrothermal veins
Smaltite	$CoAs_2$	–
Niccolite	$NiAs_2$	Vein deposits and norites
Realgar	AsS	Vein deposits, often associated with orpiment, clays and limestones, also deposits from hot springs
Orpiment	As_2S_3	Hydrothermal veins, hot springs, volcanic sublimation product
Cobaltite	CoAsS	High-temperature deposits, metamorphic rocks
Arsenopyrite	FeAsS	The most abundant As mineral, dominantly mineral veins
Tennantite	$(Cu,Fe)_{12}As_4S_{13}$	Hydrothermal veins
Enargite	Cu_3AsS_4	Hydrothermal veins
Arsenolite	As_2O_3	Secondary mineral formed by oxidation of arsenopyrite, native arsenic and other As minerals
Claudetite	As_2O_3	Secondary mineral formed by oxidation of realgar, arsenopyrite and other As minerals
Scorodite	$FeAsO_4 \cdot 2H_2O$	Secondary mineral
Annabergite	$(Ni,Co)_3(AsO_4)_2\ 8H_2O$	Secondary mineral
Hoernesite	$Mg_3(AsO_4)_2\ 8H_2O$	Secondary mineral, smelter wastes
Haematolite	$(Mn,Mg)_4Al(AsO_4)(OH)_8$	–
Conichalcite	$CaCu(AsO_4)(OH)$	Secondary mineral
Adamite	$Zn_2(OH)(AsO_4)$	Secondary mineral
Domeykite	Cu_3As	Found in vein and replacement deposits formed at moderate temperatures
Loellingite	$FeAs_2$	Found in mesothermal vein deposits
Pharmacosiderite	$Fe_3(AsO_4)_2(OH)_3\ 5H_2O$	Oxidation product of arsenopyrite and other As minerals

1.2.3. Environmental Cycles

Understanding As cycling between water, soil, air and biota is essential to better predict the fate and transport of As in the environment. Figure 1.1 shows the simplified comprehensive As cycling in the lithosphere, hydrosphere, biosphere and atmosphere with the main As transfers shown by bolder arrows.

As discussed previously, As enters the environment from both natural and anthropogenic sources. As enters soil, sediment and rock through the use of pesticides, wood preservatives, feed additives, fossil fuels, and industrial and municipal wastes. Once As enters these environments it is mostly found in inorganic forms, and several processes dictate where it will travel. For example, microbes can increase the rate of As release from oxide ores into the environment by catalyzing the oxidation of sulfide to sulfate and ferrous to ferric iron (Tamaki and Frankenberger, 1992). Arsenic may be released from soil to water when phosphate effectively competes for adsorption sites, displacing As into solution (Bhumbla and Keefer, 1994). Microbes methylate inorganic As species to form methylarsenic compounds such as $CH_3AsO(OH)_2$, $(CH_3)_2AsH$, and $(CH_3)_3As$, which may either remain in the soil or volatilize into the atmosphere (Sadqi, 1997; Smith et al., 1998). Arsenic is more mobile in coarser textured soils than finer textured soils due to adsorption phenomena (Smith et al., 1998). Although As is mobile, it accumulates rapidly in soil because depletion by plant uptake, leaching, methylation and erosion occur at slower rates than deposition (Smith et al., 1998).

After As enters the soil, it may enter water, where it will either remain, volatilize, or be consumed by biota. From the atmosphere, As may enter the water or soil through atmospheric fallout or be consumed by biota. The As consumed by biota may cycle back to the water, soil, or atmosphere. When As enters the environment due

to mining, smelting, volcanoes, fossil fuels, and wastes, it travels directly to the water and atmosphere, where it cycles through the lithosphere, hydrosphere, biosphere and atmosphere.

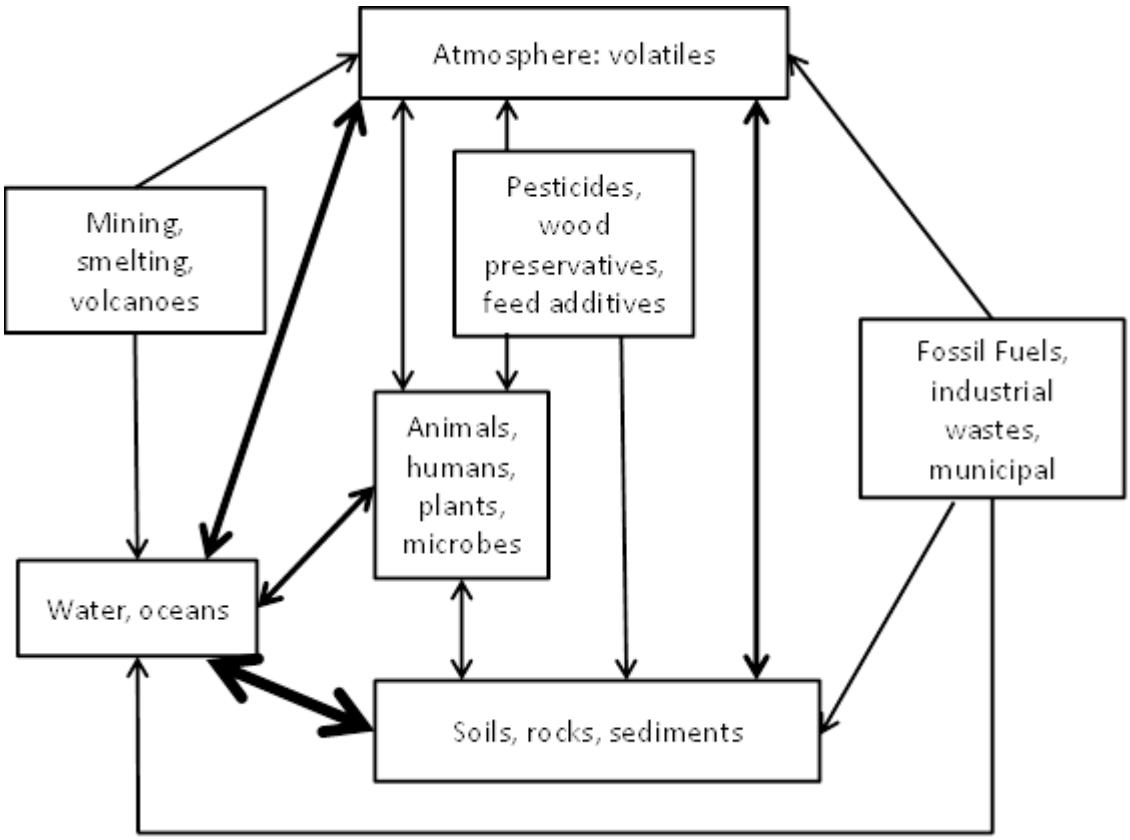

Figure 1.1 Simplified comprehensive As cycling (Kirk, 2003).

1.3 Arsenic Chemistry and Toxicity

1.3.1 General Chemistry

As a metalloid, period four, group V element, arsenic is located beneath nitrogen and phosphorus in the periodic table. The electron configuration for neutral

arsenic is $[Ar]3d^{10}4s^2 4p_x^1 4p_y^1 4p_z^1$, a state that supplies up to five valence electrons for participation in chemical bonding and empty p orbitals for electron occupation. Although As is chemically similar to P in its acid-base properties and affinity for mineral surfaces, it may volatilize from soil through biological transformations while P cannot (Scott and Morgan, 1995; Smith et al., 1998). Secondly, As differs from P by exhibiting higher mobility and is found in multiple oxidation states (Scott and Morgan, 1995; Smith et al., 1998).

Arsenic exists in the −3, 0, +3 and +5 oxidation states. Environmental forms include arsenious acids (H_3AsO_3, $H_2AsO_3^-$, $HAsO_3^{2-}$), arsenic acids (H_3AsO_4, $H_2AsO_4^-$, $HAsO_4^{2-}$), arsenites, arsenates, methylarsenic acid, dimethylarsinic acid, arsine, etc. (Mohan and Pittman, 2007). Two forms are common in natural waters: arsenite (AsO_3^{3-}) and arsenate (AsO_4^{3-}), referred to as As(III) and As(V). As(III) is a hard acid and preferentially complexes with oxides and nitrogen. Conversely, As (V) behaves like a soft acid, forming complexes with sulfides (Mohan and Pittman, 2007; Bodek et al., 1998). Figure 1.2 shows the pKa values for arsenous acid and arsenic acid.

Redox potential (Eh) and pH control arsenic speciation. The Eh-pH diagram of arsenic is shown in Figure 1.3. As(V) species predominate and are stable in oxygen rich aerobic environments. As(III) species predominate in moderately reducing anaerobic environments such as groundwater (Bodek et al., 1998). $H_2ASO_4^-$ dominates at low pH (less than about pH 6.9) in oxidizing conditions. At higher pH, $HAsO_4^{2-}$ is dominant (H_3AsO_4 and AsO_4^{3-} may be present in strong acid or base conditions, respectively). Under reducing conditions at pH < 9.2, the uncharged H_3AsO_4 predominates.

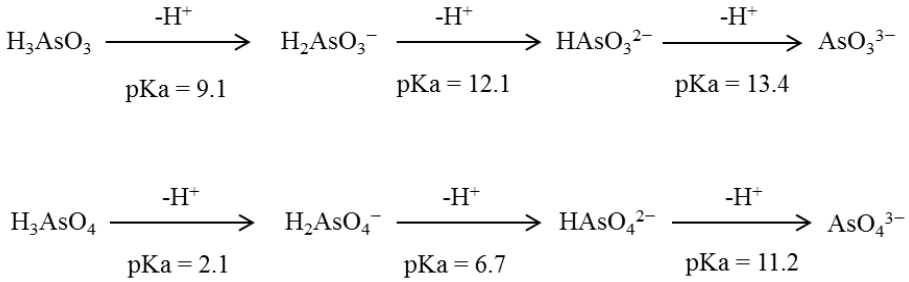

Figure 1.2 The pK_a values for arsenous acid and arsenic acid (Mohan and Pittman, 2007).

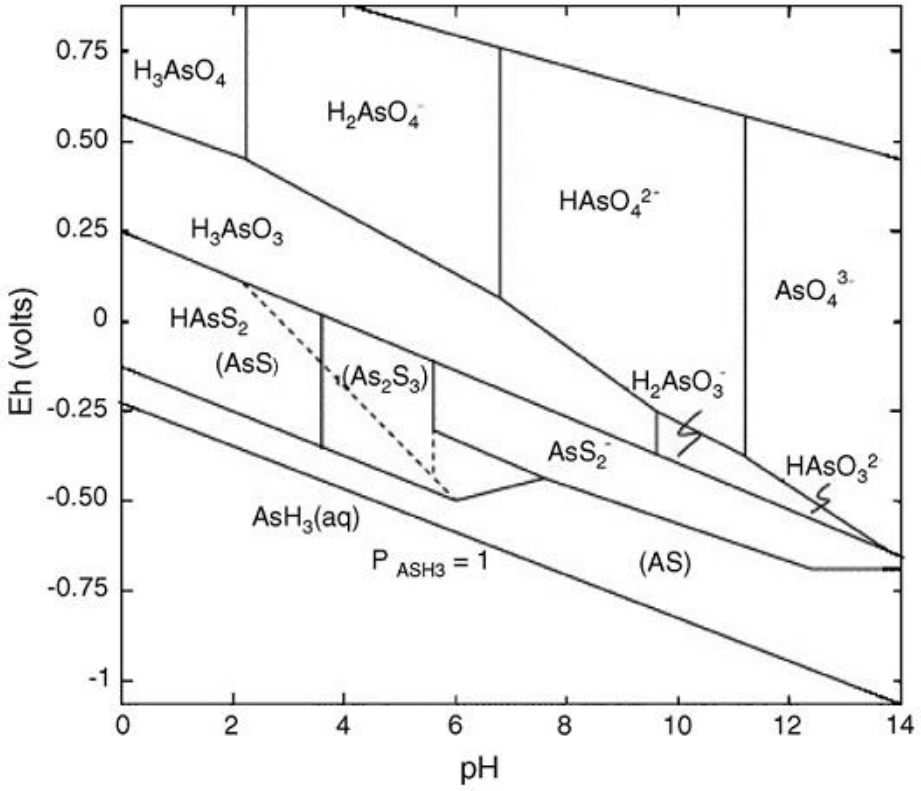

Figure 1.3 The Eh–pH diagram for arsenic at 25 ℃ and 101.3 kPa (Mohan and Pittman, 2007).

1.3.2 Arsenic Toxicity and Mobility

The oxidation state determines As toxicity, bioavailability, and mobility. In general, As(III) is 25–60 times more toxic than As(V) and more mobile (Miretzky and Cirelli, 2010). As(III) inhibits more than 200 different enzymes (Abernathy et al., 1999). It can form strong bonds with sulfhydryl and can alter protein structure, leading to disruptions of metabolic processes (Gochfeld, 1997). The binding of As(III) compounds with sulfhydryl groups has the potential to influence cellular glucose uptake, gluconeogenesis, fatty acid oxidation, and the production of glutathione (Gardner, 2009). Alternatively, the toxic effects of As(V) are due to its tendency to compete with phosphate in cells. Since there is a chemical similarity between phosphate compounds and As(V) compounds, As(V) may be substituted for PO_4 in vital compounds or reactions important to human health. Although As(V) does not interact directly with DNA, indirect effects of As(V) may create an alteration of gene expression via disruption of DNA methylation, inhibition of DNA repair, oxidation stress, or altered modulation of signal transduction pathways (Gamble et al., 2005; Cohen et al., 2006).

The mobility of As in terrestrial environments is generally determined by the extent to which it is adsorbed on mineral surfaces. Metal oxides tend to be the primary sorbents of As in the environment, especially the oxides of iron (Fe) and aluminum (Al) (Arai et al., 2001; Dixit and Hering, 2003). Mn-oxides can also sorb As to some extent (Foster et al., 2003; Manning et al., 2002; Parikh et al., 2008). Although metal oxides are generally thought to bind As(V) more readily than As(III), the extent to which each species is sorbed depends greatly on pH. For example, As(V) sorption by Fe-oxides is greater at acidic pH values, whereas As(III) sorption by Fe -oxides is

greater at basic pH values (Dixit and Hering, 2003; Raven et al., 1998). Although As sorption is pH dependent, As(III) is generally regarded as more mobile than As(V).

1.4 Manganese Oxides in the Environment

Manganese (Mn) oxides are commonly found in a wide variety of geological settings. They are ubiquitous in soils and sediments and participate in various chemical reactions, such as adsorption, surface precipitation and redox reactions, that affect groundwater and soil composition (Post, 1999). Although Mn oxides exist in much smaller amounts in the natural environments compared to ion oxides and aluminum oxides, they are very reactive. Owing to their small particle size and large surface area, Mn oxides are potent adsorbents and scavengers of heavy metals and other trace elements, therefore playing pivotal roles in the transport and fate of metal/metalloid contaminants in both terrestrial and aquatic environments (Nelson and Lion, 2003).

In the environment, Mn exists in three oxidation states: +2, +3, and +4. The presence of multiple Mn oxidation states, in part, leads to the occurrence of a wide variety of Mn-oxide minerals in the environment (Post, 1999). Mn(IV)-oxides can be divided into two structural classes: tunneled structure and layered structure. The basic building block for both structures is the MnO_6 octahedron. In tunneled structures (i.e. tectomanganates), MnO_6 octahedra share both edges and corners (Figure 1.4 a), while in layered structures (i.e. phyllomanganates), MnO_6 octahedra are arranged in sheets by sharing edges (Figure 1.4 b, c, and d) (Doxin and White, 2002). It is important to understand the structure of Mn oxides, especially as it relates to the reactivity.

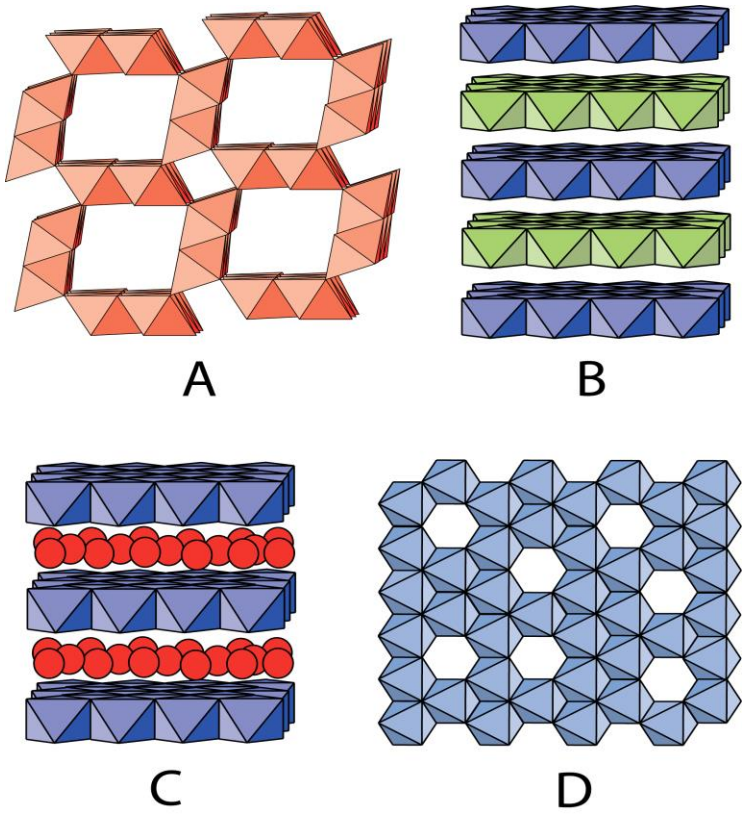

Figure 1.4 Schematic representations of: A) hollandite, a 2x2 tectomanganate, B) lithiophorite, a phyllomanganate with alternating layers of MnO_6 octahedra (blue) and $(Al/Li)(OH)_6$ octahedra (green), C) Na birnessite with unstructured hydrated Na^+ in interlayers (red) to balance the negative charge of Mn octahedral layers (blue), and D) top view of one Mn octahedral sheet in hexagonal birnessite with vacancy sites (Dixon and White, 2002).

The most commonly identified Mn oxide minerals in soils are birnessites. Birnessite group minerals are layered type Mn(III, IV) oxides of variable unit cell symmetry, sheet stacking order, and crystallinity that are commonly encountered in soils and sediments (Post, 1999). However, within the birnessite group the structure could vary. It was pointed out that natural birnessites become less crystalline as the

concentration of Mn^{3+} in their structures decreases (Villalobos and Sposito, 2005). Triclinic birnessite contains the maximum amount of Mn^{3+} substitution, about one-fourth of the octahedra, and has no cation vacancies, whereas δ-MnO_2 exhibits no Mn^{3+} substitution but has several mol percent of cation vacancies. Well crystallized hexagonal birnessite has about 10% Mn^{3+} substitution and about 16% cation vacancies that bind interlayer Mn^{2+} and Mn^{3+}. However, many Mn-oxides observed in nature are poorly-crystalline and are not able to be identified (Post, 1999).

Microorganisms, especially bacteria, but also fungi, are known to catalyze the oxidation of Mn(II) and the formation of Mn(III,IV) oxide minerals. Biological Mn(II) oxidation is generally fast relative to abiotic Mn(II) oxidation processes, including surface-catalyzed reactions, suggesting that biological Mn(II) oxidation dominates in the environment (Tebo et al., 2004). A number of investigations at specific field sites have shown that biological processes are responsible for Mn(II) oxidation at those locations. For these reasons, the majority of naturally occurring environmental Mn oxides are believed to be derived either directly from biogenic Mn(II) oxidation processes or from the subsequent alteration of biogenic oxides (Tebo et al., 2004).

1.5 As(III) Oxidation by Mn-oxides

Due to its toxicity even at low concentrations, As contamination of groundwaters and soils is one of the most important environmental problems worldwide. In the last few decades, a number of studies were devoted to As adsorption on natural or synthetic iron (Fe) and aluminum (Al) oxides, which play a major role in arsenic speciation in the environment and are often used as adsorbents for water treatment purposes. However, adsorption methods usually fail in lowering the more toxic and mobile As(III) concentrations to acceptable levels, for As(III) is less

effectively absorbed by Fe or Al oxides than As(V) (Deschamps and Ciminelli, 2005). Thus, transformation of As(III) to As(V) is of importance in considering remediation of As contaminated waters. Although Mn oxides have not been studied anywhere near the extent that Fe and Al oxides have been, Mn oxides are powerful oxidizing agents and have shown their efficiency in oxidizing As(III) to As(V) (Manning et al., 2002; Scott and Mogan, 1995; Nelson and Lion, 2003; Mohan and Pittman, 2007). Among natural and synthetic Mn oxides, their efficiencies for As(III) oxidation could vary greatly due to structural differences. For example, Mn oxides with layered structures are more reactive than other types of Mn oxides (Manning et al., 2002; Scott and Mogan, 1995). Also, different Mn(IV)/Mn(III) proportions in triclinic and hexagonal birnessites are expected to affect their redox potentials. Vacancies may prove to be highly reactive sites promoting high denticity inner-sphere complex formation, whereas a completely occupied sheet (as in triclinic birnessite) may show lower denticity or predominantly involve outer-sphere processes at interlayer sites (Villalobos et al., 2003).

Synthetic birnessite has been extensively investigated because it is representative of many naturally occurring manganese oxide materials (Manning et al., 2002). The Na^+ and K^+ substituted birnessites are phyllomanganates, possessing layered sheet structures with edge-sharing Mn octahedra. These materials have been described as nearly vacancy-free layers of Mn octahedra influenced by Jahn-Teller distortion when Mn(III) substitutes for Mn(IV). The chemical formula for sodium birnessite has been given as $Na_{0.333}(Mn_{0.7224}{}^{+}Mn_{0.2223}{}^{+}Mn_{0.0552}{}^{+})O_2$ (Manning et al., 2002), indicating a partial negative charge per unit cell. For simplicity, the birnessite chemical formula will be simplified to MnO_2 in this paper. Elucidation of the chemical

mechanisms of As(III) heterogeneous oxidation by birnessite have advanced over time (Scott and Mogan, 1995; Nesbitt et al., 1998). Oxidation of As(III) by synthetic birnessite is coupled with the reductive dissolution of the MnO_2 surface and results in the release of both As(V) and Mn(II) to solution at low pH (Scott and Mogan, 1995). The net stoichiometry of the reaction is

$$MnO_2 + H_3AsO_3 + H^+ \rightarrow Mn^{2+} + H_2AsO_4^- + H_2O \quad (1)$$

Previous work by Nesbitt et al. (1998), using X-ray photoelectron spectroscopy (XPS), has shown that the oxidation of As(III) by the synthetic 7 Å birnessite surface proceeds by a two-step pathway with an electron transfer at a time, involving the reduction of Mn(IV) to Mn(III),

$$2MnO_2 + H_3AsO_3 + H_2O \rightarrow 2MnOOH^* + H_2AsO_4^- + H^+ \quad (2)$$

where MnOOH* is a Mn(III) intermediate reaction product. The reaction in equation (2) is followed by the reaction of As(III) with MnOOH*,

$$2MnOOH^* + H_3AsO_3 + 3H^+ \rightarrow 2Mn^{2+} + H_2AsO_4^- + 3H_2O \quad (3)$$

However, there is more than one pathway that can produce Mn(II) from the oxidation of As(III) by MnO_2. Some studies (Luther and Popp, 2002) show that As(III) oxidation occurs as a two electron transfer to MnO_2, without the formation of a Mn(III) intermediate. This two electron transfer process can be presented using equation (1).

More recent work by Lafferty et al. (2010 a and b), using a stirred-flow technique, X-ray absorption spectroscopy (XAS) and X-ray diffraction (XRD), has shown that the Mn(III) in the δ-MnO_2 structure during As(III) oxidation is formed by conproportionation of sorbed Mn(II) and Mn(IV) in the mineral structure.

1.6 As Sorption on Fe-oxides

Iron hydroxides such as goethite and ferrihydrite, commonly found in soils, greatly influence the mobility of As (Aguilar et al., 2007). Two principal processes are responsible for As geochemistry in soils in the presence of iron compounds: adsorption of As(V) and As(III) on iron hydroxides and precipitation of secondary phases such as iron arsenates. The most common iron oxides are ferrihydrite (β-FeOOH), lepidocrocite (γ-FeOOH), goethite (α-FeOOH), and hematite (α-Fe_2O_3), with goethite and hematite the most stable ones. Conversion of ferrihydrite to goethite or to other crystalline iron oxide phases may occur gradually over time (Pedersen et al., 2006) affecting arsenic adsorption/desorption as the density of adsorption sites diminishes with crystallization (Fuller et al., 1993).

Under oxidizing conditions, As(V) in soil is retained in the solid phases by interaction with Fe(III) oxy-hydroxide coatings on soil particles (Bose and Sharma, 2002). Several types of interactions have been reported: As(V) adsorption on amorphous iron hydroxide (Pierce and Moore, 1980 and 1982), As(V) adsorption on ferrihydrite (Paige et al., 1997; Manning et al., 1998; Raven et al., 1998), and co-precipitation of As(III) and As(V) with iron oxy-hydroxide (Manning et al., 1998; Ford, 2002). The mechanism involved in the adsorption of As species onto iron oxides, including poorly crystalline oxides such as ferrihydrite, is the replacement of OH_2 and OH^- for the anionic As species in the coordination spheres of surface structural Fe atoms, resulting in monodentate, bidentate, mononuclear, or binuclear bridging complexes (Jain et al., 1999; Goldberg, 1986; Raven et al., 1998). The ligand exchange mechanism has been confirmed by extended x-ray absorption fine structure (EXAFS) and infrared (IR) spectroscopic techniques (Sun and Doner, 1996; Fendorf et al., 1997; Waychunas et al., 1993).

Several authors have reported that As(V) binds strongly to Fe(III) oxide minerals under fully oxidized conditions, as an inner-sphere complex, probably predominately as a bidentate, binuclear surface complex (Sun and Doner, 1996; Fendorf et al., 1997; Sherman and Randall, 2003; Fukushi and Sverjensky, 2007; Waychunas et al., 1996). In this case, competition between arsenate and phosphate ions for sorption sites on iron oxides can be a significant factor in decreasing As(V) adsorption (O'Day, 2006; Sarkar et al., 2007). Fendorf et al.(1997) reported that adsorption of As(V) on goethite occurs as a monodentate complex at low coverage, bidentate complex at intermediate coverage, and bidentate complexes, including binuclear bridging complexes at high coverage. A change in the environmental conditions to reducing ones, such as flooding, leads to the dissolution of iron oxide coatings causing release of As(III), As(V), and Fe(II).

Under reducing soil conditions, As(III) in soil is associated with sulfides, with arsenopyrite (FeAsS) being the most common, plus realgar (AsS), enargite ($CuAsS_4$), and orpiment (As_2S_3) (Bose and Sharma, 2002). Once exposed to the atmosphere by natural or anthropogenic activities, arsenopyrite is oxidized releasing As(III), SO_4^{2-}, and Fe(II). As(III) can be oxidized to As(V) and Fe(II) to Fe(III) by reactions bacterially mediated (Lloyd and Oremland, 2006).

The adsorption of As(V) and As(III) anions (AsO_4^{3-} and AsO_3^{3-}) on iron hydroxides depends also on pH, being higher at pH 4–6, below the pH of zero point of charge (pH_{ZPC}) where the oxides are positively charged (pH_{ZPC} of magnetite is 6.5, goethite is 6.8, hematite is 6.7) (Gimenez et al., 2007). Under acidic conditions the protonation of mineral surfaces favors the adsorption of As(V) poly-anions $H_2AsO_4^-$ or $HAsO_4^{2-}$, while As(III) remains soluble under such conditions as arsenious acid

H_3AsO_3 (Sun and Doner, 1998). Instead, under alkaline conditions, As(III) is adsorbed on iron oxides surfaces. Near neutral pH, As(V) and As(III) both adsorb at the surface of hydrous iron oxides and crystalline iron oxides via the formation of strong inner sphere surface complexes (Morin and Calas, 2006). It has been reported that As(III) adsorbs through a mix of inner and outer sphere surface complexes (Goldberg and Johnston, 2001), and bidentate binuclear inner sphere complexes (Manning et al., 1998), however, a bidentate mononuclear complex of As(III) with hematite and ferrihydrite was also reported (Ona-Nguema et al., 2005).

1.7 Effects of Fe(II) on As(III) Oxidation

The oxidation of As(III) is an important process in the natural cycling of As. Previous studies have demonstrated rapid oxidation of As(III) by Mn oxides which produces the less toxic and less mobile As(V) that can be sorbed on mineral surfaces. However, the presence of other mineral surfaces, bacteria, organic matter, and ions in solution can serve to influence As(III) oxidation. In natural conditions, arsenic in alluvial sediments is often associated with Fe oxides and can be mobilized by the reductive dissolution of Fe oxides. Thus, arsenic contaminated groundwater is often associated with the occurrence of elevated concentrations of dissolved Fe^{2+} (He and Hering, 2009). Some water wells in Bangladesh, one of the most As contaminated countries, often contain 0~30 mg/L Fe^{2+} and up to 1 mg/L As(III) (Han et al., 2011). Since Mn oxides are also effective oxidants for Fe^{2+}, reaction of Fe^{2+} and MnO_2 results in the formation of the solids $Fe(OH)_3$ and FeOOH (He and Hering, 2009). We could expect that the presence of Fe^{2+} will substantially alter the behavior of As on Mn-oxides in the following ways: i) Fe^{2+} can be oxidized by Mn oxides and thus could compete with As(III) in terms of oxidation by the Mn oxides; ii) the newly formed

Fe(III) oxides, as a result of the oxidation process, could scavenge As and thus have the potential to sequester As on the mineral phases.

Although a lot of previous studies have focused on As immobilization by reductive dissolution of Fe oxides and As(III) oxidation by Mn oxides, few studies have focused on systems containing both Mn and Fe, where the competitive effects could profoundly affect As behavior. Such systems better represent the natural environment. Zhang et al. (2007) used a novel Fe-Mn binary oxide adsorbent to remove As from water and showed that this synthetic adsorbent had high As(III) removal efficiency. In this Fe-Mn oxide, Mn oxide was dominant for oxidizing As(III) to As(V), while iron oxide was dominant for adsorbing the formed As(V). The effect of amendment with synthetic birnessite on As sequestration in a sediment suspension was examined in the absence and presence of Fe^{2+} by He et al. (2009). This study shows that in the absence of Fe^{2+}, the extent of As(III) oxidation to As(V) increased with increasing birnessite amendment, but As sequestration was not increased. In the presence of Fe^{2+}, however, As sequestration did increase with increasing birnessite amendment. A study by Choi et al. (2009) also showed increasing As sorption by Mn bearing sediments in the presence of Fe^{2+}. It is noted that in the presence of dissolved Fe^{2+}, the precipitation of Fe(III) hydrous oxide phases will be an effective mechanism for As scavenging only if there exists sufficient dissolved oxygen in groundwater to oxidize Fe. Once the aqueous oxidative capacity is exhausted, dissolved Fe^{2+} may compete with As(III) for the limited abiotic oxidation supplied by sediment Mn-bearing phases.

1.8 Research Rationale and Objectives

Arsenic contamination of groundwater and soils is a major global environmental challenge and poses a significant health risk to millions of people throughout the world. Both As(III) and As(V) are carcinogens, but As(III) is more toxic and more mobile. Thus, oxidation of As(III) to As(V) is an effective way to reduce As toxicity. Mn-oxides are the strongest oxidizing agents other than O_2 and facilitate the rapid transformation of As(III) to As(V). As(III) oxidation by Mn-oxides has been extensively studied in the laboratory, however, the oxidation/sorption kinetics and mechanisms of As(III) under natural heterogeneous environments remains unclear.

As(III) and Fe(II) coexist in many anoxic As contaminated environments. Some water wells in Bangladesh, one of the most As contaminated countries, often contain 0~30 mg/L Fe(II) and up to 1 mg/L As(III). The presence of Fe(II) could affect As(III) oxidation by Mn oxides in the following ways: (1) Fe(II) can be oxidized by Mn oxides and thus could compete with As(III) in terms of oxidation by the Mn oxides; (2) the newly formed Fe(III)-(hydr)oxides, as a result of the oxidation process, could scavenge As and thus have the potential to sequester As on the mineral phases. Although a lot of previous studies have focused on As immobilization by reductive dissolution of Fe-oxides and As(III) oxidation by Mn-oxides, few studies have focused on systems containing both Mn and Fe, where the competitive effects could profoundly affect As behavior. Such systems better represent the natural environment. Thus, a comprehensive understanding of As(III) oxidation and As sorption on Mn-oxides as impacted by Fe(II) is essential and will provide significant information that can be used to better predict the fate and toxicity of As in the environment as well as a possible way to solve the As contamination of soils and groundwater.

The major goal of this study is to provide insights into the complex process of As(III) oxidation by poorly crystalline hexagonal birnessite in the presence of dissolved Fe(II) and the impacts that Fe(II) has on As fate, transport and transformations in the environment. Two core objectives are crucial to achieve this goal:

(1) To examine the kinetics and mechanisms of As(III) oxidation and As sorption on poorly crystalline hexagonal birnessite in the presence of dissolved Fe(II).

(2) To determine the mobility of As sorbed on poorly crystalline hexagonal birnessite and newly formed Fe(III)-(hydr)oxides.

REFERENCES

Abernathy, C.O., Y.P. Liu, D. Longfellow, H.V. Aposhianm, B. Beck, B. Fowler, R. Goyer, R. Menzer, T. Rossman, C. Thompson, and M. Waalkes. 1999. Arsenic: Health Effects, Mechanisms of Actions , and Research Issues. Environmental Health Perspectives 107:593-597.

Abernathy, C.O. 2001. Exposure and health effects., In U. S. E. P. Agency, (ed.).

Aguilar, J., Dorronsoro, C., Fernandes, J., Fernandes, E. 2007. Remediation of As contaminated soils in the Guadiamar River Basin (SW, Spain). Water Air Soil Poll. 180: 109–118.

Alpharma. 1999. 3-Nitro is safe for the consumer and environment. Technical Bulletin. Alpharma, Ft. Lee, New Jersey.

Arai, Y., E.J. Elzinga, and D.L. Sparks. 2001. X-ray absorption spectroscopic investigation of arsenite and arsenate adsorption at the aluminum oxide -water interface. J. Colloid Interface Sci. 235:80 -88.

Bhumbla, D.K., and R.F. Keefer. 1994. Cycling and characterization., In J. O. Nriagu, ed. Arsenic in the Environment. Part I. Wiley and Sons, New York.

Bodek, I., Lyman, W.J., Reehl, W.F., Rosenblatt, D.H. 1998. Environmental Inorganic Chemistry: Properties, Processes and Estimation Methods, Pergamon Press, USA.

Bose, P., and Sharma, A. 2002. Role of iron in controlling speciation and mobilization of arsenic in subsurface environment. Water Res., 36:4916–4926.

Christen, K. 2001. The arsenic threat wors ens. Environmental Science & Technology. 35:286A-291A.

Choi, S., Day, P. A., Hering, J. G. 2009. Natural attenuation of arsenic by sediment sorption and oxidation, Environ. Sci. Technol. 43:4253-4259.

Cohen, S.M., L.L. Arnold, M. Eldan, A.S. Lewis, and B.D. Beck. 2006. Methylated arsenicals: The implications of metabolism and carcinogenicity studies in rodents to human risk assessment. Critical Review of Toxicology. 26:99-133.

Deschamps, E., Ciminelli, V. S. T., Holl, W. H. 2005. Removal of As(III) and As(V) from water using a natural Fe and Mn enriched sample. Water Research. 39:5212-5220.

Dixit, S., and J.G. Hering. 2003. Comparison of arsenic(V) and arsenic(III) sorption onto iron oxide minerals: Implications for arsenic mobility. Environ. Sci. Technol. 37:4182-4189.

Dixon, J.B., and G.N. White. 2002. Manganese oxides, p. 367 -388, In J. B. Dixon and D. G. Schulze, eds. Soil mineralogy with environmental implications. Soil Science Society of America, Inc., Madison, Wisconsin.

Fendorf, S., M.J. Eick, and P. Grossl. 1997. Arsenate and chromate retention mechanisms on goethite. 1. Surface structure. Environ. Sci. Technol. 31:315-320.

Ford, R.G. 2002. Rates of hydrous ferric oxide crystallization and the influence on coprecipitated arsenate. Environ. Sci. Technol., 36: 2459–2463.

Foster, A.L., G.E. Brown, and G.A. Parks. 2003. X-ray absorption fine structure study of As(V) and Se(IV) sorption complexes on hydrous Mn oxides. Geochim. Cosmoch im. Ac. 67:1937 -1953.

Fuller, C.C., Dadis, J. A.; Waychunas, G. A. 1993. Surface chemistry of ferrihydrite, part 2: Kinetics of arsenate adsorption and coprecipitation. Geochim Cosmochim. Acta,57: 2271–2282.

Fukushi, K., and Sverjensky, D. 2007. A predictive model (ETLM) for arsenate adsorption and surface speciation on oxides consistent with spectroscopic and theoretical molecular evidence. Geochim. Cosmochim. Acta, 71: 3717–3745.

Gamble, M.V., X. Liu, H. Ahsan, J.R. Pilsner, V. Llievski, V. Slavkovich, F. Parvez, D. Levy, P. Factor-Litvak, and J.H. Graziano. 2005. Folate, homocysteine, and arsenic metabolism in arsenic exposed individuals in Bangladesh. Environmental Health Perspective. 113:1683-1688.

Gardner, S. 2009. Fate, transport, and bioavailability of arsenic in manured and contaminated soils of Delaware. University of Delaware Ph.D dissertation.

Gimenez, J., Martinez, M., Pablo, J., Rovira, M. 2007. Arsenic sorption onto natural hematite, magnetite and goethite. J. Hazard. Mater., 141: 575–580.

Gochfeld, M. 1997. Factors influencing susceptibility to metals. Environmental Health Perspective. 105(Suppl. 4):817-833.

Goldberg, S. 1986. Chemical modeling of arsenate adsorption on aluminum and iron oxide minerals. Soil Sci. Soc. Am. J., 50: 1154–1157.

Goldberg, S., and Johnston, C.T. 2001. Mechanisms of arsenic adsorption on amorphous oxides evaluated using macroscopic measurements, vibrational spectroscopy, and surface complexation modeling. J. Colloid Interf. Sci., 234: 204–216.

Han, X., Li, Y. L., Gu, J. D. 2011. Oxidation of As(III) by MnO2 in the absence and presence of Fe(II) under acidic aonditions, Geochimica et Cosmochimica Acta. 75:368-379.

He, Y. T., Hering, J. G. 2009. Enhancement of arsenic(III) sequestration by manganese oxides in the presence of iron(II), Water, Air, Soil Pollut. 203:359-368.

Jain, A., Raven K.P., Leoppert, R.H. 1999. Arsenite and arsenate adsorption on ferrihydrite: Surface charge reduction and net OH-release stoichiometry.Environ. Sci. Technol., 33: 1179–1184.

Kirk, L. 2003. Metal sorption effects on arsenic(III) oxidation kinetics at the birnessite-water interface. University of Delaware M.S. thesis.

Lafferty, B., M. Ginder-Vogel and D.L. Sparks. 2010 a. Arsenite oxidation by a poorly crystalline manganese-oxide 1. Stirred-flow experiments. Environ. Sci. Technol. 44:8460-8466.

Lafferty, B., M. Ginder-Vogel, M. Zhu, K.J.T. Livi and D.L. Sparks. 2010 b. Arsenite oxidation by a poorly crystalline manganese-oxide 2.Results from X-ray absorption spectroscopy and X-ray diffraction. Environ. Sci. Technol. 44:8467–8472.

Lloyd, J., and Oremland, R. 2006. Microbial transformations of As in the environment: From soda lakes to aquifers. Elements, 2: 85–90.

Luther, G., Popp, J. 2002. Kinetics of abiotic reduction of polymeric manganese dioxide by nitrite: An anaerobic nitrification reaction, Aquatic Geochem. 8:15-36.

Mandal, B.K., and K.T. Suzuki. 2002. Arsenic Round the World: a review. Talanta. 58:201-235.

Manning, B.A., Fendorf, S.E., Goldberg, S. 1998. Surface structures and stability of arsenic (III) on goethite: Spectroscopic evidence for inner-sphere complexes. Environ. Sci. Technol., 32: 2383–2388.

Manning, B.A., Fendorf, S.E., Bostick, B., Suarez, D.L. 2002. Arsenic(III) oxidation and arsenic(V) adsorption reactions on synthetic birnessite. Environ. Sci. Technol. 36:976-981.

Miretzk, P. and Cirelli, A.F. 2010. Remediation of Arsenic-Contaminated Soils by Iron Amendments: A Review. Critical Reviews in Environmental Science and Technology 40:93–115.

Mohan, D., Pittman, C. U. 2007. Arsenic removal from water/wastewater using adsorbents-a critical review, J. Hazard. Mater. 142:1-53.

Morin, G., and Calas, G. 2006. Arsenic in soils, mine tailings and former industrial sites. Elements, 2: 97–101.

Nelson, Y. M., Lion, L. W. 2003. Formation of biogenic manganese oxides and their influence on the scavenging of toxic trace metals, In: Selim HM, Kingerly WL (eds), Geochemical and Hydrological Reactivity of Heavy Metals in Soils, CRC Press, Boca Raton, pp169-186.

Nesbitt, H.W., G.W. Canning, and G.M. Bancroft. 1998. XPS study of reductive dissolution of 7 angstrom-birnessite by H3AsO3, with constraints on reaction mechanism. Geochim. Cosmochim. Ac. 62:2097-2110.

Nriagu, J.O. 1990. Human Influence On The Global Cycling Of Trace-Metals. Global And Planetary Change 82:113-120.

O'Day, P. 2006. Chemistry and mineralogy of arsenic. Elements, 2: 77–83.

Ona-Nguema, G., Morin, G., Juillot, F., Calas, G., Brown, G. 2005. EXAFS analysis of Arsenic (III) sorption onto 2-lineferrihydrite, hematite, goethite, and lepidocrocite under anoxic conditions. Influence of the surface structure. Environ. Sci. Technol., 39: 9147–9155.

Paige, C.R., Nicholson, R.V., Scharer, J.M. 1997. An arsenate effect on ferrihydrite dissolution kinetics under acidic oxic conditions. Water Res., 31: 2370–2382.

Parikh, S.J., B.J. Lafferty, and D.L. Sparks. 2008. An ATR -FTIR spectroscopic approach for measuring rapid kinetics at the mineral/water interface. J. Colloid Interface Sci. 320:177.

Pedersen, H., Postma, D., Jakobsen, R. 2006. Release of arsenic associated with the reduction and transformation of iron oxides. Geochim. Cosmochim. Acta,70: 4116–4129.

Pierce, M.L., and Moore, C.B. 1980. Adsorption of arsenite on amorphous iron hydroxide from dilute aqueous solution. Environ. Sci. Technol., 14: 214–216.

Pierce, M.L., and Moore, C.B. 1982. Adsorption of arsenite and arsenate on amorphous iron hydroxide. Water Res., 16: 1247–1253.

Post, J.E. 1999. Manganese oxide minerals: Crystal structures and economic and environmental significance. Proc. Natl. Acad. Sci. 96:3447 -3454.

Raven, K.P., A. Jain, and R.H. Loeppert. 1998. Arsenite and arsenate adsorption on ferrihydrite: kinetics, equilibrium, and adsorption envelopes. Environ. Sci. Technol. 32:344-349.

Sadiq, M. 1997. Arsenic chemistry in soils: An overview of thermodynamic predictions and field observations. Water Air And Soil Pollution 93:117-136.

Sarkar, D., Quazi, S., Makris, K.C., Datta, R., Khairom, A. 2007. Arsenic bioaccessibility in a soil amended with drinking-water treatment residuals in the presence of phosphorous fertilizer. Arch. Environ. Contam. Toxicol., 53: 329–336.

Scott, M.J., and J.J. Morgan. 1995. Reactions at Oxide Surfaces. 1. Oxidation of As(III) by Synthetic Birnessite. Environm ental Science & Technology 29:1898-1905.

Sherman, D.M., and Randall, S.R. 2003. Surface complexation of arsenic (V) to iron (III) (hydr)oxides: Structural mechanism from ab initio molecular ge-ometries and EXAFS spectroscopy. Geochim. Cosmochim. Acta, 67: 4223–4230.

Smith, E., R. Naidu, and A.M. Alston. 1998. Arsenic in the Soil Environment: A Review. Advances in Agronomy 64:149-195. Academic Press, San Diego, CA.

Sparks, D.L., Sims, T.J., Seiter., J., Gardner, S. 2007. Fate and transport of arsenic in Delaware soils: assessing potential impacts on water quality. DNREC, DWR, Watershed Assessment Branch.

Sun, X., and Doner, H.E. 1996. An investigation of arsenate and arsenite bonding structures on goethite by FTIR.Soil Sci., 161: 865–872.

Tamaki, S., and W.T. Frankenberger. 1992. Environm ental Biochemistry of Arsenic. Reviews of Environmental Contamination and Toxicology 124: 79-110.

Tebo, B.M., J.R. Bargar, B.G. Clement, G.J. Dick, K.J. Murray, D. Parker, R. Verity, and S.M. Webb. 2004. Biogenic manganese oxides: Properties and mechanisms of formation. Ann. Rev. Earth and Plan. Sci. 32: 287 -328.

USEPA. 2001. National primary drinking water regulations; arsenic and clarifications to compliance and new source contaminants monitoring, pp. 6976 -7065, Vol. Rule 66 FR 6976. Federal Register.

Villalobos, M., B. Toner, J. Bargar, and G. Sposito. 2003. Characterization of the manganese oxide produced by Pseudomonas putida strain MnB1. Geochim. Cosmochim. Acta 67:2649 -2662.

Villalobos, M., Bargar, J., Sposito, G. 2005. Mechanisms of Pb(II) sorption on a biogenic manganese oxide, Environ. Sci. Technol. 39: 569-576.

Waychunas, G.A., B.A. Rea, C.C. Fuller, and J.A. Davis. 1993. Surface Chemistry of Ferrihydrite: Part 1. EXAFS Studies of the Geometry of Coprecipitated and Adsorbed Arsenate. Geochimica et Cosmochimica Acta 57:2251-2269.

Waychunas, G.A., Fuller, C.C., Rea, B.A., Davis, J.A.1996. Wide angle x-ray scattering (WAXS) study of two-line ferrihydrite structure: Effect of arsenate sorption and counterion variation and comparison with EXAFS results. Geochim. Cosmochim. Acta, 60: 1765–1781.

WHO. 2001. Arsenic Compounds, Environmental Health Criteria 224, 2nd ed., World Health Organisation, Geneva.

Woolson, E.A. 1975. Bioaccumulation Of Arsenicals. Advances In Chemistry Series:97-107.

Zhang, G., Qu, J., Liu, H., Liu, R., Li, G. 2007. Removal mechanism of Standard methods 3500-Fe B As(III) by a novel Fe–Mn binary oxide adsorbent: oxidation and sorption, Environ. Sci. Technol. 41:4613–4619.

Chapter 2

THE EFFECTS OF IRON(II) ON ARSENIC OXIDATION AND SORPTION ON MANGANESE OXIDES: RESULTS FROM STIRRED-FLOW AND KINETIC EXPERIMENTS

ABSTRACT

The oxidation of arsenite (As(III)) by manganese (Mn) oxides is an important process in the natural cycling of arsenic (As) in the environment. Previous studies have demonstrated rapid oxidation of As(III) by Mn oxides which produces the less toxic and less mobile arsenate (As(V)) that can be sorbed on mineral surfaces. Under natural conditions, the presence of other ions, such as Fe(II), can influence the behavior of As(III) on Mn oxides. However, very few studies have focused on the effects of Fe(II) on the redox and sorption processes. In this study, As(III) oxidation by a poorly-crystalline phyllomanganate (δ-MnO_2) in the presence and absence of dissolved Fe(II) was investigated using stirred-flow and batch experiments. Chemically synthetic δ-MnO_2 was reacted with four influent solutions, containing the same As(III) concentration but different Fe(II) concentrations, at pH 6. The results show an initial rapid As(III) oxidation by δ-MnO_2, which is followed by an appreciably slow reaction after 8 hours. In the presence of Fe(II), As(III) oxidation is inhibited due to the competitive oxidation of Fe(II) as well as the formation of Fe(III)-(hydr)oxides on the δ-MnO_2 surface. However, the sorption of As(III), As(V) and

Mn(II) are increased, for the newly formed Fe(III)-(hydr)oxides provide additional sorption sites. This study suggests that the competitive oxidation of Fe(II) and consequently the precipitation of Fe(III) compounds on the δ-MnO_2 surface play an important role in As(III) oxidation and As sequestration. Understanding these processes would be helpful in developing in situ strategies for remediation of As-contaminated waters and soils.

2.1 Introduction

Arsenic (As) contamination in soils, sediments, and water from natural and anthropogenic sources pose environmental and human health risks. The predominate species of As in soil and aquatic environments are arsenite (As(III)) and arsenate (As(V)). As(V) is the most stable species under aerobic conditions and exists as deprotonated oxyanions of arsenic acid ($H_2AsO_4^-$ and $HAsO_4^{2-}$), while As(III) is always electrically neutral, and primarily exists as the uncharged molecule H_3AsO_3 when the pH is below 9. As(III) is known to be more mobile in soil and sediment environments due to being weakly bound to mineral surfaces, and is more toxic than As(V), since it binds to sulfhydryl groups, impairing the function of many proteins (Jiang et al., 2009). Therefore, the transformation of As(III) to As(V) not only decreases the toxicity of As, but also enhances As removal from drinking water and sequestration to soils and sediments.

In environmental settings, manganese (Mn) oxide minerals commonly occur as coatings and fine-grained aggregates with large surface areas and exert chemical influences far out of proportion to their prevalence (Post, 1999; Ginder-Vogel et al., 2009). Manganese oxides minerals act as potent sorbents of heavy metals and

nutrients, serving as natural sinks for environmental contaminants. More importantly, they are powerful oxidants and play a critical role in the transformation of As(III) to As(V) under natural conditions (Scott and Morgan, 1995; Nesbitt et al., 1998; Tournassat et al., 2002; Yang et al., 2005). The oxidation process by Mn-oxides is quite rapid, compared to the direct oxidation of aqueous As(III) by molecular oxygen with a half-life around a year (Eary and Schramke, 1990). The reactivity of Mn-oxide minerals varies with their mineralogy. It has been found that layered Mn-oxide minerals, such as phyllomanganates, are more reactive than other types of Mn-oxides (Oscarson et al., 1983; Chiu and Hering, 2000; Manning et al., 2002). The most reactive Mn-oxides have a great potential in terms of As(III) oxidation even when present in small quantities. There is evidence that a large number of Mn-oxides found in surface environments are poorly crystalline and of biogenic origin (Tebo et al., 2004; Shiller and Stephens, 2005). Also, these poorly crystalline biogenic Mn-oxides may be among the most reactive Mn-oxides in the environment (Tebo et al., 2004). It is important to understand the reactivity of poorly crystalline Mn-oxides, as it relates to As speciation, not only because of their higher reactivity but also because of their abundance in the environment.

Under natural conditions, various ions may coexist with As(III). However their impact on the As (III) oxidation process has attracted less attention. Power et al. (2005) found that the competitive sorption of Zn(II) on the birnessite surface decreased the As(III) oxidation rates under all reaction conditions and this inhibition became more pronounced when Zn(II) was pre-sorbed onto the birnessite surface as opposed to when it was added simultaneously with As(III). Parikh et al. (2010) reported that initial reaction rates of As(III) oxidation by hydrous Mn-oxides (δ-

MnO_2) are reduced when high phosphate concentrations strongly passivate δ-MnO_2 and reduce As(III) interactions with the mineral surface. Naturally occurring As in soils and sediments is often associated with Fe-oxides and, hence, As can be mobilized by the reductive dissolution of the carrier phase (Herbel and Fendorf, 2006; He and Hering, 2009). Thus, co-occurrence of elevated concentrations of As(III) and Fe(II) are often observed under moderately reducing conditions (Nickson et al. 2000; Swartz et al. 2004). There is a report that in Bangladesh, one of the most arsenic contaminated countries, some water wells contains 0-30 mg/L Fe(II) and up to 1 mg/L As(III) (Nickson et al., 1998). As(III) and Fe(II) may also coexist in aerobic conditions. Acid mine drainage (AMD), which is caused by the biological oxidation of sulfidic materials, frequently contains sulfate, As(III) and/or As(V), along with much higher concentrations of dissolved Fe(II) and/or Fe(III) (Wang et al., 2003; Han et al., 2011).

Unlike other ions such as Zn(II) and phosphate, Fe(II) could also be oxidized by Mn-oxides, and thus can compete with As(III). The reaction of Fe(II) with Mn-oxides results in the formation of solid Fe(III)-(hydr)oxides on Mn-oxide surfaces (Postma and Appelo, 2000), which may cause surface passivation and inhibit further oxidation of As(III) and Fe(II). Also, the newly formed Fe(III)-(hydr)oxides could adsorb both As(III) and As(V) in solution due to the high affinity of As(III) and As(V) to Fe-oxides (Dixit and Hering, 2003; He and Hering, 2009; Han et al., 2011). Therefore, the presence of Fe(II) could substantially alter As(III) oxidation on Mn-oxides, however, the effect of Fe(II) has not been elucidated to date. The aim of this study is to explore the extent to which dissolved Fe(II) could affect the oxidation of As(III) by Mn-oxides and the mechanism involved in this process. To achieve this goal, the following stirred-flow experiments were conducted: (1) oxidation of As(III)

and Fe(II) individually by δ-MnO_2; (2) oxidation of As(III) and Fe(II) simultaneously by δ-MnO_2 under different Fe(II) concentrations; and (3) Oxidation of As(III) first by δ-MnO_2 and then addition of Fe(II) at different time periods. A unique benefit of the stirred-flow technique is that reaction products are removed from the reactor, thus limiting potential reactions between products and the mineral surface being studied.

In addition, quantification of the initial rates of environmental reactions at the mineral/water interface is a fundamental prerequisite to determining reaction mechanisms and contaminant transport modeling and predicting environmental risk. Many important mineral surface processes (e.g., adsorption, oxidation-reduction, precipitation) are characterized by a rapid initial reaction on time scales of milliseconds to minutes in which a significant portion of the reaction process may occur (Scheidegger and Sparks, 1996; Ginder-Vogel et al., 2009). In this study, we are also interested in knowing how Fe(II) could affect the initial As(III) oxidation rate by δ-MnO_2. Therefore, batch kinetic experiments (up to 30min) were performed under different Fe(II) additions to quantify initial As(III) oxidation rates. Knowledge of these initial reaction rates is critical to determining chemical kinetic rate constants and reaction mechanisms, both of which are required to fully understand environmental chemical processes involving As.

2.2 Methods and Materials

2.2.1 Chemicals

All chemicals used in this study met or exceeded American Chemical Society standards. 18.2 MΩ deionized (DI) water was used for all solutions. $NaAsO_2$ and $FeSO_4 \cdot 7H_2O$ were used as sources of As(III) and Fe(II), respectively. As(III) stock

solution (100 mmol/L) was stored at 4 ℃ and prepared every month. Fe(II) solution was freshly prepared every time in the glove box and the DI water used to make the Fe(II) solution was degased, using nitrogen gas, for 2 hours before use.

2.2.2 δ-MnO_2 Synthesis

δ-MnO_2, a poorly-crystalline, phyllomanganate, was used in the studies presented here because of its high reactivity as well as its similarities to biogenic Mn-oxides (Villalobos et al., 2003). δ-MnO_2 is a form of hexagonal birnessite with a low degree of stacking of phyllomanganate sheets (Drits et al., 1997; Silvester et al., 1997). δ-MnO_2 was synthesized by drop wise addition of a 100 mL solution containing 11.29 g $Mn(NO_3)_2$ ·4H_2O to a 100 mL solution containing 2.4 g NaOH and 4.74 g KMnO4, corresponding to a final Mn(II):Mn(VII):OH ratio of 3:2:4 (Morgan and Stumm, 1964). After adding Mn(II) to the basic permanganate solution, the resulting suspension was stirred overnight (at least 12 hours) to allow complete conproportionation of Mn(II) and Mn(VII) to Mn(IV). Following synthesis, δ-MnO_2 was centrifuged at 10,000 RCF for 15 min, then the supernatant was removed and replaced with 18.2 MΩ deionized (DI) water. This wash step was repeated 6 times. Following washing, δ-MnO_2 was transferred to a polypropylene bottle, resuspended in DI water, and stored at 4 ℃ prior to use in experiments. Experiments were conducted using δ-MnO_2 within a month of synthesis. Characterization of synthetic δ-MnO_2 is provided in Appendix A.

2.2.3 Stirred-flow Experiments

The stirred-flow system is shown in Figure 2.1. The reactor is a modified version of the stirred-flow reactor described by Wielinga et al. (2001). The chamber

volume is 12.0 mL. All stirred-flow reactions were conducted by pumping a solution of As(III) or Fe(II) or both in a 0.01 M $NaNO_3$ background electrolyte buffered at a certain pH at a rate of 1.0 mL/min into a stirred-flow chamber containing 2.0 g/L δ-MnO_2. For reactions involving Fe(II), nitrogen gas was pumped into the solution to maintain anoxic conditions. All suspensions in the reaction chamber were mixed at 100 rpm via a magnetic stir bar. Effluent solutions were filtered with a 0.22 μm pore size filter and then collected by a fraction collector. Effluent solutions which contained Fe(II) were immediately transferred into a glove box until analysis, and all other solutions were stored at 4 ºC in the dark until analysis. All stirred-flow experiments were conducted at least in duplicate.

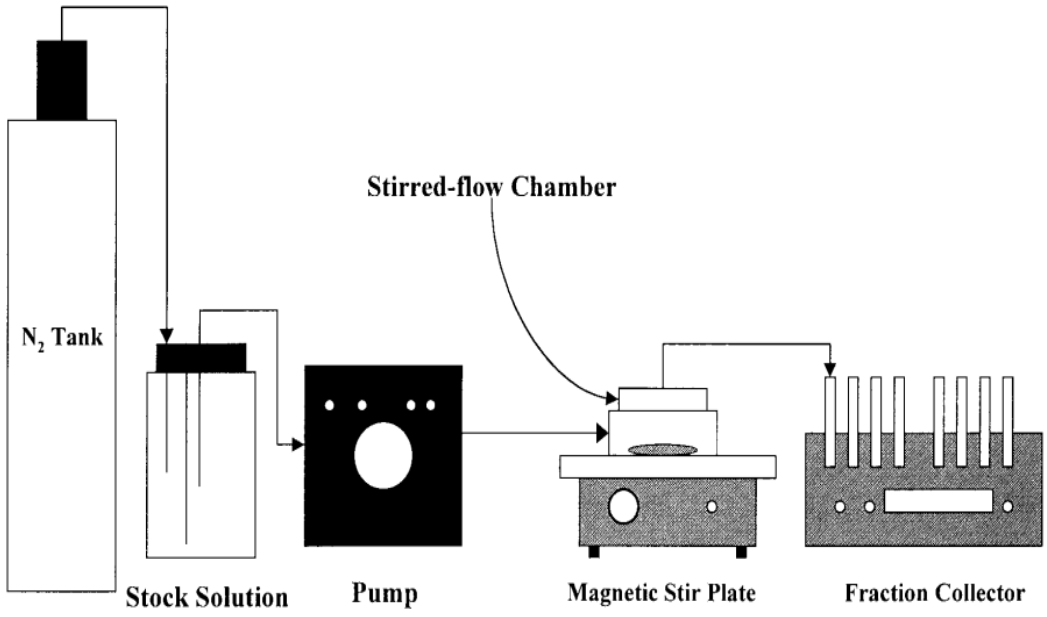

Figure 2.1 Schematic illustration of the stirred-flow experiments (Strawn and Sparks, 2000).

2.2.4 Kinetic Experiments

All kinetic experiments were conducted under batch conditions using 500 mL of reaction solution, which was prepared in 0.01 mol/L $NaNO_3$ (or NaF) background electrolyte buffered at a particular pH. The reaction was then initiated by adding a certain amount of HMO stock solution to achieve a HMO concentration of 0.1 g/L. All reaction mixtures were stirred at 200 rpm via a magnetic stir bar and for those containing Fe(II), nitrogen gas was pumped during reaction to maintain anoxic conditions. The reaction was sampled every 15 seconds for the first 2 minutes, every 1 minute from 2 to 10 minutes and then every 5 minutes until 30 minutes by removal of 2 mL of the reaction mixture using a syringe. Within 2 second of removal, the reaction mixture was filtered through a 0.2 μm polypropylene syringe filter to quench the reaction. The filtered solutions which contained Fe(II) were immediately transferred into a glove box until analysis, and all other solutions were stored at 4 ^{o}C in the dark until analysis. All kinetic experiments were conducted at least in triplicate.

2.2.5 Determination of Metal Concentrations

As(III) and As(V) were quantified by liquid chromatography inductively coupled plasma mass spectrometry (LC-ICP-MS). As(III) and As(V) were separated using a Phenomenex Prodigy 5 μm ODS-3 100 Å (150 x 4.6) column with a flow rate of 1 mL/min, using a 10 μm sample injection before quantification by LC-ICP-MS. The mobile phase consisted of 5% methanol in 5 mM tetra-butyl ammonium hydroxide, and the pH was adjusted to 5.9 using malonic acid (final concentration of about 3 mM). Arsenic species separated by LC were directly introduced via a nebulizer into an Agilent 7500ce inductively coupled plasma mass spectrometer operated in helium mode. Fe(II) concentration was determined by the ferrozine

method (Stookey, 1970). In order to eliminate the interference of Fe(III) in Fe(II) measurements, 0.05 mol/L NaF was added to mask Fe(III) in Fe(II) determination. Total Fe was determined by reducing total Fe(III) to Fe(II) and then Fe(II) was measured by the ferrozine method without addition of NaF solution. The Fe(III) content in the liquid solution was obtained by difference. Mn(II) concentration was quantified by inductively coupled plasma optical emission spectrometry (ICP-OES), where 5 mL of sample were acidified using 1% (w/v) nitric acid mixed with 0.5% (w/v) hydrochloric acid. The amount of As sorbed during the reaction was determined by calculating the difference between the mass of As (μmol) introduced into the reactor and the mass of As (μmol) removed from the reactor over time (more details please see Appendix B).

2.3 Results and Discussion

2.3.1 Oxidation of As(III) and Fe(II) Individually by δ-MnO_2

As(III) Oxidation by δ-MnO_2. The reaction shows a similar pattern at both pH 3 (Fig 2.2 a) and 6 (Fig 2.2 b). As(V) appears immediately in the effluent solution and reaches a maximum within 2 hours, indicating a fast initial oxidation rate of As(III) by δ- MnO_2. After that the As(V) concentration starts to decrease and gradually reaches equilibrium. The decrease of As(V) in the effluent is due to both the decreased As(III) oxidation rate, producing less As(V), and the sorption of As(V) onto δ-MnO_2 surface. Changes in Mn(II) concentration in the effluent resembles As(V). It reaches a maximum in a few hours and then decreases. However, Mn(II) appears relatively late in the effluent, compared to As(V). This late appearance could be attributed to either the complete retention of Mn(II) by δ-MnO_2, or the formation of a

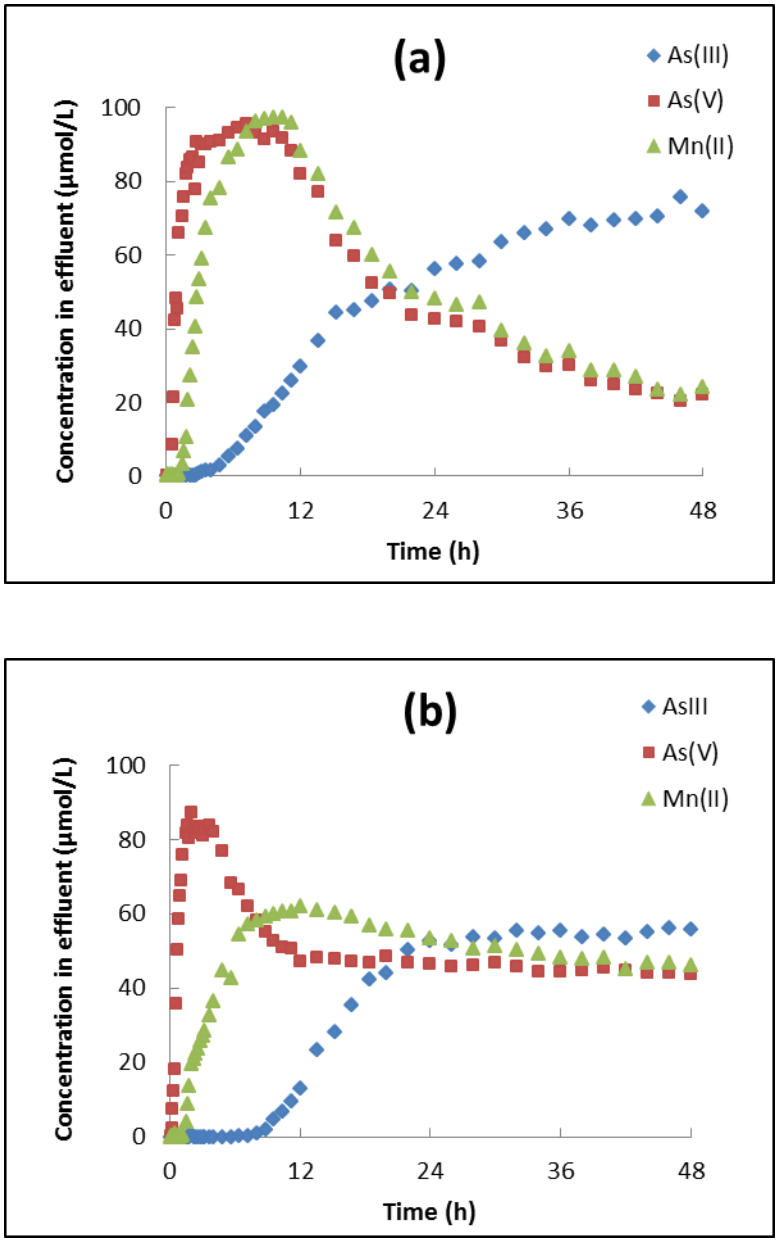

Figure 2.2 Concentrations (µmol/L) of As(III), As(V) and Mn(II) in the effluent of a stirred-flow experiment where 100 µmol/L As(III) was reacted with 2 g/L δ-MnO_2 for 48 hours at (a) pH 3 and (b) pH 6.

Mn(III) intermediate early in the reaction process (Nesbitt et al., 1998; Lafferty et al., 2010a), since no Mn(II) is produced when Mn(IV) is reduced to Mn(III). At both pHs, there are two clear As(III) oxidation phases, a fast oxidation phase in the first few hours followed by a gradual decrease in the oxidation process. During the fast oxidation phase, no As(III) is detected in the effluent. After that, As(III) starts to appear as the oxidation rate decreases and finally reaches equilibrium. As(III) appears at 3.6 h at pH 3 , which is about 5 hours earlier than what occurs at pH 6, indicating a higher As(III) oxidation rate by δ-MnO_2 at the higher pH.

The two-phase As(III) oxidation by Mn-oxides has been observed previously (Scott and Morgan, 1995; Manning et al., 2002; Tournassat et al., 2002; Parikh et al., 2008 and 2010; Ginder-Vogel et al., 2009; Lafferty et al., 2010a) and was attributed to surface passivation of Mn-oxides (Manning et al., 2002; Tournassat et al., 2002; Parikh et al., 2010; Lafferty et al., 2010a). Three possible causes could contribute to the passivation of the Mn-oxides surface. First is the sorption of Mn(II) and As(V). The reaction of As(III) with Mn-oxides produces Mn(II) and As(V). Typically, Mn(II) and As(V) are not released into solution in stoichiometric amounts during the reaction, indicating that some of the Mn(II) and As(V) are re-adsorbed onto the Mn-oxide surface (Scott and Morgan, 1995; Lafferty et al., 2010a). The sorption is thought to occur at the reactive sites where As(III) is oxidized, thus blocking the potential sites for further As(III) oxidation. A possible second reason could be the formation of a Mn-As precipitate. Under certain reaction conditions, a Mn(II)-As(V) precipitate that compositionally resembles the mineral krautite ($Mn^{II}HAs^{V}O_4 \cdot H_2O$) has been observed during As(III) oxidation by birnessite. This precipitate could also block the reactive site for As(III) oxidation (Tournassat et al., 2002). Third is the formation of a Mn(III)

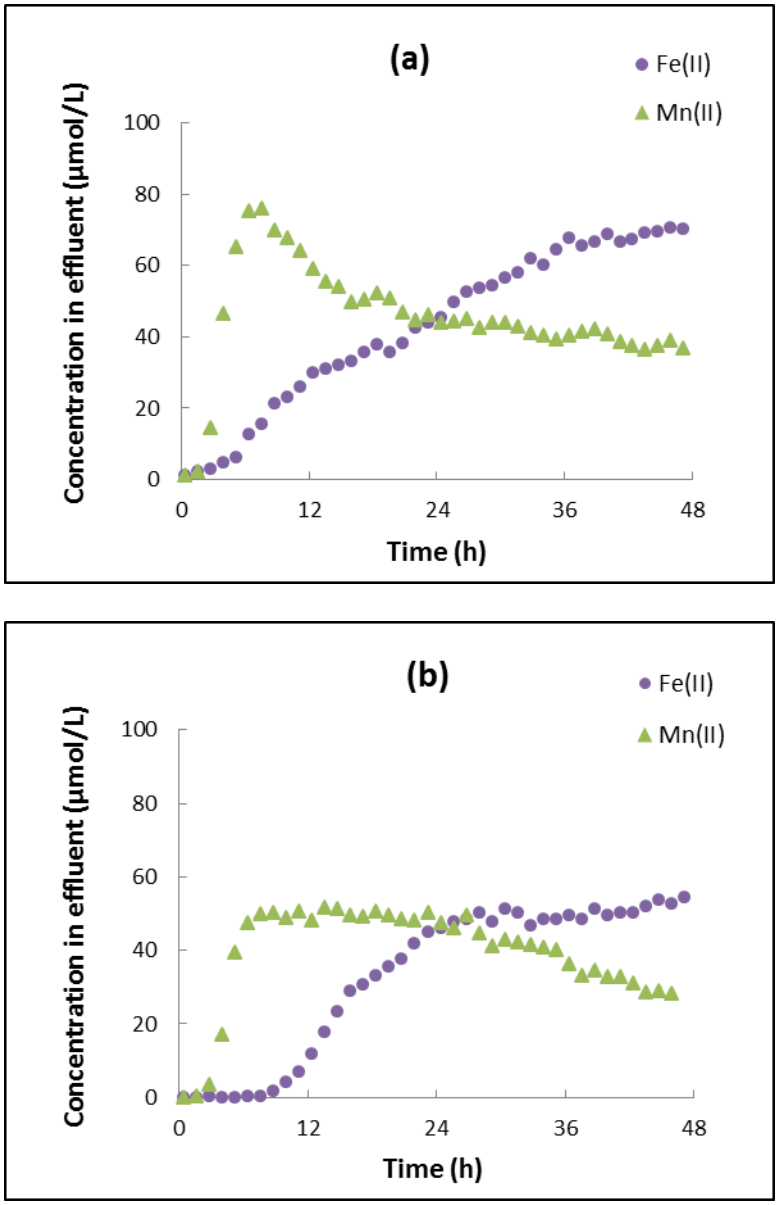

Figure 2.3 Concentrations (µmol/L) of Fe(II) and Mn(II) in the effluent from a stirred-flow experiment reacting 100 µmol/L Fe(II) with 2 g/L δ-MnO_2 for 48 hours at (a) pH 3 and (b) pH 6.

intermediate. Studies have shown that As(III) oxidation by birnessite proceeds in two discrete electron transfers, where one electron was transfered from Mn(IV) at first, involving the reduction of Mn(IV) to Mn(III), and then another one electron was transfered from either Mn(IV) or Mn(III) (Nesbitt et al., 1998). The formation of a Mn(III) intermediate could contribute to Mn-oxide passivation because Mn(III) sites are thought to be less reactive than Mn(IV) sites on the Mn-oxide surface (Chiu and Hering, 2000; Zhu et al., 2009; Lafferty et al., 2010a).

Fe(II) Oxidation by δ-MnO_2. Fe(II) can be readily oxidized by δ-MnO_2 at both pH 3 (Fig 2.3 a) and 6 (Fig 2.3 b), however, the reaction rate varies at different pHs. At pH 3, Fe(II) appears in the effluent after 0.5 h of the reaction, while at pH 6 Fe(II) appears after 8 h. The delayed appearance of Fe(II) indicates a faster oxidation rate at higher pH. Similar to As(III) oxidation, the oxidation of Fe(II) by δ-MnO_2 shows a two-phase trend, a fast initial oxidation followed by a decrease in oxidation rate, indicating passivation of δ-MnO_2 surface also exists during Fe(II) oxidation. The reaction of Fe(II) with Mn-oxides can result in the formation of solid $Fe(OH)_3$ and FeOOH (Postma and Appelo, 2000), and also release Mn(II) to solution. Therefore, the sorption of Mn(II) and the formation of Fe(III)-(hydr)oxides can both cause the surface passivation of δ-MnO_2 by blocking reactive sites on the δ-MnO_2 surface.

2.3.2 Oxidation of As(III) and Fe(II) Simultaneously by δ-MnO_2

In order to investigate the effects of Fe(II) on As(III) oxidation by δ-MnO_2, stirred-flow experiments were conducted using influent solutions containing 100 μmol/L As(III) and simultaneously adding 100, 200, or 1000 μmol/L Fe(II) to react with 2 g/L δ-MnO_2 at both pH 3 and 6. Due to the similarity of reactions at both pHs, results are shown only at pH 6.

Effects of Fe(II) on As(III) Oxidation. As(III) oxidation by δ-MnO_2 was strongly influenced by the addition of Fe(II) (Fig 2.4 and Fig 2.5 a). In the absence of Fe(II) (Fig 2.4 a), no As(III) appears in the effluent during the initial 8 hours, indicating that all As(III) introduced into the reactor is oxidized to As(V) or sorbed onto the δ-MnO_2 surface. In the presence of Fe(II), As(III) appears earlier in the effluent. Compared to 8 hours with no Fe(II) addition, As(III) appears after 2.3 hours with 100 μmol/L of Fe(II) addition (Fig 2.4 b), 0.8 hours with 200 μmol/L of Fe(II) addition (Fig 2.4 c), and As(III) appears almost immediately with 1000 μmol/L of Fe(II) addition (Fig 2.4 d). The higher the concentration of added Fe(II), the earlier the As(III) appears in the effluent, which suggests that the As(III) oxidation rate is lowered in the presence of Fe(II). This decreased As(III) oxidation rate could be explained by two reasons: (1) since δ-MnO_2 can also effectively oxidize Fe(II) (Fig 2.3), Fe(II) may compete with As(III) for oxidation by sorbing on some of the reactive sites on δ-MnO_2 surface, thus lowering the As(III) oxidation rate; (2) the reaction of Fe(II) and δ-MnO_2 could result in the formation of solid Fe(III)-(hydr)oxides (Postma and Appelo, 2000) on the δ-MnO_2 surface, blocking some of the reactive sites, therefore decreasing the As(III) oxidation rate. Furthermore, the finding that the final As(III) concentration in the effluent increases with increasing Fe(II) addition (Fig 2.5 a), except for the 1000 μmol/L Fe(II) addition, shows that less As(III) is oxidized by δ-MnO_2 in the presence of Fe(II). This also indicates the inhibitive impact that Fe(II) has on As(III) oxidation, either through competing with As(III) or the formation of sorbed Fe(III)-(hydr)oxides. Some previous studies also observed a decrease in As(III) oxidation rate by Mn-oxides when other ions were present. Power et al. (2005) confirmed competitive sorption of Zn(II) on birnessite

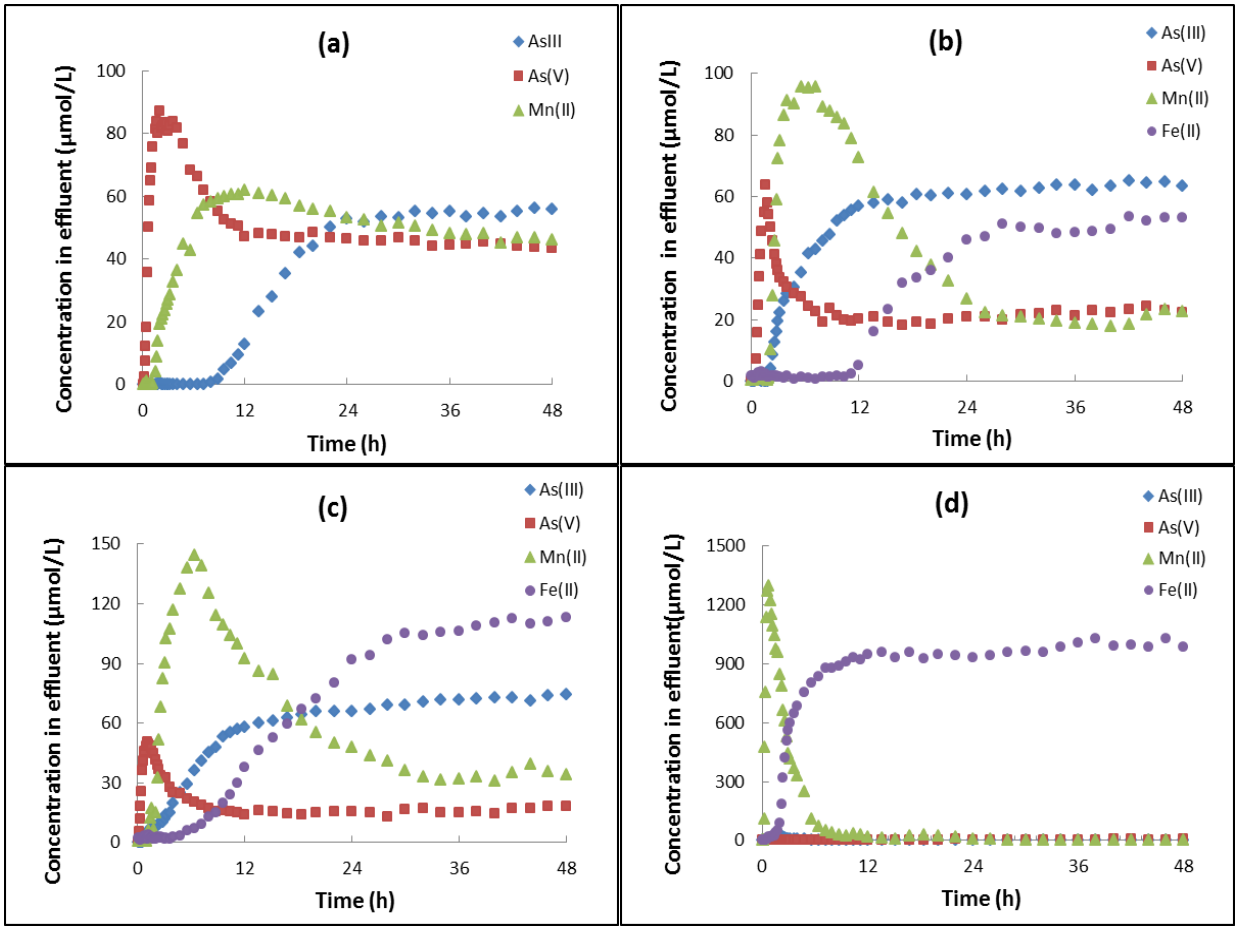

Figure 2.4 Concentrations (µmol/L) of As(III), As(V), Mn(II) and Fe(II) in the effluent of a stirred-flow experiment reacting 2g/L δ-MnO2 with simultaneously (a) 100 µmol/L As(III) and no Fe(II); (b) 100 µmol/L As(III) and 100 µmol/L Fe(II); (c) 100 µmol/L As(III) and 200 µmol/L Fe(II) and (d) 100 µmol/L As(III) and 1000 µmol/L Fe(II), at pH 6 for 48 hours.

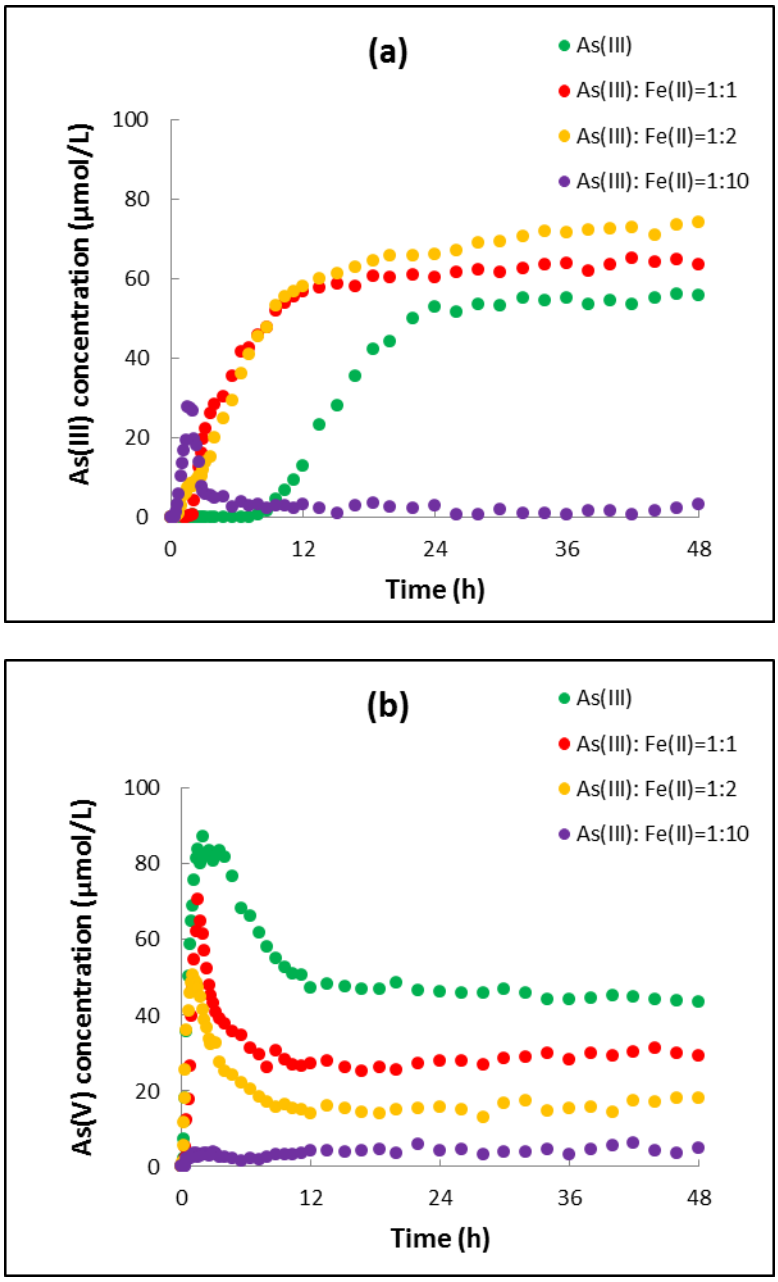

Figure 2.5 (a) As(III) and (b) As(V) concentrations in effluents of stirred-flow experiments reacting 2g/L δ-MnO_2 with 100 µmol/L As(III) and 0, 100, 200, or 1000 µmol/L Fe(II) simultaneously at pH 6 for 48 hours.

decreased the oxidation rate of As(III). Choi et al. (2009) assumed competition between Fe(II) and As(III) for sorption sites on manganese oxides further blocked the oxidation rate of As(III). Parikh et al. (2010) showed a reduced As(III) oxidation in the presence of phosphate (PO_4^{3-}) caused by competitive adsorption between As(III) and PO_4^{3-}. He also reported a decrease in As(III) oxidation when goethite (α-FeOOH) was present, resulting from the competition between δ-MnO_2 and α-FeOOH for As(III). Han et al. (2011) found that the removal rate of As(III) significantly decreased with an increasing ratio of Fe(II):As(III) from 1/64:1 to 1:1. He also pointed out that the presence of As(III) significantly inhibited the oxidation of Fe(II) by MnO_2 significantly as well.

Effects of Fe(II) on As Sequestration. The concentration of As(V) in the effluent decreases with increasing Fe(II) addition (Fig 2.5 b). This decreased As(V) concentration could be attributed to two reasons: (1) less As(V) is produced with Fe(II) addition; (2) more As(V) is sorbed with Fe(II) addition. The first reason is confirmed in the last section since less As(III) is oxidized as more Fe(II) added. The second reason can be proved by noting that the decrease in As(V) concentration in the effluent is more pronounced than the increase of As(III) concentration in the effluent (Fig 2.5 a). Also, we calculated the total As (both As(III) and As(V)) sorption amounts at different Fe(II) addition (Fig 2.6). The results show that as more Fe(II) is added, more As is sorbed on the solid phase due to more Fe(III)-(hydr)oxides being formed, providing additional sorption sites for both As(III) and As(V). He and Hering (2009) confirmed that As(III) and As(V) predominantly adsorbed on the freshly formed Fe(III) precipitates when Fe(II) is added in the presence of birnessite. Chio et al. (2009) also showed that in the presence of dissolved Fe(II), the precipitation of Fe(III)

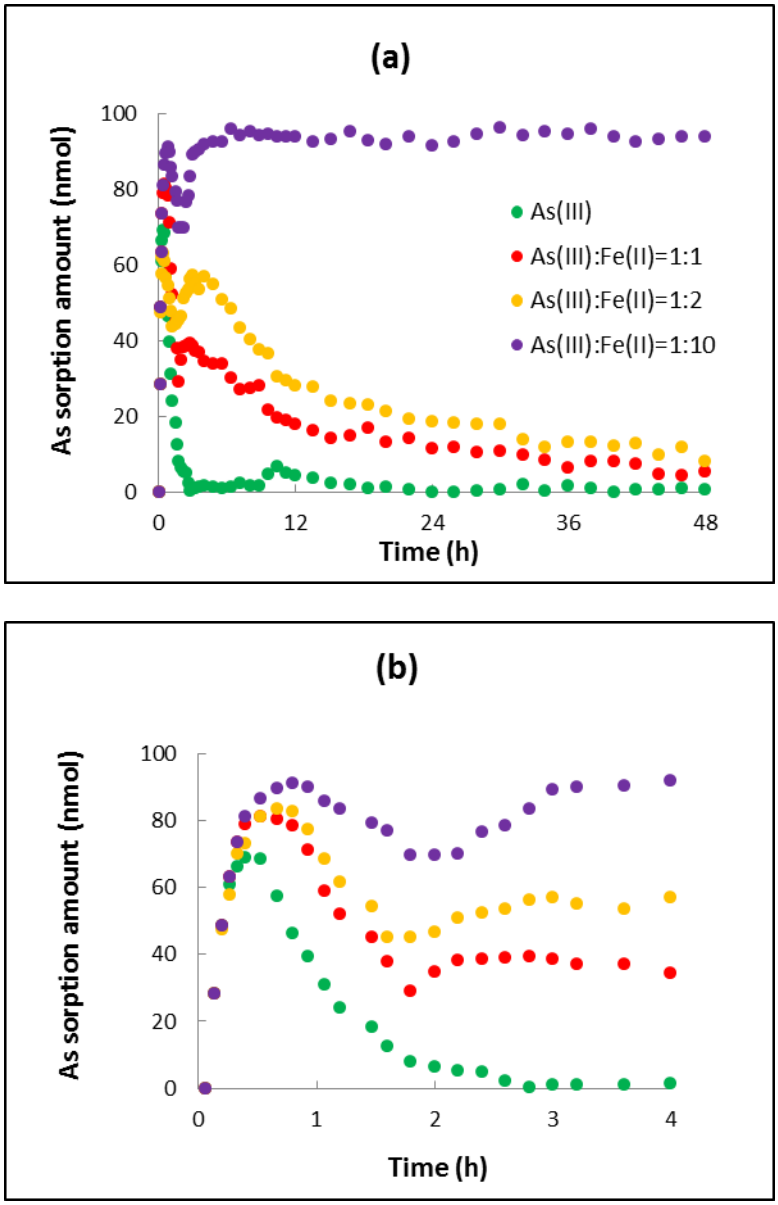

Figure 2.6 (a) Calculated amount of As sorption (nmol) in stirred-flow experiments where 2 g/L δ-MnO_2 was reacted with 100 µmol/L As(III) and 0, 100, 200, or 1000 µmol/L Fe(II) simultaneously at pH 6 for 48 hours; (b) Plot of (a) for the first 4 hours.

hydrous oxides was an effective mechanism for As scavenging from groundwater if there exists sufficient oxidants to oxidize Fe(II). In some environments, oxygen is available as the oxidant for Fe(II) and microbial mediation can be important in catalyzing this reaction (Roberts et al. 2004; Berg et al. 2006). Native manganese oxides in soils and sediments can also serve as the oxidants for Fe(II). This enhancement in Fe(II) oxidation could be an effective strategy for augmenting the natural attenuation of As.

Effects of Fe(II) on Mn(II) Sequestration. Apart from As(III) and As(V), we are also interested in the changes of Mn(II) concentration in the effluent. The Mn(II) concentration reaches a maximum after a few hours of reaction, and this maximum value increases as more Fe(II) is added to the system (Fig 2.4). After 24 hours, the concentration of Mn(II) remains stable, and the final concentration of Mn(II) in the effluent decreases with increasing Fe(II) addition. This suggests more Mn(II) is re-sorbed onto the newly formed Fe(III)-(hydr)oxides.

2.3.3 Oxidation of As(III) by δ-MnO_2 with Fe(II) Added at Different Times

In order to fully investigate the effects of Fe(II) on the As(III) oxidation by δ-MnO_2 over time, since the oxidation rate is decreasing as δ-MnO_2 becomes passivated, 100 μmol/L Fe(II) was introduced into the reaction of 100 μmol/L As(III) with 2 g/L δ-MnO_2 at different times (4, 10 and 24 hours) at pH 6. The reason why 4, 10 and 24 hours were chosen is that during the As(III) oxidation by δ-MnO_2 (Fig 2.2 b), maximum As(V) appeared at 4 hours, As(III) starts to appears in solution at about 10 hours, which is the changing point from rapid As(III) oxidation to a slower oxidation rate, and after 24 hours, the whole system reaches a steady state, where the change in concentration of As(III), As(V) and Mn(II) with time are negligible. The results show

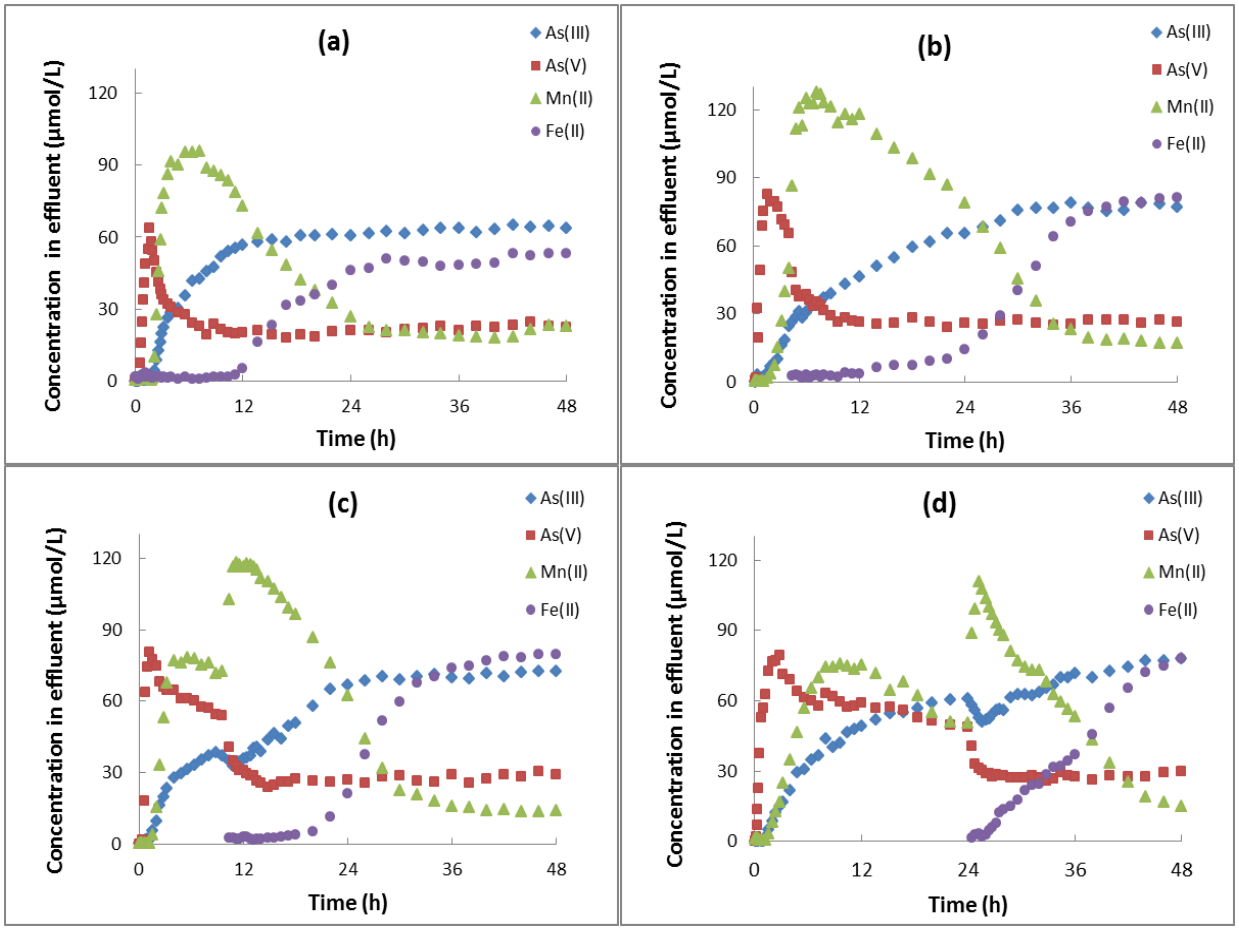

Figure 2.7 Concentrations (µmol/L) of As(III), As(V), Mn(II) and Fe(II) in the effluent from a stirred-flow experiment where 2g/L δ-MnO_2 reacts with 100 µmol/L As(III) first and then 100 µmol/L Fe(II) is added to the influent solution at (a) 0 hour (simultaneously); (b) 4 hours; (c) 10 hours and (d) 24 hours, at pH 6.

that immediately after Fe(II) is introduced to the system at each time point, there is a dramatic increase in Mn(II) as well as a marked drop in As(V) in the effluent (Fig 2.7 b, c and d). The boost in Mn(II) can be attributed to the readily oxidation of Fe(II) by δ-MnO_2, releasing a large amount of additional Mn(II) to the solution. The concentration jump in Mn(II) is about the same value (~ 40 μmol/L), regardless of when Fe(II) is added to the system. This is different from our expectation that as δ-MnO_2 becomes passivated with time, the oxidation rate of Fe(II) by δ-MnO_2 should decrease from 4 hours to 24 hours. Thus, the concentration jump of Mn(II) would be less pronounced at 24 hour compared to 10 or 4 hours. We have shown that the very initial oxidation rate of Fe(II) by δ-MnO_2 is independent of the surface passivation of δ-MnO_2 during As(III) oxidation, which suggests that the initial rapid Fe(II) oxidation might occur at certain reactive sites that are not blocked by the oxidation of As(III). The large drop in As(V) right after Fe(II) is added could be the result of the formation of Fe(III)-(hydr)oxides, which provides extra sorption sites for As(V). This result also confirms that the sorption of As(V) on the newly formed Fe(III)-(hydr)oxides takes place as soon as As(III) is oxidized to As(V). Interestingly, when Fe(II) is involved in the reaction, the concentration of As(III) in the effluent doesn't increase as expected, but rather As(III) decreases (not that obvious in Fig 2.7 b) and then increases. Once Fe(II) is added to the system, there are two contradictory effects on As(III). One is the competitive oxidation of Fe(II), which causes As(III) to increase; the other one is the sorption of As(III) on the newly formed Fe(III)-(hydr)oxides, resulting in a decrease in As(III). The decrease in As(III) concentration after Fe(II) is added could be the result of the sorption effect, which outcompetes the competitive effect.

2.3.4 Initial As(III) Oxidation Rate by δ-MnO_2 in the Presence of Fe(II)

In order to investigate how the initial As(III) oxidation rate changes when Fe(II) is present, batch kinetic experiments were conducted under different Fe(II) additions and the As(III) depletion rates were quantified (Fig 2.8). The oxidation of As(III) by δ-MnO2 proceeds very rapidly and follows first-order kinetics nicely (Fig 2.8). When no Fe(II) is present (Fig 2.8 a), As(III) concentration decreases to 60% of the initial value within 15 seconds and As(V) appears immediately in the solution after reaction starts. As(III) concentration continues to decrease while As(V) increases over the course of 30 minutes reaction. Similar to many environmental redox reactions, this reaction exhibits biphasic kinetics. The depletion of As(III) is fast in the first couple of minutes and then slows down after 5 minutes. Therefore, two sets of apparent first-order rate constants were calculated using data from either the initial (0 to 60 second, shown in Fig 2.8) or final (10 to 30 minute) portion of the reaction. Under all reaction conditions, the rate constants after 10 minutes are approximately 1/10 of the rate constants within 1 minute as a result of surface passivation of δ-MnO2 (Table 2.1).

As discussed in the previous sections, when Fe(II) is present, the depletion of As(III) in solution could be ascribed to two factors. First, As(III) is oxidized by δ-MnO_2 to As(V). Second, As(III) is sorbed on the produced Fe(III)-(hydr)oxide products as Fe(II) is oxidized by δ-MnO_2. In order to differentiate the two effects, batch kinetic experiments were performed in two background electrolyte solutions, $NaNO_3$ and NaF. For reactions in the $NaNO_3$ solutions, the As(III) depletion rate can be considered as the summation of As(III) oxidation by δ-MnO_2 and As(III) sorption by the Fe(III)-(hydr)oxides products. For reactions in NaF solutions, the As(III)

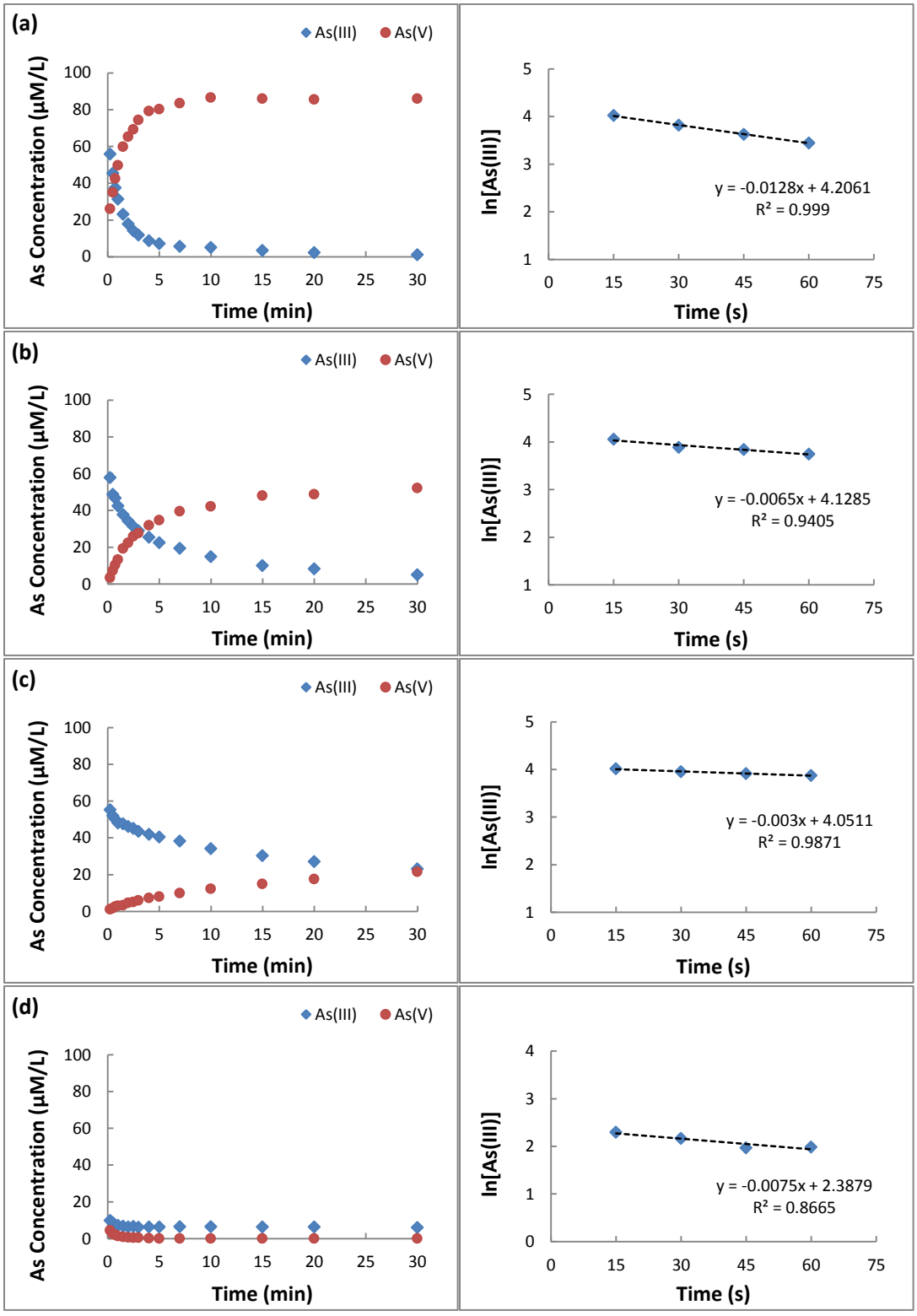
(a)
As(III)
As(V)
As Concentration (µM/L)
Time (min)
ln[As(III)]
y = -0.0128x + 4.2061
R² = 0.999
Time (s)
(b)
As(III)
As(V)
As Concentration (µM/L)
Time (min)
ln[As(III)]
y = -0.0065x + 4.1285
R² = 0.9405
Time (s)
(c)
As(III)
As(V)
As Concentration (µM/L)
Time (min)
ln[As(III)]
y = -0.003x + 4.0511
R² = 0.9871
Time (s)
(d)
As(III)
As(V)
As Concentration (µM/L)
Time (min)
ln[As(III)]
y = -0.0075x + 2.3879
R² = 0.8665
Time (s)

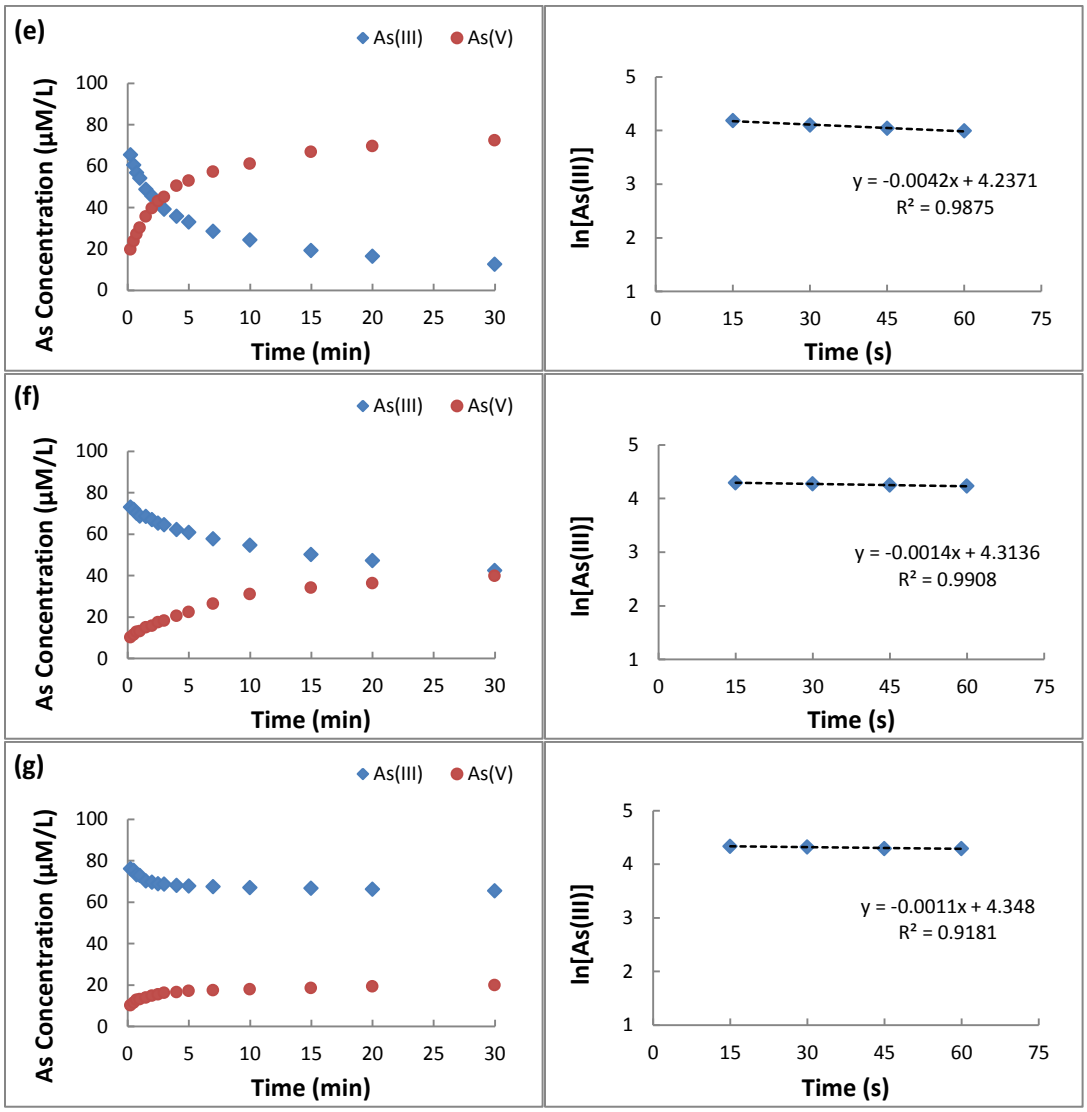

Figure 2.8 Concentrations (µmol/L) of As(III) and As(V) determined from batch kinetic experiments, reacting 0.1 g/L δ-MnO_2 with (a) 100 µmol/L As(III); (b) 100 µmol/L As(III) and 100 µmol/L Fe(II); (c) 100 µmol/L As(III) and 200 µmol/L Fe(II); (d) 100 µmol/L As(III) and 1000 µmol/L Fe(II); (e) 100 µmol/L As(III) and 100 µmol/L Fe(II); (f) 100 µmol/L As(III) and 200 µmol/L Fe(II); (g) 100 µmol/L As(III) and 1000 µmol/L Fe(II), at pH 6. Reactions (a), (b), (c) and (d) were conducted in 0.01 mol/L $NaNO_3$ background electrolyte, while reactions (e), (f) and (g) were conducted in 0.01 mol/L NaF background electrolyte. Plots to the right are the corresponding first-order As(III) depletion rates within 60 seconds.

depletion is due only to As(III) oxidation by δ-MnO_2, since F^- would complex with the produced Fe^{3+} to form soluble FeF_6^{3-} in solution, and thus prevent the formation of Fe(III)-(hydr)oxides. The initial As(III) oxidation rate by δ-MnO_2 decreases when Fe(II) is added to the system and the more Fe(II) that is added, the slower the As(III) oxidation rate (Table 2.1, reaction a, e,f and g). This result proves the competitive oxidation between As(III) and Fe(II), which also agrees with the results from the stirred-flow experiments. The As(III) depletion rates of reactions in $NaNO_3$ solutions are higher than those of reactions in NaF solutions (Table 2.1, reaction b vs. e, c vs. f and d vs. g), indicating that some amount of As(III) is sorbed by the produced Fe(III)-(hydr)oxides. This effect is even more obvious at the highest Fe(II) concentration (Table 2.1, reaction d vs. g) and is also shown in Figure 2.8 d, where both As(III) and As(V) concentrations are much lower than those in Figure 2.8 g.

Table 2.1 Apparent first-order rate constants of As(III) depletion, determined by linear regression analysis of data from batch kinetic experiments. All reactions were conducted at pH 6 with 0.1 g/L δ-MnO_2 and 0.01 mol/L $NaNO_3$ or NaF.

Reaction Conditions	≤ 1 min		≥ 10 min	
	k (s^{-1})	R^2	k (s^{-1})	R^2
a. 100 μmol/L As(III), $NaNO_3$	1.3×10^{-2}	1.00	1.3×10^{-3}	1.00
b. 100 μmol/L As(III) + 100 μmol/L Fe(II), $NaNO_3$	6.5×10^{-3}	0.94	9.0×10^{-4}	0.99
c. 100 μmol/L As(III) + 200 μmol/L Fe(II), $NaNO_3$	3.0×10^{-3}	0.99	3.0×10^{-4}	0.99
d. 100 μmol/L As(III) + 1000 μmol/L Fe(II), $NaNO_3$	7.5×10^{-3}	0.87	5.0×10^{-5}	0.83
e. 100 μmol/L As(III) + 100 μmol/L Fe(II), NaF	4.2×10^{-3}	0.99	5.0×10^{-4}	0.98
f. 100 μmol/L As(III) + 200 μmol/L Fe(II), NaF	1.4×10^{-3}	0.99	2.0×10^{-4}	0.99
g. 100 μmol/L As(III) + 1000 μmol/L Fe(II), NaF	1.1×10^{-3}	0.92	2.0×10^{-5}	1.00

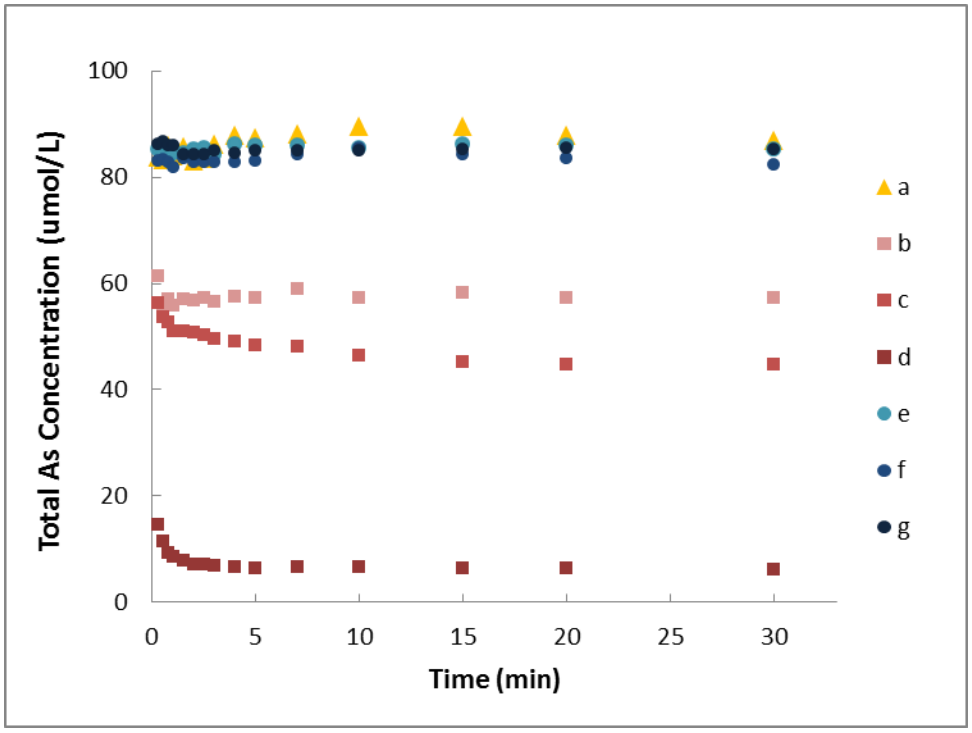

Figure 2.9 Concentrations (μmol/L) of total As, As(III) plus As(V), determined from batch kinetic experiments, reacting 0.1 g/L δ-MnO_2 with (a) 100 μmol/L As(III); (b) 100 μmol/L As(III) and 100 μmol/L Fe(II); (c) 100 μmol/L As(III) and 200 μmol/L Fe(II); (d) 100 μmol/L As(III) and 1000 μmol/L Fe(II); (e) 100 μmol/L As(III) and 100 μmol/L Fe(II); (f) 100 μmol/L As(III) and 200 μmol/L Fe(II); (g) 100 μmol/L As(III) and 1000 μmol/L Fe(II), at pH 6. Reactions (a), (b), (c) and (d) were conducted in 0.01 mol/L $NaNO_3$ background electrolyte, while reactions (e), (f) and (g) were conducted in 0.01 mol/L NaF background electrolyte.

Total As concentration is also observed during the reaction (Fig 2.9). When Fe(II) is absent (Fig 2.9, set a), total As concentration is quite constant over the course of the reaction, however, total As concentration (about 85 μmol/L) is lower than the initial value of 100 μmol/L. This might be the reason that some As is sorbed on δ-MnO_2. For reactions in NaF solutions (Fig 2.9, set e, f and g), since there is no

formation of Fe(III)-(hydr)oxides, total As concentration doesn't change with Fe(II) addition. For reactions in $NaNO_3$ solutions (Fig 2.9, set b, c and d), total As concentration decreases over the course of reaction as more Fe(III)-(hydr)oxides are formed. Also, the more Fe(II) that is added, the lower the total As concentration in solution, suggesting that the newly formed Fe(III)-(hydr)oxides provide additional sorption sites for both As(III) and As(V). The results are consistent with our stirred-flow experiments as well as some previous studies (He and Hering, 2009; Chio et al. 2009).

2.4 Conclusions

The oxidation of As(III) via Mn-oxides is an important process for natural As cycling and for developing in situ strategies for remediation of As-contaminated waters and soils. The present study shows that both As(III) and Fe(II) can be efficiently oxidized by δ-MnO_2. Both oxidation reactions are rapid initially, followed by a decrease in oxidation rates as a result of the surface passivation of δ-MnO_2. As(III) oxidation is inhibited in the presence of Fe(II), due to both the competitive oxidation of Fe(II) and the formation of Fe(III)-(hydr)oxides on the δ-MnO_2 surface. The Fe(III) precipitate products also play an important role in the sorption of As(III) and As(V). As the amount of added Fe(II) (simultaneously) increased, less As(III) is oxidized, but the total sorption of both As(III) and As(V) increases as well as more sorption of Mn(II). These results demonstrate a possible remediation strategy for increasing As removal through addition of Mn-oxides and Fe(II) (or Fe-oxides) to As contaminated waters and soils.

REFERENCES

Berg, M. M., Luzi, S., Trang, P. T. K., Viet, P. H., Giger, W., Stuben, D. 2006. Arsenic removal from groun dwater by household sand filters: Comparative field study, model calculations, and health benefits. Environmental Science and Technology, 40: 5567-5573.

Chiu, V. Q., and Hering, J. G. 2000. Arsenic adsorption and oxidation at manganite surfaces. 1. Method for simultaneous determination of adsorbed and dissolved arsenic species. Environ. Sci. Technol. 34: 2029–2034.

Choi, S., Day, P. A., Hering, J. G. 2009. Natural attenuation of arsenic by sediment sorption and oxidation, Environ. Sci. Technol. 43:4253-4259.

Dixit, S., and J.G. Hering. 2003. Comparison of arsenic(V) and arsenic(III) sorption onto iron oxide minerals: Implications for arsenic mobility. Environ. Sci. Technol. 37:4182-4189.

Drits, V.A., E. Silvester, A.I. Gorshkov, and A. Manceau. 1997. Structure of synthetic monoclinic Na -rich birnessite and hexagonal birnessite. 1. Results from X – ray diffraction and selected-area electron diffraction. Am. Mineral. 82: 946 - 961.

Eary, L. E., and Schramke, J. A. 1990. Rates of inorganic oxidation reactions involving dissolved oxygen. In Chemical Modeling in Aqueous Systems II, vol. 416 (eds. D. C. Melchior and R. L. Bassett). ACS Symposium Series, American Chemical Society, Washington, DC, pp. 379–396.

Ginder-Vogel, M., G. Landrot, J. S. Fischel, and D. L. Sparks. 2009. Quantification of rapid environmental redox processes with quick-scanning x-ray absorption spectroscopy (Q-XAS). PNAS 106 (38): 16124–16128.

Han, X., Li, Y. L., Gu, J. D. 2011. Oxidation of As(III) by MnO2 in the absence and presence of Fe(II) under acidic aonditions, Geochimica et Cosmochimica Acta. 75:368-379.

He, Y. T., Hering, J. G. 2009. Enhancement of arsenic(III) sequestration by manganese oxides in the presence of iron(II), Water, Air, Soil Pollut. 203:359-368.

Herbel, M. and Fendorf , S. 2006. Biogeochemical processes controlling the speciation and transport of arsenic within iron coated sands. Chem. Geol. 228: 16–32.

Jiang J., Bauer I., Paul A. and Kappler A. 2009 Arsenic redox changes by microbially and chemically formed semiquinone radicals and hydroquinones in a humic substance model quinone. Environ. Sci. Technol. 43: 3639–3645.

Lafferty, B., M. Ginder-Vogel and D.L. Sparks. 2010 a. Arsenite oxidation by a poorly crystalline manganese-oxide 1. Stirred-flow experiments. Environ. Sci. Technol. 44:8460-8466.

Manning, B.A., Fendorf, S.E., Bostick, B., Suarez, D.L. 2002. Arsenic(III) oxidation and arsenic(V) adsorption reactions on synthetic birnessite. Environ. Sci. Technol. 36:976-981.

Morgan, J.J., and W. Stumm. 1964. Colloid-chemical properties of manganese dioxide. J. Colloid Sci. 19:347-359.

Nesbitt, H.W., G.W. Canning, and G.M. Bancroft. 1998. XPS study of reductive dissolution of 7 angstrom-birnessite by H3AsO3, with constraints on reaction mechanism. Geochim. Cosmochim. Ac. 62:2097-2110.

Nickson, R., McArthur, J., Burgess, W., Ahmed, K. M., Ravenscroft, P. and Rahman, M. 1998. Arsenic poisoning of Bangladesh groundwater. Nature. 395: 338.

Nickson, N. T., M cArthur, J. M., Ravenscroft, P., Burgess, W. G., Ahmed, K. M. 2000. Mechanism of arsenic release to groundwater, Bangladesh and West Bengal. Applied Geochemistry, 15: 403–413.

Oscarson, D. W., Huang, P. M., Liaw, W. K., and Hammer, U. T. 1983. Kinetics of oxidation of arsenite by various manganese dioxides. Soil Sci. Soc. Am. J. 47: 644–648.

Paktunc, D., Dutrizac J., and Gertsman, V. 2008. Synthesis and phase transformations involving scorodite, ferric arsenate and arsenical ferrihydrite: implications for arsenic mobility. Geo-chim. Cosmochim. Acta72: 2649–2672.

Parikh, S.J., B.J. Lafferty, and D.L. Sparks. 2008. An ATR -FTIR spectroscopic approach for measuring rapid kinetics at the mineral/water interface. J. Colloid Interface Sci. 320:177.

Parikh, S.J., B. J. Lafferty, T. G. Meade and D.L. Sparks. 2010. Evaluating environmental influences on AsIII oxidation kinetics by a poorly crystalline Mn-oxide. Environ. Sci. Technol. 44: 3772-3778.

Post, J.E. 1999. Manganese oxide minerals: Crystal structures and economic and environmental significance. Proc. Natl. Acad. Sci. 96:3447 -3454.

Postma, D., and Appelo, C. A. J. (2000) Reduction of Mn-oxides by ferrous iron in a flow system: column experiment and reactive transport modeling. Geochim. Cosmochim. Acta 64: 1237–1247.

Power, L. E., Arai, Y., and Sparks, D. L. 2005. Zinc adsorption effects on arsenite oxidation kinetics at the birnessite–water interface. Environ. Sci. Technol. 39: 181–187.

Roberts, L. C., Hug, S. J., Ruettimann, T., Billah, M. M., Khan, A. W., Rahman, M. T. 2004. Arsenic removal with Iron(II) and Iron(III) in waters with high silicate and phosphate concentrations. Environmental Science and Technology, 38: 307–315.

Scott, M.J., and J.J. Morgan. 1995. Reactions at Oxide Surfaces. 1. Oxidation of As(III) by Synthetic Birnessite. Environm ental Science & Technology 29:1898-1905.

Shiller, A.M., and T.H. Stephens. 2005. Microbial manganese oxidation in the lower Mississippi river: methods and evidence. Geomicrobiol. J. 22:117 -125.

Silvester, E., A. Manceau, and V.A. Drits. 1997. Structure of synthetic monoclinic Na-rich birnessite and hexagonal birnessite. 2. Results from chemical studies and EXAFS spectroscopy. Am. Mineral. 82: 962-978.

Strawn, D. G. and D. L. Sparks. 2000. Effects of soil organic matter on the kinetics and mechanisms of Pb(II) sorption and desorption in the soil. Soil Sci. Soc. Am. J. 64: 144-156.

Stookey, L.L. 1970. Ferrozine – a new spectrophotometric reagent for iron. Anal. Chem. 42: 779–781.

Swartz, C . H ., Blute, N. K., Badru zzman, B., Ali, A., Brabander, D., Jay, J. B. 2004. Mobility of arsenic in a Bangladesh aquifer: inferences from geochemical profiles, leaching data, and mineralogical characterization. Geochemical et Cosmochimica Acta, 68: 4539 – 4557.

Tebo, B.M., J.R. Bargar, B.G. Clement, G.J. Dick, K.J. Murray, D. Parker, R. Verity, and S.M. Webb. 2004. Biogenic manganese oxides: Properties and mechanisms of formation. Ann. Rev. Earth and Plan. Sci. 32: 287 -328.

Tournassat, C., Charlet, L., Bosbach, D. and Manceau, A. 2002. Arsenic(III) oxidation by birnessite and precipitation of man-ganese(II) arsenate. Environ. Sci. Technol. 36, 493–500.

Villalobos, M., B. Toner, J. Bargar, and G. Sposito. 2003. Characterization of the manganese oxide produced by Pseudomonas putida strain MnB1. Geochim. Cosmochim. Acta 67:2649 -2662.

Wang J. W., Bejan D. and Bunce N. J. 2003. Removal of arsenic from synthetic acid mine drainage by electrochemical pH adjustment and coprecipitation with iron hydroxide.Environ. Sci. Technol. 37: 4500–4506.

Wielinga, B., M.M. Mizuba, C.M. Hansel, and S. Fendorf. 2001. Iron promoted reduction of chromat e by dissimilatory iron reducing bacteria. Environ. Sci. Technol. 35: 522-527.

Yang, J., Barnett, M. O., Zhuang, J., Fendorf, S. E., and Jardine, P. M. 2005. Adsorption, oxidation, and bioaccessibility of As(III) in soils. Environmental Science & Technology, 39: 7102 –7110.

Zhu, M., K. W. Paul, J. D. Kubicki and D.L. Sparks. 2009. Quantum chemical study of arsenic (III, V) adsorption on Mn-oxides: Implications for arsenic(III) oxidation. Environ. Sci. Technol. 43: 6655–6661.

Chapter 3

THE EFFECTS OF IRON(II) ON ARSENIC OXIDATION AND SORPTION ON MANGANESE OXIDES: RESULTS FROM SPECTROSCOPY STUDIES

ABSTRACT

The redox state and speciation of metalloid arsenic (As) determine its toxicity and mobility. Knowledge of biogeochemical processes influencing the As redox state is therefore necessary to understand and predict its environmental behavior. Many previous studies examined As(III) oxidation by various Mn-oxides, but few were focused on the environmental influences (e.g. co-existing ions) on such process. Here we investigated the mechanisms of As(III) oxidation by a poorly crystalline hexagonal birnessite (δ-MnO_2) in the presence of Fe(II) using X-ray absorption spectroscopy (XAS), Mössbauer spectroscopy and transmission electron microscopy coupled with energy-dispersive X-ray spectroscopy (TEM-EDS). As K-edge XANES analysis revealed that at low Fe(II) concentration, As(V) was the predominant As species on the solid phase, while at high Fe(II) concentration, both As(III) and As(V) were sorbed on the solid phase. As K-edge EXAFS analysis showed an increasing As-Mn/Fe distance over time, indicating As prefers to bind with the newly formed Fe(III)-(hydr)oxides. As adsorbed on Fe(III)-(hydr)oxides as a bidentate binuclear corner-sharing complex. Both Mössbauer and TEM-EDS study demonstrated that the Fe(III)-(hydr)oxides formed during Fe(II) oxidation by δ-MnO_2 were predominantly

ferrihydrite and goethite. However, Fe EXAFS analysis also suggested the formation of a small amount of lepidocrocite. The Mn K-edge XANES data indicated that As(III) and Fe(II) oxidation occurs as a two electron transfer with δ-MnO_2 and the observed Mn(III) is due to conproportionation of sorbed Mn(II) with Mn(IV) on δ-MnO_2. This study reveals that the mechanisms of As(III) oxidation by δ-MnO_2 in the presence of Fe(II) are very complex, involving many simultaneous reactions, and the formation of Fe(III)-(hydr)oxides plays a very important role in reducing As mobility.

3.1 Introduction

Arsenic (As) is a toxic element, which is widespread in soils and groundwater as a result of human activities and natural geologic occurrence (Nordstrom, 2002; Frankenberger, 2002). The maximum As concentration level in drinking water is set at 10 ppb by both the U.S. Environmental Protection Agency (EPA) and the World Health Organization (WHO) (Mohan and Pittman, 2007). The fate and transport of As in the environment are greatly dependent on speciation and sorption to minerals. Under most natural conditions, As is primarily present in inorganic forms and exists in two predominant species: arsenate (As(V)) and arsenite (As(III)), with As(III) being more toxic, soluble and mobile than As(V). Hence, the transformation of As(III) to As(V) is essential in both the natural cycling of As and in developing remediation technologies for As removal from water and soils.

Manganese (Mn) oxide minerals have important environmental chemistry applications, for they readily oxidize many reduced toxic metals, such as As(III) (Manning et al., 2002; Tournassat et al., 2002; Lafferty et al., 2010 a and b). The mechanisms of As(III) oxidation by Mn-oxides can be quite complex, involving

several reactions simultaneously. For example, As(III) oxidation by birnessite (MnO_2) produces As(V) and Mn(II), and then both As(V) and Mn(II) can be adsorbed by MnO_2. A previous study by Manning et al. (2002), using extended X-ray absorption fine structure (EXAFS) spectroscopy, showed that the As(V)-MnO_2 complex formed after As(III) oxidation was a bidentate binuclear corner-sharing (bridged) complex occurring at MnO_2 edges and interlayer domains, with a coordination number near 2 and an As(V)–Mn interatomic distance of 3.22 Å. A study by Foster et al. (2003) also confirmed a As(V)–Mn bidentate binuclear adsorption complex but with a shorter distance at 3.16 Å. A more recent study by Lafferty et al. (2010b) found a possible monodentate mononuclear As(V)-Mn complex with a As(V)–Mn interatomic distance of 3.48 Å, in addition to the bidentate binuclear As(V)-Mn complex. They also showed that the binding complex between As(V) and MnO_2 changed with time as the As(III) oxidation proceeded.

However, in natural systems, As never exists alone. As is often associated with iron (Fe) oxides and, hence, can be mobilized by the reductive dissolution of the carrier phases (Herbel and Fendorf, 2006; He and Hering, 2009). Therefore, the co-occurrence of elevated concentrations of As and Fe(II) are often observed under moderately reducing conditions (Nickson et al., 2000; Swartz et al., 2004). Mn-oxides are also effective oxidants for Fe(II) and the reaction with Mn-oxides results in the formation of secondary solid Fe(III)-(hydr)oxides. Thus, the transformation reactions of As(III) to As(V) by Mn-oxides and the resulting sorption of As might be altered due to the presence of Fe(II). Previous studies showed that As was strongly sorbed by Fe-oxides and hydroxides such as ferrihydrite, goethite, lepidocrocite, maghemite, and hematite (Waychunas et al., 1993 and 1995; Fendorf et al., 1997; Jain et al., 1999;

Sherman and Rondall, 2003; Georges et al., 2005). Based on EXAFS spectroscopy, Waychunas et al. (1993) found the dominate As-Fe complex on goethite was a bidentate binuclear corner-sharing complex, yielding an As-Fe distance near 3.26 Å. Fendorf et al. (1997) interpreted their EXAFS data as indicating three surface As-Fe complexes: a monodentate mononuclear corner sharing complex with an As-Fe distance of 3.6 Å, a bidentate binuclear corner-sharing complex with two As-Fe distances near 3.25 Å and a bidentate mononuclear edge-sharing complex with a single As-Fe distance of 2.83 ~ 2.85 Å. Fendorf et al. (1997) proposed that the relative importance of each complex depended on the degree of surface loading. Farquhar et al. (2002) obtained EXAFS data for As(V) sorption on goethite and lepidocrocite and found peaks near 2.93 Å and 3.30 ~ 3.31 Å, which were attributed to bidentate mononuclear and bidentate binuclear complexes, respectively.

In the previous study (Chapter 2), As(III) oxidation and As sorption by a synthetic poorly crystalline Mn-oxide (δ-MnO_2) in the absence and presence of Fe(II) were investigated using stirred-flow experiments. The results showed a decrease in As(III) oxidation but an increase in As sorption. In this study, the solid phases taken from stirred-flow experiments were analyzed using X-ray Absorption Spectroscopy (XAS). The aim of this study is to: (1) determine the As speciation on solid phases; (2) characterize As(III) oxidation and As binding mechanisms by δ-MnO_2 in the presence of Fe(II); and (3) identify the composition of Fe(III)-(hydr)oxides that formed during Fe(II) oxidation by δ-MnO_2. Understanding the mechanisms of As(III) oxidation by Mn-oxides as influenced by Fe(II) and the sorption of As onto solid phases at the molecular level are of critical importance in predicting the fate and transport of As in the environment.

3.2 Methods and Materials

3.2.1 Chemicals

All chemicals used in this study met or exceeded American Chemical Society standards. 18.2 MΩ deionized (DI) water was used for all solutions. $NaAsO_2$ and $FeSO_4 \cdot 7H_2O$ were used as sources of As(III) and Fe(II), respectively. As(III) stock solution (100 mmol/L) was stored at 4 ℃ and prepared every month. Fe(II) solution was freshly prepared every time in the glove box and the DI water used to make the Fe(II) solution was degased, using nitrogen gas, for 2 hours before use.

3.2.2 Synthesis of Minerals

δ-MnO_2, a poorly-crystalline, phyllomanganate, was used in the studies presented here because of its high reactivity as well as its similarities to biogenic Mn-oxides (Villalobos et al., 2003). δ-MnO_2 is a form of hexagonal birnessite with a low degree of stacking of phyllomanganate sheets (Drits et al., 1997; Silvester et al., 1997). δ-MnO_2 was synthesized by drop wise addition of a 100 mL solution containing 11.29 g $Mn(NO_3)_2 \cdot 4H_2O$ to a 100 mL solution containing 2.4 g NaOH and 4.74 g KMnO4, corresponding to a final Mn(II):Mn(VII):OH ratio of 3:2:4 (Morgan and Stumm, 1964). After adding Mn(II) to the basic permanganate solution, the resulting suspension was stirred overnight (at least 12 hours) to allow complete conproportionation of Mn(II) and Mn(VII) to Mn(IV). Following synthesis, δ-MnO_2 was centrifuged at 10,000 RCF for 15 min, then the supernatant was removed and replaced with 18.2 MΩ deionized (DI) water. This wash step was repeated 6 times. Following washing, δ-MnO_2 was transferred to a polypropylene bottle, resuspended in DI water, and stored at 4 ℃ prior to use in experiments. Experiments were conducted

using δ-MnO_2 within a month of synthesis. Characterization of synthetic δ-MnO_2 is provided in Appendix A.

Two-line ferrihydrite was synthesized using a procedure adapted from Schwertmann and Cornell (1991). Ferric sulfate, $Fe_2(SO_4)_3$ $5H_2O$, was used as the source of the ferric ion. Briefly, the Fe(III) solution was prepared by dissolving $Fe_2(SO_4)_3$ $5H_2O$ in deionized water. The pH of the solution was raised to ~7.5 in about 5 min using a 1M NaOH solution and maintained at that pH for 1 h with the slurry vigorously agitated. The solid was washed five times with deionized water and then freeze dried.

Ferric arsenate ($FeAsO_4$ ·4-$7H_2O$) was synthetized using the method described by Jia et al. (2006). Briefly, a mixture of 0.02 M As(V) (Na_2HAsO_4 ·$7H_2O$) and 0.02 M Fe(III) ($Fe_2(SO_4)_3$ $5H_2O$) was adjusted from an initial pH 1.3 to pH 1.8 with 1M NaOH solution and maintained at that pH for 1 h. The solid product was then separated by filtration, washed with deionized water and freeze dried.

3.2.3 XAS Analysis

Sample Preparation. As(III) oxidation on δ-MnO_2 in the presence of Fe(III) was investigated using the same stirred-flow protocol and reaction conditions described in Chapter 3. In order to monitor changes occurring in the solid phase during As(III) oxidation on δ-MnO_2 in the presence of Fe(II), the reaction was stopped and the solid phase collected for analysis after 0.5, 4, 10, 24, and 48 h of reaction (Fig 3.1). During As(III) oxidation by δ-MnO_2 in the presence of Fe(II), As sorption was greatest at 0.5 hours, while maximum As(V) appeared in the effluent after 4 hours of reaction. Fe(II) appeared in the effluent at 10 hours; at 24 hours, the whole system reached a steady state, where the change in concentration of As(III), As(V), Fe(II) and

Mn(II) with time was negligible. At 48 hours, the stirred-flow reaction process was stopped. To stop the reaction, influent solution was removed, and the suspension in the reaction chamber was immediately filtered (0.22 μm) to remove any background electrolyte, Mn(II), Fe(II) and As not bound to δ-MnO_2. After filtration, the residual wet paste was immediately covered by Kapton tape and stored under anoxic conditions for less than 3 days prior to spectroscopic analysis.

To monitor changes occurring in the solid phase during As(III) oxidation by δ-MnO_2 under different addition amounts of added Fe(II), solid phases were collected at 48 hours after reacting 2g/L δ-MnO_2 with 100 μmol/L As(III) and simultaneously, 0, 100, 200, or 1000 μmol/L Fe(II) at pH 6. To stop the reaction, influent solution was removed, and the suspension in the reaction chamber was immediately filtered (0.22 μm) to remove any background electrolyte, and Mn(II), Fe(II) and As not bound to δ-MnO_2. After filtration, the residual wet paste was immediately covered with Kapton tape and stored under anoxic conditions for less than 3 days prior to spectroscopic analysis.

An As(V)-δ-MnO_2 sorption standard was prepared by reacting 100 μmol/L As(V) with 2 g/L δ-MnO_2 at pH 6 for 48 h in the same background electrolyte used in the stirred-flow reactions. As(V)- and As(III)-ferrihydrite sorption standards were prepared by reacting 100 μmol/L As(V) and 100 μmol/L As(III), respectively, with 2 g/L ferrihydrite at pH 6 for 48 h in the same background electrolyte used in the stirred-flow studies. An Fe(II)-δ-MnO_2 standard was prepared by reacting 100 μmol/L Fe(II) with 2 g/L δ-MnO_2 at pH 6 for 48 h in the same background electrolyte used in the stirred-flow studies. All standards were filtered, and the residual wet paste was immediately covered with Kapton tape and stored under anoxic conditions, for less

than 3 days before spectroscopic analysis.

Data Collection. Extended X-ray absorption fine structure (EXAFS) and X-ray absorption near edge (XANES) spectroscopic data for the stirred-flow samples were collected at beamline 4-1 and beamline 4-3 at the Stanford Synchrotron Radiation Lightsource (SSRL). The electron storage ring operates at 3.0 GeV with a current ranging from 100 to 90 mA. The monochromator consisted of two parallel Si-(220) crystals with a vertical entrance slit separation of 0.5 mm. As (11.9 keV), Mn

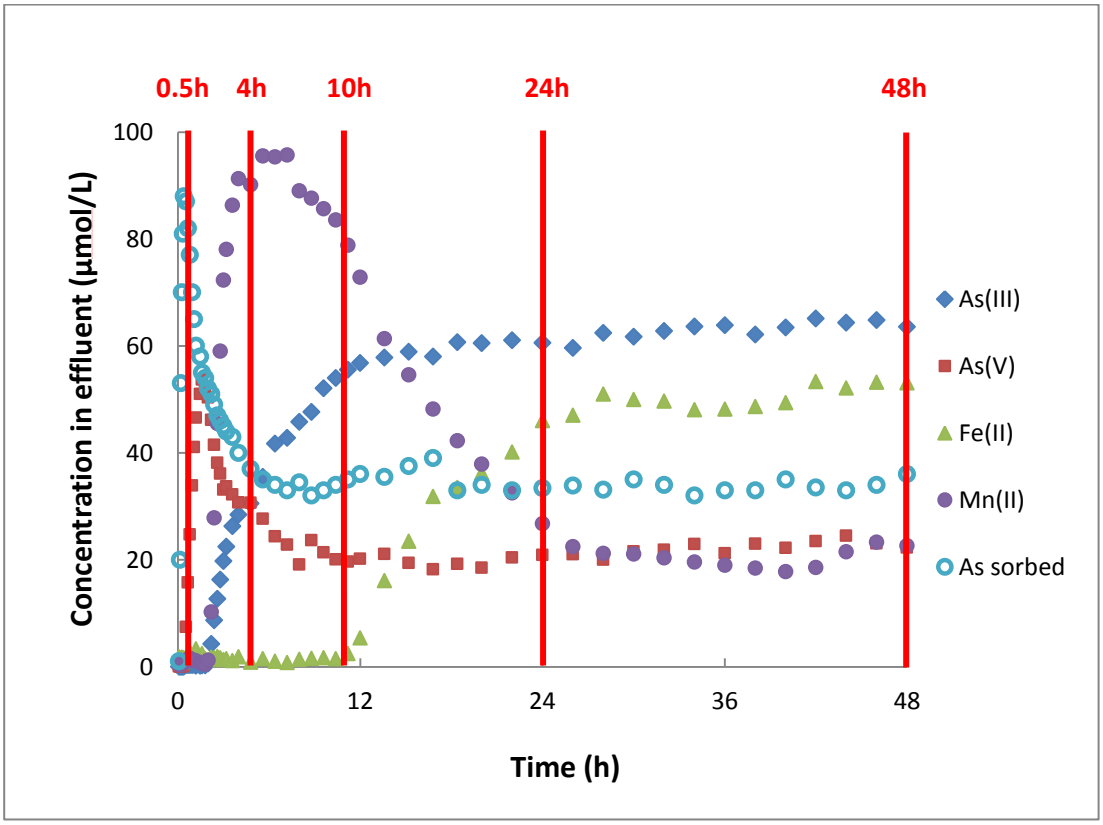

Figure 3.1 Vertical lines represent five stirred-flow reaction points of As(III) oxidation by δ-MnO_2 in the presence of Fe(II) (2 g/L δ-MnO_2 reacted with 100 µmol/L As(III) and 100 µmol/L Fe(II) at pH 6). Each reaction was stopped at the time indicated at the top of the graph (0.5, 4, 10, 24, 48 hours), at which point all remaining solid was collected for spectroscopic analysis.

(6.5 keV) and Fe (7.1 keV) K-edge EXAFS/XANES spectra were collected. All samples were oriented at 45 °to the incident beam and a Lytle detector was used to collect As, Fe and Mn spectra in fluorescence mode. The monochromator crystals were detuned by 30 % for As, 40 % for Fe and 50% for Mn in I_0 to reject higher order harmonics. A 3-path length germanium (Ge) filter for As or Mn filter for Fe or chromium (Cr) filter for Mn, and Sollier slits were used for signal optimization and removal of elastically scattered radiation. The monochromator angle was calibrated to the As(V) K-edge (11.874 keV) using diluted $Na_2HAs^VO_4$ as a standard (10% $Na_2HAs^VO_4$ with 90% boron nitride) or to the Fe(0) K-edge (7.112 keV) using a Fe metal foil or to the Mn(0) K-edge (6.539 keV) using a Mn metal foil. These standards were monitored in transmission mode simultaneous to sample collection to check for potential shifts in their respective K-edges. Multiple scans were collected at room temperature for each sample to improve the signal-to-noise ratio for data analysis.

For reference samples, EXAFS and XANES spectroscopic data were collected at beamline X-11A at the National Synchrotron Light Source (NSLS) at Brookhaven National Laboratory. The electron storage ring operates at 2.8 GeV with a current ranging from 300 to 150 mA. The monochromator consisted of two parallel Si-(111) crystals with a vertical entrance slit separation of 0.5 mm. As (11.9 keV) and Fe (7.1 keV) K-edge EXAFS spectra were collected using the same procedures as stated earlier.

Data Analysis. The As K-edge EXAFS data were analyzed by shell-by-shell fitting of the Fourier transformed EXAFS spectra (k-range 3 to 13 $Å^{-1}$, r -range 0.8 to 4 Å) using the SixPACK (Webb, 2005) interface to IFEFFIT (Newville, 2001). The theoretical scattering paths were calculated using the FEFF 7.2 code (Ankudinov and

Rehr, 1997). Flinkite ($Mn_3(OH)_4AsO_4$) was used as a structural model for As(V) sorbed on δ-MnO_2. Scorodite ($FeAsO_4 \cdot H_2O$) and tooeleite ($Fe_6(AsO_3)_4SO_4(OH)_4 \cdot 4H_2O$) were used as structural models for As(V) and As(III) sorbed on Fe-oxides (Morin et al., 2008; Wang et al., 2008). In the As EXAFS fitting, we considered As–O and As–Fe/Mn single scattering (SS) paths and one multiple scattering (MS) path (triangular As-O-O) within the AsO_4 tetrahedron or AsO_3 pyramid. The degeneracy of the As-O-O MS path was fixed to the theoretical value of 12 for As(V) and 6 for As(III).

Linear combination fitting (LCF) was performed on the Mn XANES spectra over the range of 6.4 to 6.6 keV and Fe EXAFS spectra over the k-range of 3 to 12 $Å^{-1}$ using SixPACK's least square fitting module, which is a graphical interface for IFEFFIT's minimization function (Newville, 2001). For Mn XANES, three reference standards, δ-$Mn^{IV}O_2$, $Mn_2{}^{III}O_3$ and $Mn^{II}SO_4$, were used for LCF. For Fe EXAFS, a set of reference spectra were used for LCF, including 2-line ferrihydrite, goethite, lepidocrocite, hematite, magnetite and synthetic ferric arsenate. Both shell-by-shell fitting and linear combination fitting were optimized by minimizing reduced σ^2 (Newville et al., 1995).

3.2.4 Mössbauer Analysis

Mössbauer spectra were collected at variable temperatures using ~50 mCi (1.85 MBq) ^{57}Co/Rh single-line thin sources. The velocity transducer (MVT-1000; WissEL) was operated in the constant-acceleration mode (23 Hz, ± 10 mm/sec). Data were acquired on 1,024 channels and then folded to 512 channels to give a flat background and a zero-velocity position corresponding to the center shift (CS or δ) of a metallic-Fe foil at room temperature. Calibration spectra were obtained with a 20 μm

thick α-Fe foil (Amersham, England) placed in exactly the same position as the samples to minimize any geometry error. The transmitted radiations were recorded with the Ar-Kr proportional counters.

3.2.5 TEM Analysis

TEM analysis was performed on a Philips CM 300 FEG (field emission gun) operating at 297 kV, equipped with an Oxford EDS (Energy-dispersive X-ray spectroscopy) detector. The spatial resolution of the CM 300 is 0.2 nm. Digital images were acquired using a 1024 x 1024 pixel CCD camera mounted on a Gatan GIF 200 electron energy-loss spectrometer. Powdered samples were suspended in DI water, and a drop of suspension was applied to a holey-carbon support film on a 200-mesh copper grid.

3.3 Results and Discussion

3.3.1 As Speciation and Binding Mechanisms over Time during As(III) Oxidation by δ-MnO_2 in the Presence of Fe(II)

As K-edge XANES first derivative spectra (Fig 3.2a) show only As(V) associated with solid phase during As(III) oxidation by δ-MnO2 in the presence of Fe(II) when the As(III) to Fe(II) ratio is 1:1. Previous studies have found that during As(III) oxidation by birnessite, As is bound to the solid phase only as As(V) with no evidence of As(III) (Lafferty et al., 2010b; Tournassat et al., 2002; Manning et al., 2002). We also tested the potential for synchrotron radiation induced redox change of As by comparing multiple rapid XANES scans performed on the same sample location, but no beam induced redox change was observed.

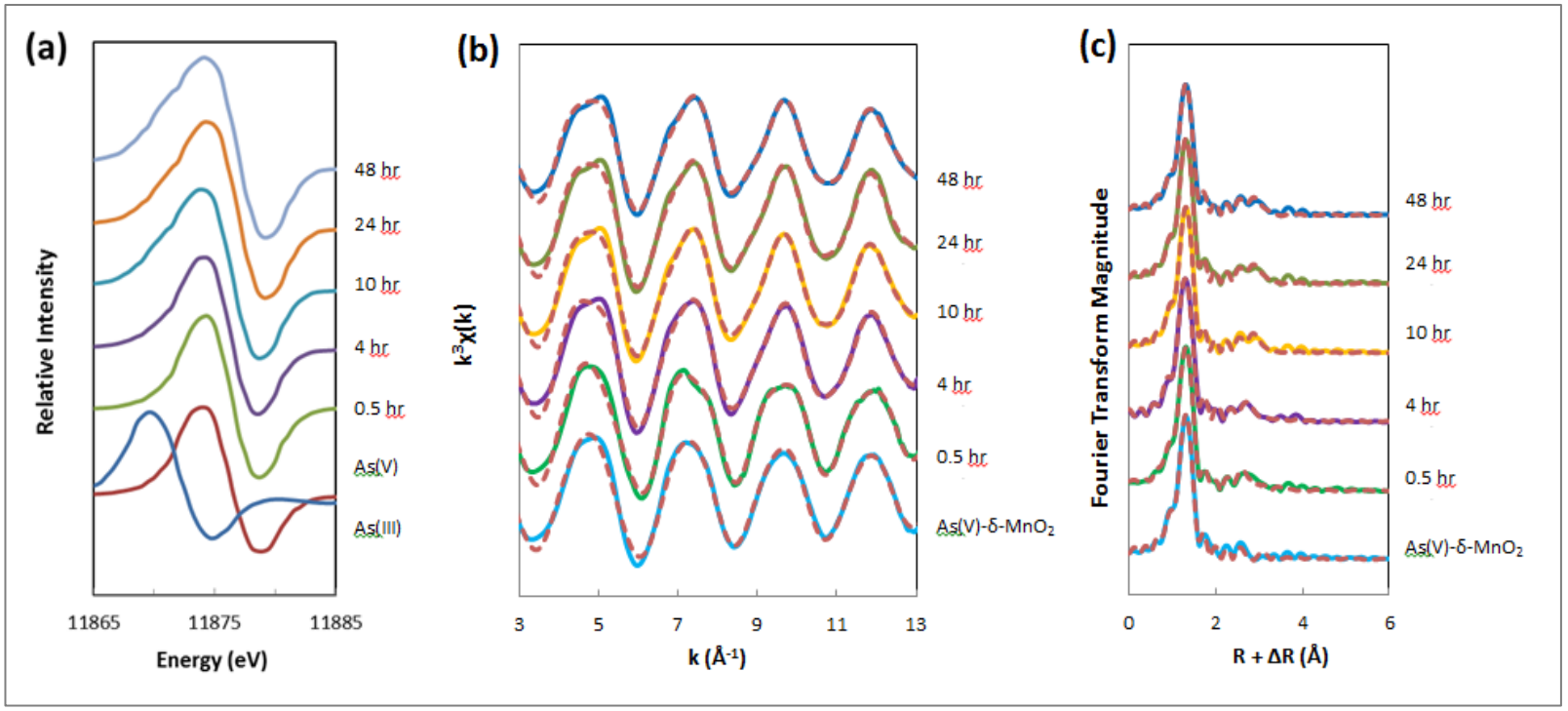

Figure 3.2 (a) Arsenic K-edge derivative XANES; (b) As K-edge EXAFS; and (c) Fourier transformed EXAFS of δ-MnO_2 (2 mg/L) reacted with 100 µmol/L As(III) and 100 µmol/L Fe(II), simultaneously, at pH 6 in a stirred-flow reactor for 0.5, 4, 10, 24, and 48 h. XAS data are presented as solid lines, and fits are presented as dashed lines (fit data are provided in Table 3.1). Sorption standards of As(V) on δ-MnO_2, As(V) on ferrihydrite, and As(III) on ferrihydrite were used.

Table 3.1 Structural parameters derived from shell-by-shell fits to k^3-weighted As EXAFS data of δ-MnO_2 (2 mg/L) reacted with 100 μmol/L As(III) and 100 μmol/L Fe(II), simultaneously, at pH 6 in a stirred-flow reactor for 0.5, 4, 10, 24, and 48 h. Fitting parameters for sorption standards of As(V) on δ-MnO2 and As(V) on ferrihydrite (Fh), as well as a standard of a synthetic ferric arsenate precipitate were also provided.

Sample	As-O			As-O-O			As-Mn/Fe			ΔE_0	S_0^2	R factor
	CN	R	σ^2	CN	R	σ^2	CN	R	σ^2			
0.5 hr	4.32	1.69	0.002	12	3.07	0.009	1.43	3.20	0.005	6.93	0.98	0.0164
4 hr	4.16	1.69	0.001	12	3.09	0.008	1.59	3.31	0.009	6.32	0.94	0.0169
10 hr	4.12	1.69	0.002	12	3.09	0.011	1.17	3.33	0.002	6.77	0.93	0.0156
24 hr	4.01	1.69	0.002	12	3.11	0.008	1.46	3.32	0.006	6.89	0.91	0.0176
48 hr	4.31	1.69	0.002	12	3.09	0.002	2.03	3.33	0.010	6.66	0.95	0.0138
Standards												
As(V)-δ-MnO_2	3.97	1.69	0.002	12	3.08	0.005	0.52	3.21	0.005	6.44	0.97	0.0167
As(V)-Fh	4.55	1.69	0.002	12	3.09	0.010	0.92	3.29	0.006	5.30	0.91	0.0097
Ferric arsenate	4.38	1.69	0.002	12	3.11	0.003	1.79	3.33	0.003	6.33	0.98	0.0086

Note: CN, coordination number, uncertainty for As-O is ±0.2-0.47, for As-Mn/Fe is ±0.24-0.97, $CN_{As\text{-}O\text{-}O}$ is fixed to 12; R(Å), interatomic distance, uncertainty for As-O is ±0.002-0.003, for As-Mn/Fe is ±0.02-0.04; σ^2, Debye-Waller factor, uncertainty for As-O is ±0.001, for As-Mn/Fe is ±0.001-0.01; ΔE_0 (eV), difference between experimentally determined threshold energy and the FEFF calculated threshold energy, uncertainty is ±0.4-1.0; S_0^2, amplitude reduction factor, uncertainty is ±0.06-0.23; R factor, goodness of fit, $R=\sum(\text{data-fit})^2/\sum\text{data}^2$.

Shell-by-shell fits of the As EXAFS spectra indicate a first shell As-O distance of 1.69 Å exclusively (Table 3.1). An As-O bond distance of 1.69 Å is consistent with findings of As(V) bound on phyllomanganates (Manning et al., 2002; Lafferty et al., 2010b; Foster et al., 2003) and is similar to As(V) bound on Fe-oxides (Fendorf et al., 1997; Waychunas et al., 1993). As K-edge EXAFS spectra exhibit a single major frequency (Fig 3.2b) which is due to the presence of four oxygen atoms surrounding As in tetrahedral coordination (Foster et al., 2003). This major frequency produces the predominant feature in the Fourier transformed data, an As-O peak at about 1.3 Å (R + ΔR) (Fig 3.2c). Aside from the As-O shell, an As-Mn/Fe distance at 3.20 Å ~ 3.33 Å was found, which is in good agreement with previous studies of As(V) bound to Mn/Fe-oxides, and is attributed to a bidentate binuclear corner-sharing (^{2}C) complex with Mn/Fe-oxides (Manning et al., 2002; Manceau et al., 2003; Fendorf et al., 1997; Waychunas et al., 1993). In some studies, several second As-Mn/Fe shells were found between 2.6 Å and 3.6 Å. An As-Mn distance at ~2.7 Å and an As-Fe distance at ~2.85 Å were attributed to the formation of a bidentate mononuclear edge-sharing (^{2}E) complex, and peaks at ~3.5 Å for As-Mn and ~3.6 Å for As-Fe were attributed to a monodentate corner-sharing (^{1}V) complex (Lafferty et al., 2010b; Fendorf et al., 1997). However, in this study, no evidence of such bidentate edge-sharing (^{2}E) complex is found possibly due to the addition of a As-O multiple scattering path to our fits. Arguments have been presented that peaks near ~2.85 Å result from As-O multiple scattering but not from As-Fe backscatters (Sherman and Randall, 2003; Waychunas et al., 2005). Additionally, according to density functional theory calculations by Sherman and Randall (2003), the bidentate corner-sharing (^{2}C) complex is predicted to be substantially (55 kJ/mol) more favored energetically over

the hypothetical edge-sharing bidentate (^{2}E) complex and the monodentate corner-sharing (^{1}V) complex is very unstable. These points also explain why we didn't observe bidentate edge-sharing (^{2}E) and monodentate corner-sharing (^{1}V) complexes in our system.

During As(III) oxidation by δ-MnO_2 in the presence of Fe(II), interestingly an increased As-Mn/Fe distance with time is observed (Table 3.1). In the beginning half hour, the As-Mn/Fe distance is 3.20 Å, which is very close to the As-Mn distance (3.21 Å) of our As(V)-δ-MnO_2 adsorption standard, indicating that at this stage, As binds mainly to the δ-MnO_2 surface. At 4 hours of reaction, the As-Mn/Fe distance increases dramatically to 3.31 Å, suggesting that the As binding structure changes greatly. This As-Mn/Fe distance of 3.31 Å is much longer than a regular As-Mn distance from 3.13 to 3.21 Å (Manning et al., 2002; Lafferty et al., 2010b), but is closer to an As-Fe distance (3.29 Å) in our adsorption standard of As(V) on ferrihydrite. During 0.5 to 4 hours, more As(III) as well as Fe(II) are oxidized by δ-MnO_2, Fe(III)-(hydr)oxides start to form and build up. The released As(V) can either be sorbed on the δ-MnO_2 surface or on the newly formed Fe(III)-(hydr)oxide surface. It is known that Fe-oxides generally have larger sorption capacity and higher affinity for As than Mn-oxides, thus at this stage, As prefers to bind with Fe, resulting in the marked increased of the As-Mn/Fe distance. During 4 to 10 hours, as oxidation is proceding, the As-Mn/Fe distance keeps increasing and after 10 hours, the As-Mn/Fe distance is stable at 3.33 Å. This As-Mn/Fe distance (3.33 Å) is longer than the reported As-Fe distance (3.25 to 3.30 Å) for As(V) adsorption samples on various Fe-oxides (Waychunas et al., 1993; Fendorf et al., 1997; Sherman and Randall, 2003; Voegelin et al., 2007), which implies there might be other As binding mechanisms

besides adsorption. A synthetic ferric arsenate was then used as a standard material in this study in order to identify the possible occurrence of a surface precipitate of As(V) and Fe(III), since some research has shown that a ferric arsenate surface precipitate formed during As adsorption on ferrihydrite (Jia et al., 2006). Ferric arsenate, a precursor to scorodite formation, naturally occurs in sea-floor hydrothermal vents (Rancourt et al., 2001), acid mine drain-age precipitates (Carlson et al., 2002), and mine tailings (Langmuir et al., 1999; Paktunc et al., 2003). Shell-by-shell fitting (Table 4.1) revealed that the As-Fe distance for ferric arsenate at 3.33 Å is in very good agreement with the As-Mn/Fe distance after 10 hours of reaction in our system. This coincidence suggests that we might have As(V) and Fe(III) precipitates (e.g. ferric arsenate) formed rather than As(V) adsorption onto Fe(III)-(hydr)oxides, although additional evidence is needed. It was also pointed out previously that surface precipitation of ferric arsenate involved an initial complexation of the arsenate iron on Fe-oxides and was favored with increasing sorbate concentration. Consequently, surface precipitation was generally a slow process (Jia et al., 2006; Carlson et al., 2002). This explains why we didn't see a large As-Mn/Fe distance (e.g. 3.33 Å) at the very beginning of the reaction, but rather after a few hours of reaction.

3.3.2 As Speciation and Binding Mechanisms during As(III) Oxidation by δ-MnO_2 with Different Fe(II) Additions

As K-edge XANES first derivative spectra (Fig 3.3a) show that only As(V) was associated with the solid phase during As(III) oxidation when Fe(II) was absent or at a low concentration (As(III) : Fe(II) = 1:1). However, when high concentrations of Fe(II) were present (As(III) : Fe(II) = 1:2 or 1:10), both As(III) and As(V) were found to associate with the solid phase. Also, we found As(III) intensity increased as Fe(II)

concentration increased, meaning that the more Fe(II) we added into the system the more As(III) was bound to the solid phase. Previous studies have shown that during As(III) oxidation by Mn-oxides, As(V) is the only species bound to the solid phase, for As(III) is readily oxidized to As(V) once it binds to Mn-oxides (Lafferty et al., 2010b; Tournassat et al., 2002; Manning et al., 2002). Therefore, the As(III) we found on the solid phase should be associated only with the Fe(III) -(hydr)oxides that formed during Fe(II) oxidation by δ-MnO_2.

Shell-by-shell fits of the As EXAFS spectra indicate the first shell As-O distance increased from 1.69 Å to 1.72 Å with increasing Fe(II) addition and the corresponding coordination number decreased from 4.3 to 3.6 (Table 3.2). This is due to the association of As(III) with the solid phase at higher Fe(II) additions. Compared to $As^{V}O_4$ tetrahedral geometry, which yields a first shell As-O distance of ~1.69 Å and a coordination number around 4, the $As^{III}O_3$ pyramid geometry yields a first shell As-O distance of ~1.79 Å and a coordination number around 3 (Hohmann et al., 2011). The shell-by-shell fits predict an average As binding environment, therefore, we would expect a longer As-O distance and a higher coordination number in samples containing both As(III) and As(V) than those samples having only As(V). Besides the As-O shell, only one second As-Mn/Fe shell is found between 3.19 Å to 3.35 Å with a coordination number about 2, indicating As forms a bidentate binuclear corner-sharing (^{2}C) complex on the solid phase. In the presence of Fe(II), the As-Mn/Fe distance (3.33~3.35 Å) is much greater than the As-Mn distance (3.21 Å) in the As(V) adsorption standard on δ-MnO_2, but is close to the As-Fe distance of As adsorption/precipitation standards on Fe(III) -(hydr)oxides. This suggests that most of the As is bound with Fe(III) -(hydr)oxides either through adsorption or precipitation.

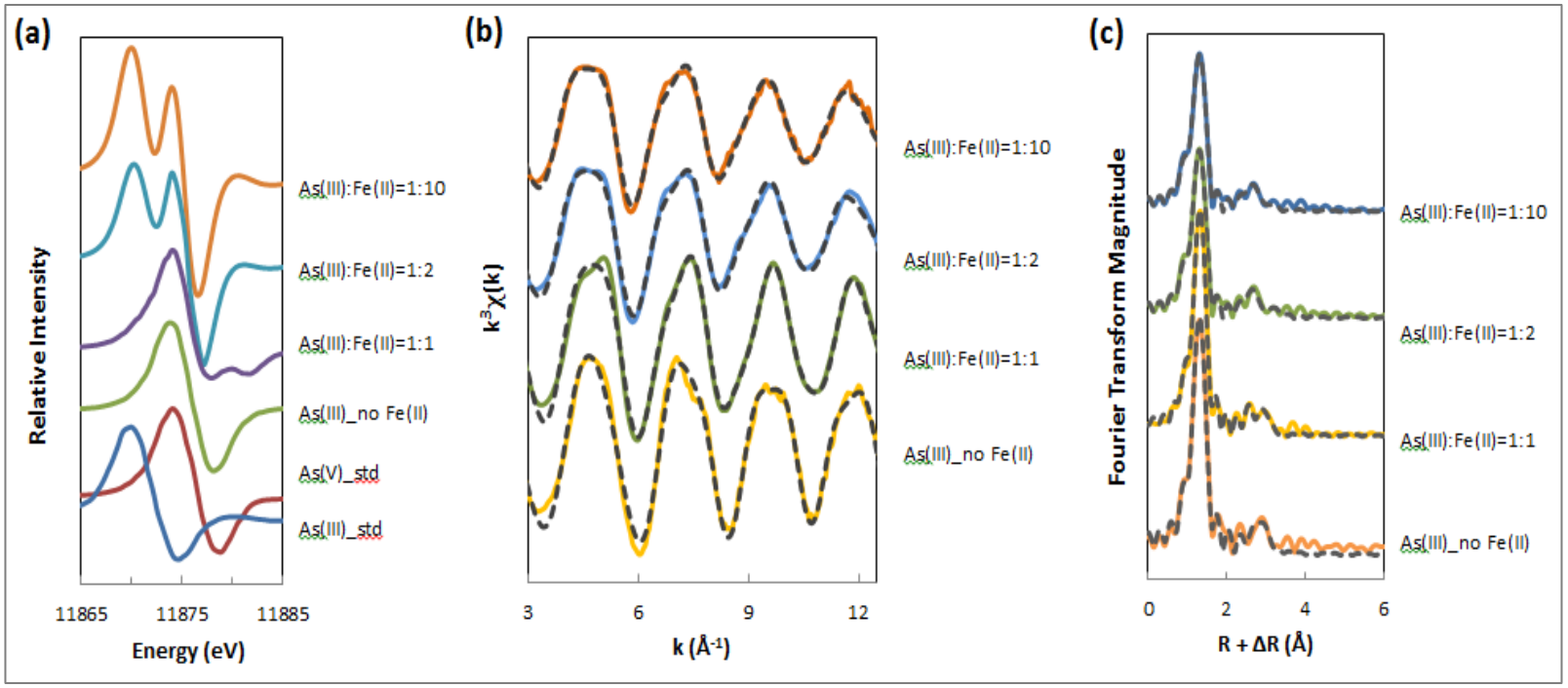

Figure 3.3 (a) Arsenic K-edge derivative XANES; (b) As K-edge EXAFS; and (c) Fourier transformed EXAFS of δ-MnO_2 (2 mg/L) reacted with 100 µmol/L As(III) and 0 µmol/L, 100 µmol/L, 200 µmol/L, and 1000 µmol/L Fe(II), respectively, in a stirred-flow reactor at pH 6 for 48 h. XAS data are presented as solid lines, and fits are presented as dashed lines (fit data are provided in Table 3.2). Sorption standards of As(V) and As(III) on ferrihydrite were used.

Table 3.2 Structural parameters derived from shell-by-shell fits to k^3-weighted As EXAFS data of δ-MnO_2 (2 mg/L) reacted with 100 μmol/L As(III) and 0 μmol/L, 100 μmol/L, 200 μmol/L, and 1000 μmol/L Fe(II), respectively, in a stirred-flow reactor at pH 6 for 48 h. Fitting parameters for sorption standards of As(V) on δ-MnO_2, As(V) on ferrihydrite (Fh) and As(III) on ferrihydrite, as well as a precipitation standard of synthetic ferric arsenate were also provided.

Sample	As-O			As-O-O			As-Mn/Fe			ΔE_0	S_0^2	R factor
	CN	R	σ^2	CN	R	σ^2	CN	R	σ^2			
As(III)	4.29	1.69	0.002	12	3.07	0.001	0.69	3.19	0.002	6.57	0.99	0.0195
As(III):Fe(II)=1:1	4.31	1.69	0.002	12	3.09	0.002	2.03	3.33	0.010	6.66	0.95	0.0138
As(III):Fe(II)=1:2	4.06	1.71	0.004	12	3.11	0.001	2.21	3.33	0.013	4.50	0.88	0.0175
As(III):Fe(II)=1:10	3.60	1.72	0.004	12	3.15	0.010	2.12	3.35	0.007	4.89	0.84	0.0154
Standards												
As(V)-δ-MnO_2	3.97	1.69	0.002	12	3.08	0.005	0.52	3.21	0.005	6.44	0.97	0.0167
As(V)-Fh	4.55	1.69	0.002	12	3.09	0.010	0.92	3.29	0.006	5.30	0.91	0.0097
As(III)-Fh	2.96	1.79	0.004	6	3.20	0.007	1.05	3.35	0.006	9.05	0.91	0.0146
Ferric arsenate	4.38	1.69	0.002	12	3.11	0.003	1.79	3.33	0.003	6.33	0.98	0.0086

Note: CN, coordination number, uncertainty for As-O is ±0.1-0.5, for As-Mn/Fe is ±0.35-1.02, for As-O-O is fixed; R(Å), interatomic distance, uncertainty for As-O is ±0.002-0.006, for As-Mn/Fe is ±0.01-0.04; σ^2, Debye-Waller factor, uncertainty for As-O is ±0.001-0.002, for As-Mn/Fe is ±0.002-0.01; ΔE_0 (eV), difference between experimentally determined threshold energy and the FEFF calculated threshold energy, uncertainty is ±0.2-1.3; S_0^2, amplitude reduction factor, uncertainty is ±0.06-0.23; R factor, goodness of fit, $R=\sum(\text{data-fit})^2/\sum\text{data}^2$.

In the sample with the highest Fe(III) concentration (As(III):Fe(II)=1:10), an observed As-Mn/Fe distance at 3.35 Å is in good agreement with the As-Fe distance of the As(III) adsorption standard on ferrihydrite. This indicates that although the presence of a high concentration of Fe(II) inhibits As(III) oxidation, a large amount of As(III) is not released to the solution but sorbed on newly formed Fe(III)-(hydr)oxides.

3.3.3 Fe(III)-(hydr)oxides Formed during Fe(II) Oxidation by δ-MnO_2

Fe K-edge XANES first derivative spectra (Fig. 3.4 a) show that most of the Fe exists as Fe(III) (peak at ~7128 eV) in the solid phase, but a small amount of Fe(II) (peak at ~7124 eV) is observed in samples containing Fe(II) as well as in samples having high Fe(II) concentrations (As(III):Fe(II)=1:10 or 1:2). Similar to As(III), we assume no Fe(II) is bound to δ-MnO_2, for Fe(II) can be readily oxidized once it binds to δ-MnO_2. Thus, the Fe(II) we found on the solid phase should be associated only with the Fe(III) -(hydr)oxides that formed during the Fe(II) oxidation by δ-MnO_2. We also tested the potential for synchrotron radiation induced redox change of Fe by comparing multiple rapid XANES scans performed on the same sample location, but no beam induced redox change was observed.

Linear combination fitting (LCF) of Fe K-edge EXAFS spectra were conducted using five common Fe (hydr)oxides standards, including ferrihydrite, goethite, lepidocrocite, hematite and magnetite. Besides, a As(V)-Fe(III) precipitate standard, ferric arsenate, was also included in the fitting when As(III) is present. LCF reveals that when As(III) is absent, the oxidation products of Fe(II) on δ-MnO_2 consist of 54% ferrihydrite, 25% goethite and 21% lepidocrocite (Table 3.3). This result is consistent with previous studies that found ferrihydrite was the predominant mineral formed by abiotic Fe(II) oxidation during a pH range of 5 to 8 with lesser amounts of

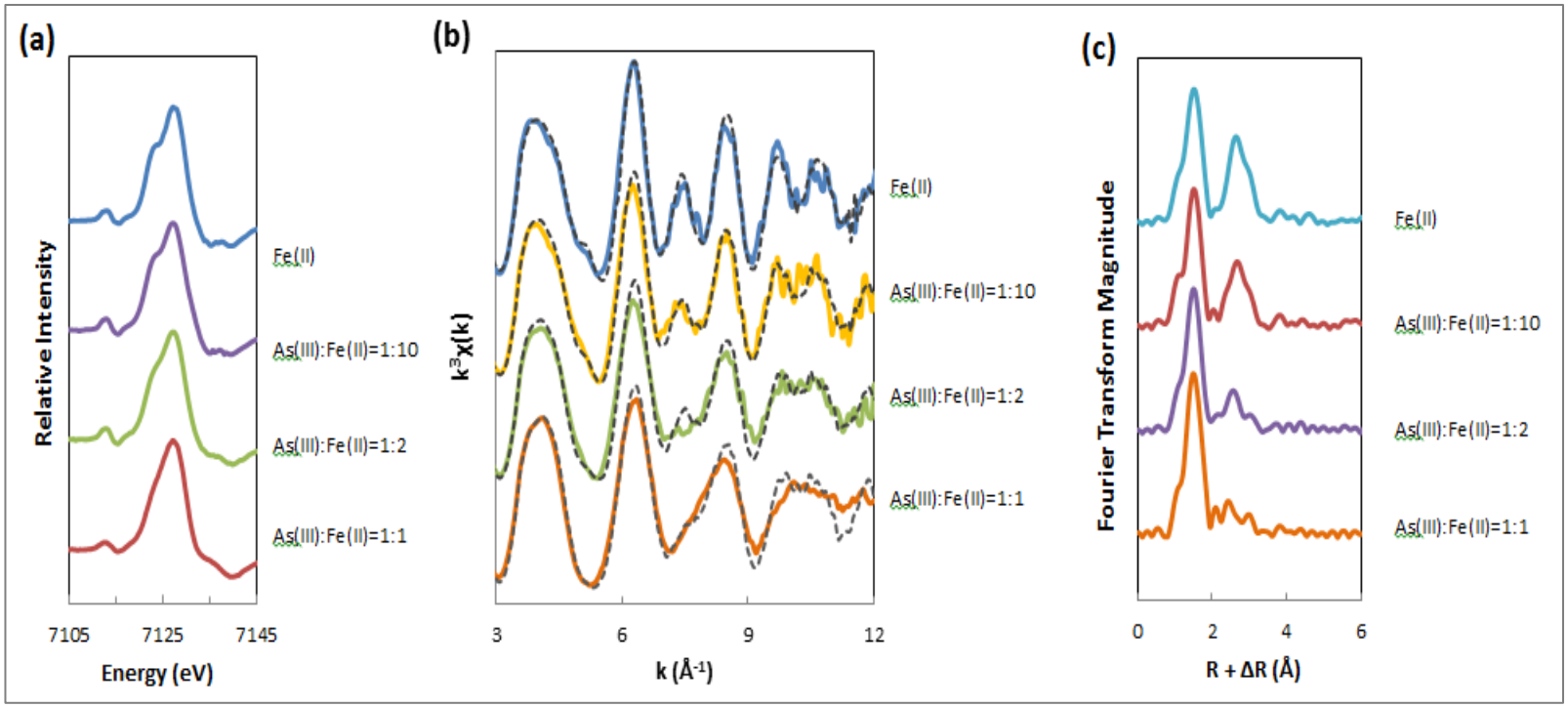

Figure 3.4 (a) Fe K-edge derivative XANES; (b) Fe K-edge EXAFS; and (c) Fourier transformed EXAFS of δ-MnO_2 (2 mg/L) reacted with 100 µmol/L Fe(II) alone, 100 µmol/L As(III) and 100 µmol/L, 200 µmol/L, and 1000 µmol/L Fe(II), respectively, in a stirred-flow reactor at pH 6 for 48 h. XAS data are presented as solid lines, and fits are presented as dashed lines (fit data are showed in Table 3.3).

Table 3.3 Mineralogical composition of Fe(III)-(hydr)oxides derived from linear combination fits to k^3-weighted Fe EXAFS data of δ-MnO_2 (2 mg/L) reacted with 100 μmol/L Fe(II) alone, and 100 μmol/L As(III) and 100 μmol/L, 200 μmol/L, and 1000 μmol/L Fe(II), respectively, in a stirred-flow reactor at pH 6 for 48 h.

Sample	Standards				R factor
	Ferrihydrite	Goethite	Ferric arsenate	Lepidocrocite	
Fe(II)	54.2 ± 3.7 %	25.0 ± 3.2 %	-	20.8 ± 1.4 %	0.04363
As(III):Fe(II)=1:1	43.9 ± 4.3%	-	56.1 ± 2.5%	-	0.05488
As(III):Fe(II)=1:2	60.1 ± 2.7%	-	38.2 ± 2.7%	1.7 ± 3.9%	0.07378
As(III):Fe(II)=1:10	62.3 ± 2.7%	-	21.5 ± 2.6%	16.2 ± 3.8%	0.06097

Note: R factor, goodness of fit, $R=\sum(data-fit)^2/\sum data^2$.

goethite, lepidocrocite, schwertmannite and green rusts (Cornell and Schwertmann, 2003; Kappler and Straub, 2005; Hohmann et al., 2011; Burgos et al., 2012). It was also pointed out previously that abiotic Fe(II) oxidation leads in many cases to precipitation of amorphous or poorly crystalline Fe(III)-bearing phases (Cornell and Schwertmann, 2003), whereas bio-mineral formation by Fe(II)-oxidizing bacteria has been shown to produce not only poorly crystalline ferrihydrite-type solids, but also crystalline phases such as goethite, hematite, and magnetite (Hohmann et al., 2011). Mössbauer spectroscopy analysis of the same sample (Fig. 3.5 a) confirms that Fe(II) oxidation by δ-MnO_2 produces ferrihydrite and goethite. Both a ferrihydrite doublet and a goethite sextet are found at 77 K. However, the goethite sextet seems to be more pronounced than the ferrihydrite doublet, which suggests that the solid contains more goethite. Compared to the Fe EXAFS study, the increased goethite fraction in Mössbauer analysis can be explained by the aging of ferrihydrite. Transformation of

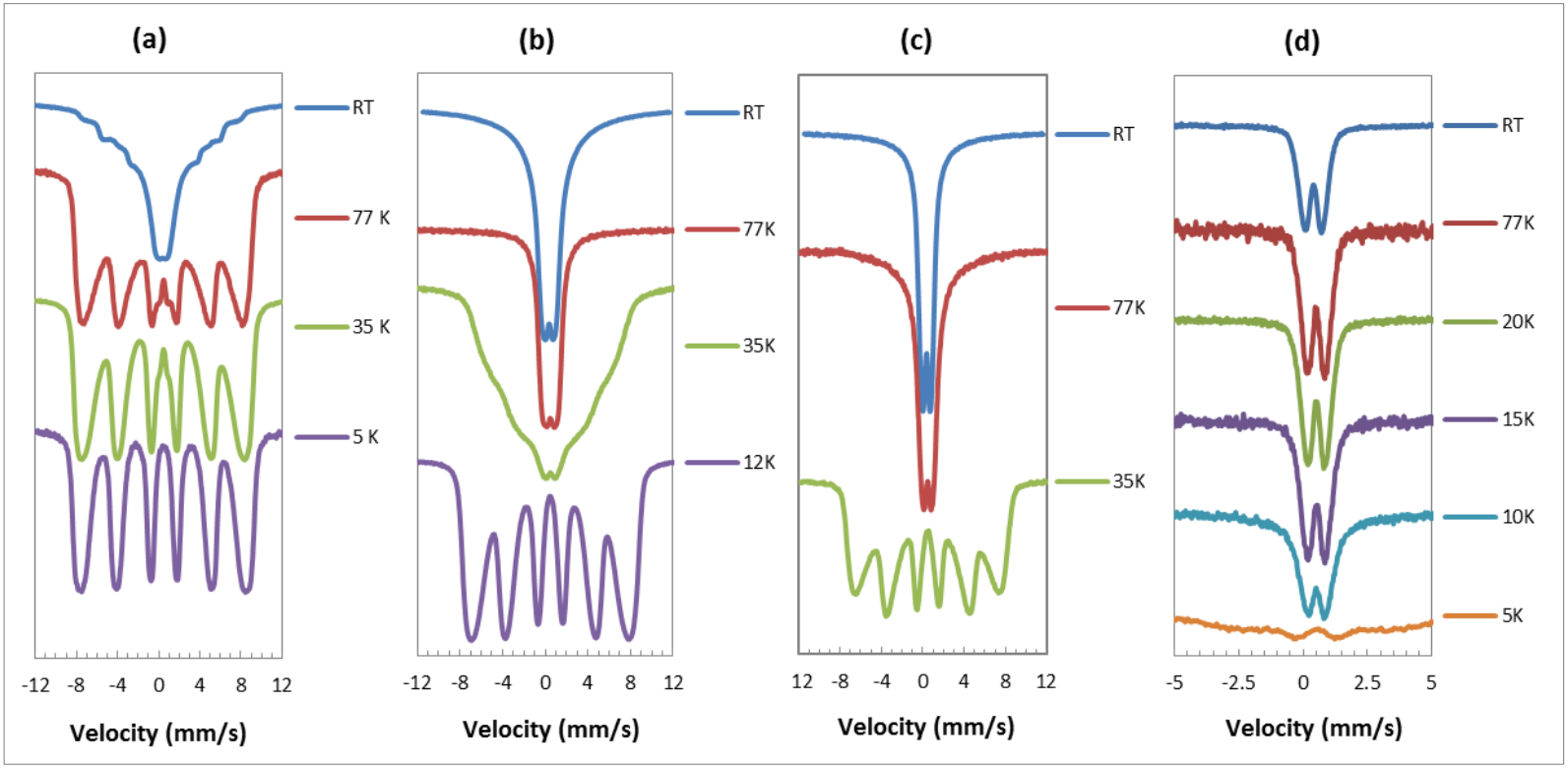

Figure 3.5 Mössbauer spectra at variable temperatures of δ-MnO_2 (2 mg/L) reacted with (a) 100 µmol/L Fe(II) alone; (b) 100 µmol/L As(III) and 100 µmol/L Fe(II); (c) 100 µmol/L As(III) and 1000 µmol/L Fe(II), at pH 6 for 48 h; and (d) synthetic ferric arsenate.

ferrihydrite to more crystalline Fe oxides such as goethite, lepidocrocite and hematite are widely documented (Cornell and Schwertmann, 2003; Hansel et al., 2003 and 2004; Yang et al., 2010; Boland et al., 2013 and 2014). It is possible that ferrihydrite in our sample is partially transformed to goethite due to longer transporting and waiting time before Mössbauer analysis. Transmission electron microscopy (TEM) analysis of the Fe(II) oxidation products by δ-MnO_2 observes at least two different phases of Fe-oxides (Fig. 3.6), and one of them agrees well with the ferrihydrite observed by previous studies (Kukkadapu et al., 2003; Michel et al., 2007; Wang et al., 2013). It shows uniform morphology, poor crystallinity and irregular shaped particle aggregates with a size of about 5 to 10 nm (Fig. 3.6 b). Some of the crystallites also exhibit lattice fringes. The other Fe-oxide observed is more tightly packed and some of the particles show a rod like shape. Although a goethite like Fe oxide is not found in this sample, we do observe a needle shaped Fe oxide formed in the sample containing 1000 μmol/L Fe(II) with 100 μmol/L As(III) (Fig. 3.8 c). Therefore, TEM analysis confirms both the EXAFS and Mössbauer studies that Fe(II) oxidation by δ-MnO_2 results in the formation of ferrihydrite and goethite. The TEM analysis is also coupled with energy-dispersive X-ray spectroscopy (EDS) to characterize the elemental composition of the sample (Fig. 3.7). It shows the Fe-oxides formed during Fe(II) oxidation and the reacted δ-MnO_2 are very pure. Neither Mn substitution into the Fe-oxide structure nor Fe substitution into Mn-oxide structure is found.

When As(III) is oxidized simultaneously with Fe(II), the LCF of the Fe EXAFS spectra shows the composition of the oxidation product changes greatly. Although ferrihydrite is still a main component, goethite is excluded, but ferric arsenate becomes an important component. One thing should be pointed out that

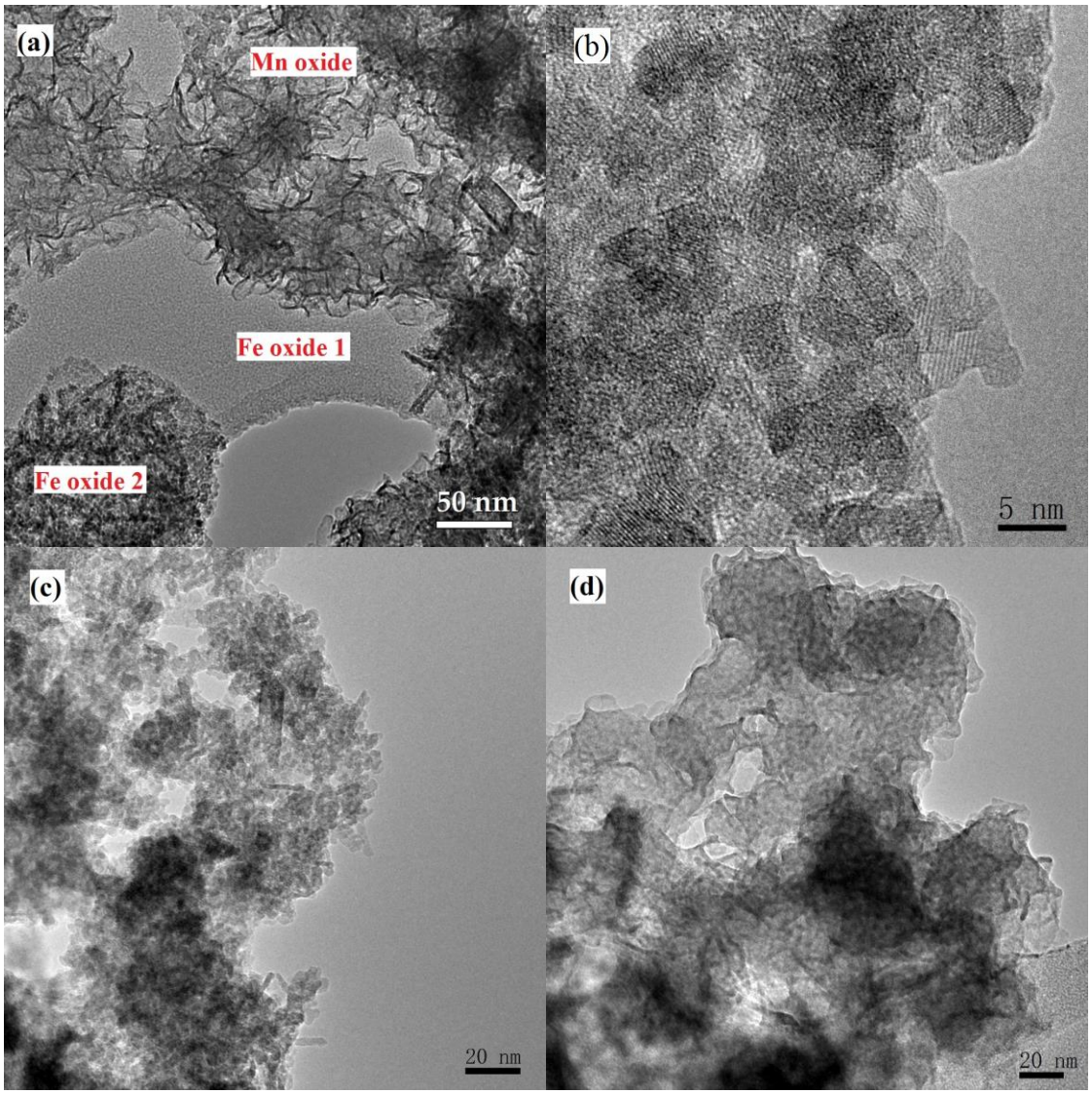

Figure 3.6 Transmission electron micrographs of δ-MnO_2 (2 mg/L) reacted with 100 µmol/L Fe(II) after 48 hours at pH 6. (a) Reacted δ-MnO_2 and two produced Fe-oxides; (b) detail of the Fe-oxide 1; (c) detail of the Fe-oxide 2; (d) detail of the Mn-oxide (reacted δ-MnO_2).

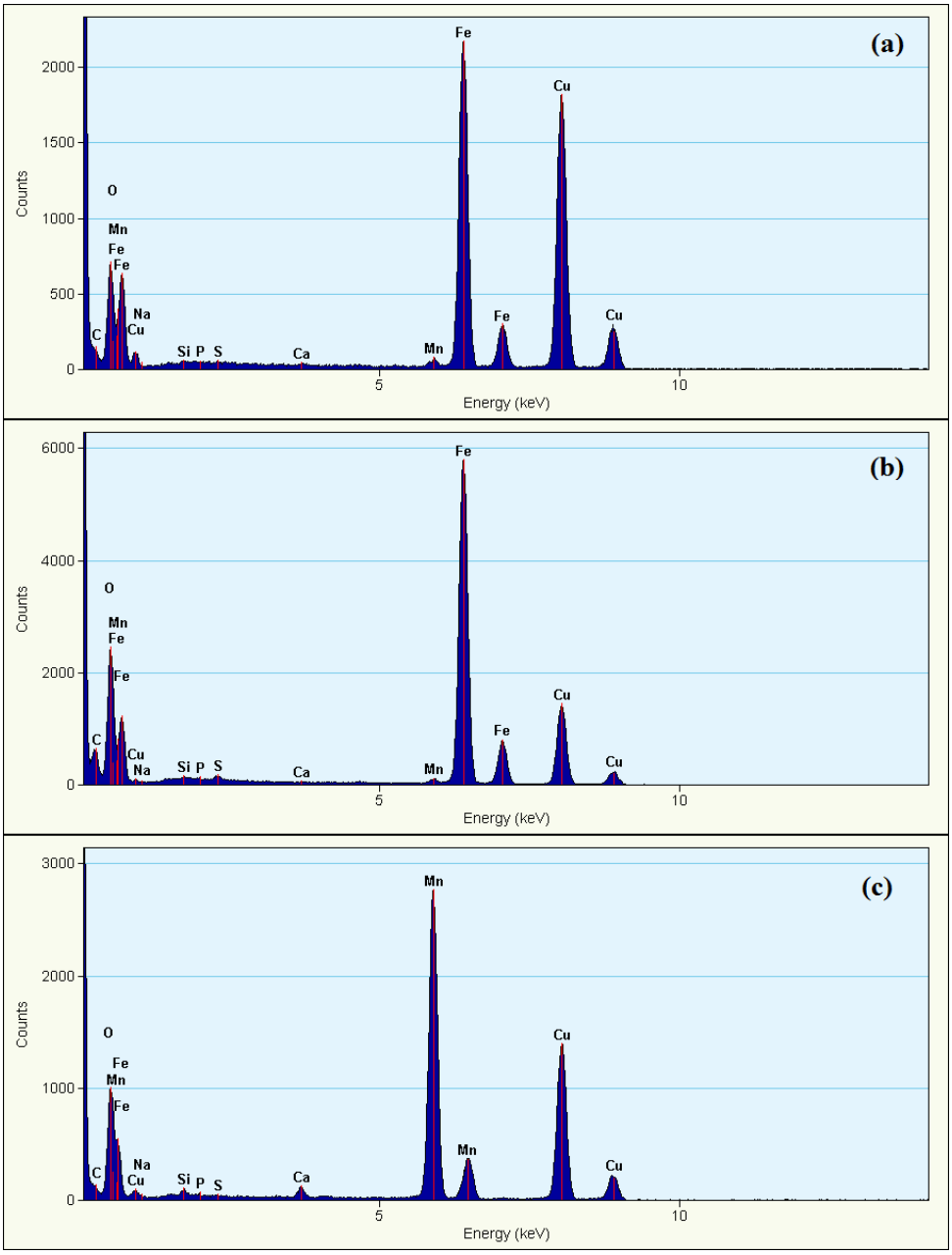

Figure 3.7 (a), (b) and (c) EDS spectra of Fe-oxide 1, Fe-oxide 2, and Mn-oxide shown in Fig 3.5 a, respectively.

among the six Fe mineral standards we used in the fitting, only one showed As binding with Fe. No As adsorption standard is included. However, due to the similarity among the EXAFS spectra for As adsorbed on ferrihydrite and goethite, and As co-precipitated with Fe(III) (Cancès et al., 2005; Paktunc et al., 2008; Hohmann et al., 2011), the ferric arsenate standard could be considered as a model representing As association with Fe either through precipitation or though adsorption. In a sample containing equal amounts of Fe(II) and As(III), LCF shows about 56% of the oxidation product is ferric arsenate, indicating that more than half of the Fe(III) (hydr)oxides are associated with As, while in the sample containing Fe(II):As(III) = 10:1, 21% of the oxidation product is ferric arsenate, indicating that less than one quarter of the Fe(III) (hydr)oxides are associated with As. The decreasing fraction of ferric arsenate with increasing Fe(II) concentration is reasonable, since more Fe(III) (hydr)oxides are formed but As remains the same amount. Mössbauer analysis shows that ferric arsenate exhibits a doublet spectrum until temperature decreases to below 10 K, however, the spectrum of the sample containing Fe(II):As(III) = 1:1 or 10:1 collapses to a sextet at a temperature higher than 10 K, suggesting that both of them are free of ferric arsenate (Fig. 3.5 b, c and d). In addition, TEM-EDS analysis of the sample with Fe(II):As(III) = 1:1 or 10:1 demonstrates that the produced Fe(III) (hydr)oxides have a Fe/As from 2 to 5 (Fig. 3.9 a, b and c), which is different from ferric arsenate that has a Fe/As=1 (Fig. 3.9 d). Although As EXAFS data indicate a ferric arsenate like precipitate might be formed when As(III) oxidized simultaneously with Fe(II) by δ-MnO_2, this is not supported by Mössbauer and TEM-EDS study. However, formation of a As(V)-Fe(III) precipitate other than ferric arsenate is not precluded.

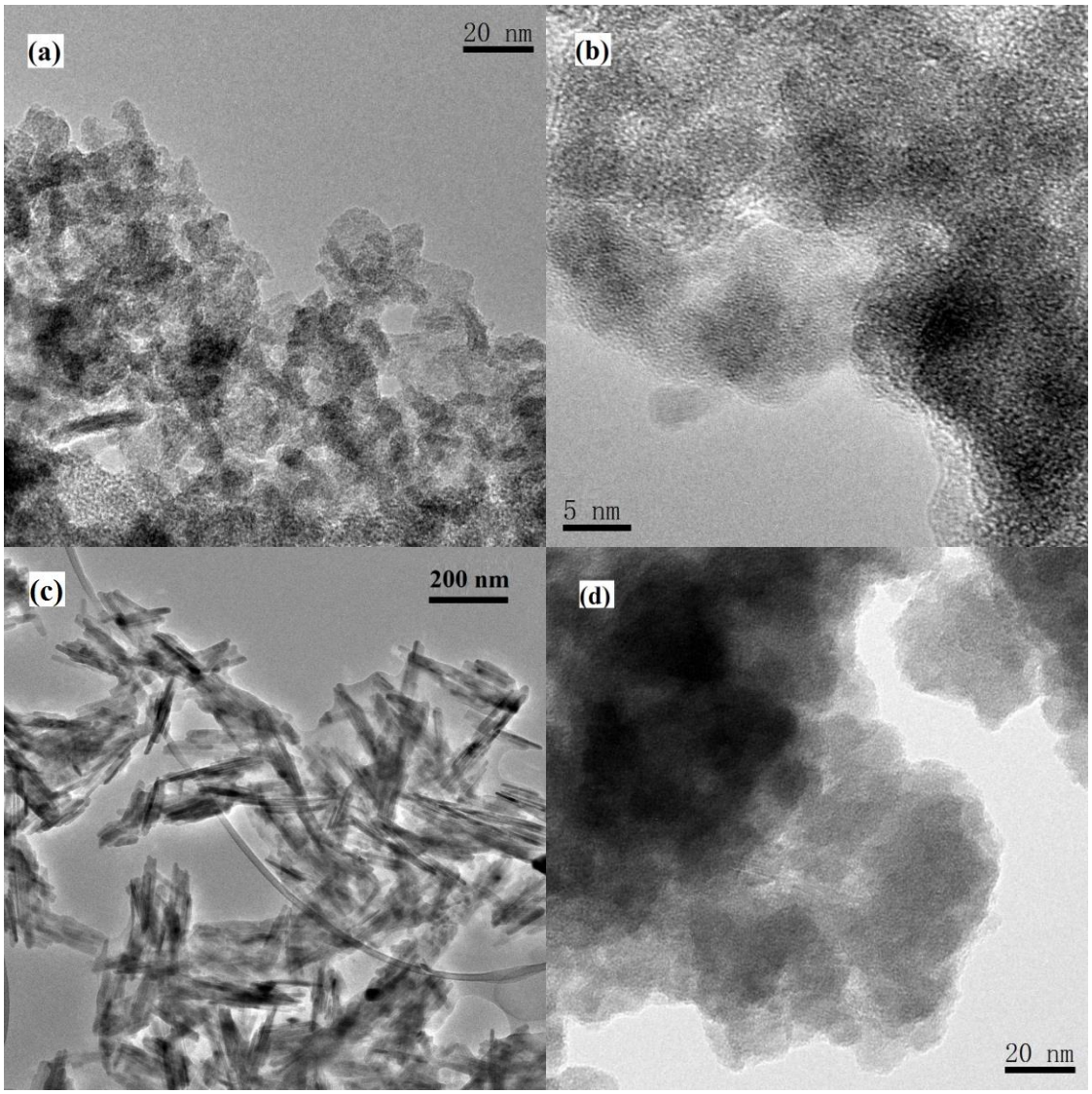

Figure 3.8 Transmission electron micrographs of (a) and (b) Fe-oxides produced in reaction of δ-MnO_2 (2 mg/L) with 100 μmol/L As(III) and 100 μmol/L Fe(II) for 48 hours at pH 6; (c) Fe-oxides produced in reaction of δ-MnO_2 (2 mg/L) with 100 μmol/L As(III) and 1000 μmol/L Fe(II) for 48 hours at pH 6; (d) Synthetic ferric arsenate.

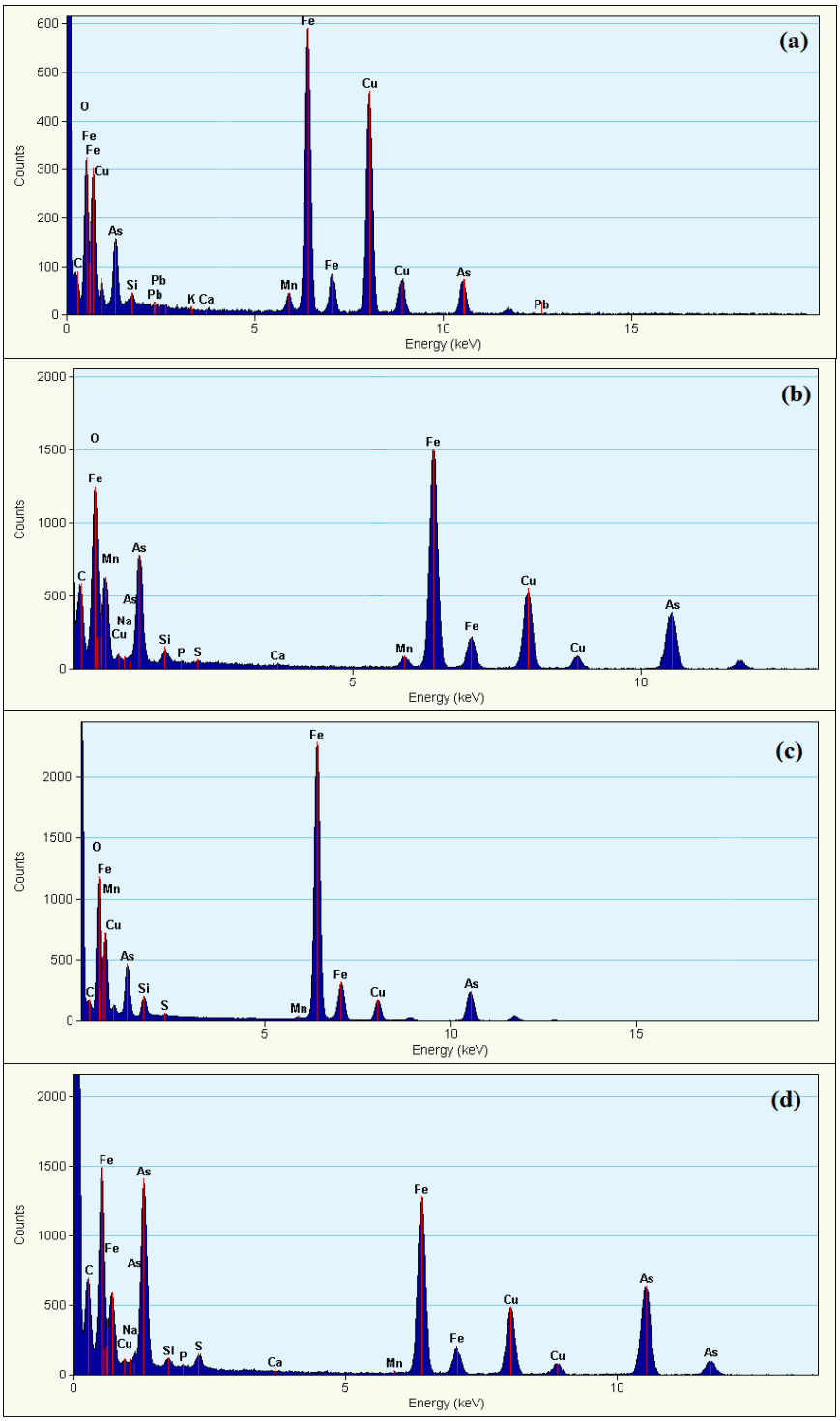

Figure 3.9 (a), (b), (c) and (d) EDS spectra of minerals shown in Fig 3.7 a, b, c and d, respectively.

3.3.4 Mn Speciation Over Time during As(III) Oxidation by δ-MnO_2 in the Presence of Fe(II)

Although unreacted δ-MnO_2 has neither Mn(II) nor Mn(III) in its structure, the amount of Mn(II) and Mn(III) appear to increase as As(III) oxidation proceed. From Mn XANES spectra (Fig. 3.10), one can see shoulders starting to build up at 6552.5 eV (Mn^{II} peak) and 6556 eV (Mn^{III} peak) after 4 hours of reaction. Linear combination fits of the data (Table 3.4) shows that Mn(II) appears at the very beginning of the reaction and increases to a maximum of 12.7 % at 4 hours. However, in the first 4 hours of the reaction, which is the fast oxidation stage, no Mn(III) is detected in δ-MnO_2. This suggests that no Mn(III) is formed during the first 4 hours of reaction. At this stage, Mn(IV) was reduced directly to Mn(II) when As(III) was oxidized. Mn(III) appears after 10 hours of reaction and reaches a maximum of 23.5 % at 48 hours. There are two possible mechanisms for the formation of Mn(III) during As(III) oxidation by δ- MnO_2. First, Mn(III) could be formed directly through Mn(IV) oxidation of As(III) (Eq. 1).

$$2MnO_2 + H_3AsO_3 + H_2O \rightarrow 2MnOOH + H_2AsO_4^- + H^+ \quad (1)$$

Although this process does not occur in the first 4 h of reaction in this study (18), it has been reported previously for As(III) oxidation by birnessite (Nesbitt et al., 1998; Tournassat et al., 2005). Another possible pathway for Mn(III) formation is through conproportionation of Mn(II) sorbed at Mn(IV) sites on the δ-MnO_2 surface (Webb et al., 2005; Perez-Benito, 2002). In this conproportionation reaction, Mn(II) is oxidized, Mn(IV) is reduced, and the resulting product is Mn(III) (Eq. 2).

$$MnO_2 + Mn^{2+} + 2H_2O \rightarrow 2Mn^{3+} + 4OH^- \quad (2)$$

This conproportionation reaction very well explains our findings that no Mn(III) is observed in the first 4 hours and during 10 to 48 hours, when Mn(III)

accumulates in δ-MnO_2, the Mn(II) fraction decreases by contrast. Therefore, it is reasonable to conclude that As(III) oxidation occurs as a two electron transfer with δ-MnO_2 and does not proceed through a Mn(III) intermediate.

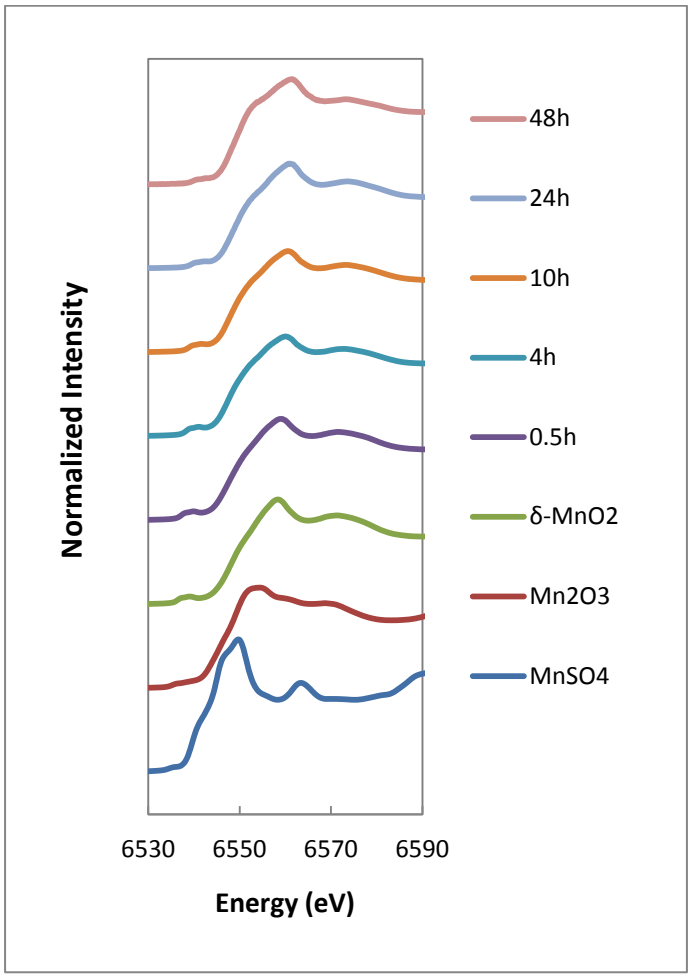

Figure 3.10 Mn K-edge XANES Spectra of δ-MnO_2 (2 mg/L) reacted with 100 µmol/L As(III) and 100 µmol/L Fe(II), simultaneously, at pH 6 in a stirred-flow reactor for 0.5, 4, 10, 24, and 48 h. Three standards, δ-$Mn^{IV}O_2$, $Mn_2{}^{III}O_3$ and $Mn^{II}SO_4$, were used.

Table 3.4 Mn(II), Mn(III) and Mn(IV) composition derived from linear combination fits to Mn K-edge XANES data of δ-MnO_2 (2 mg/L) reacted with 100 μmol/L As(III) and 100 μmol/L Fe(II), simultaneously, at pH 6 in a stirred-flow reactor for 0.5, 4, 10, 24, and 48 h. Three standards, δ-$Mn^{IV}O_2$, $Mn_2{}^{III}O_3$ and $Mn^{II}SO_4$, were used.

Sample	Mn(IV)	Mn(III)	Mn(II)	Energy Shift (eV)	R factor
0.5 h	92.1 ± 0.3 %	-	7.9 ± 0.1%	-0.56	0.0057
4 h	87.3 ± 0.4 %	-	12.7 ± 0.3%	-0.14	0.0113
10 h	85.3 ± 0.3 %	2.3 ± 0.4 %	12.4 ± 0.1%	-1.78	0.0116
24 h	84.0 ± 0.4 %	7.2 ± 0.4 %	8.7 ± 0.1%	-2.06	0.0136
48 h	68.3 ± 0.5 %	23.5 ± 0.6 %	8.2 ± 0.2 %	-2.11	0.0032

Note: R factor, goodness of fit, $R=\sum(data-fit)^2/\sum data^2$.

3.3.5 Proposed As(III) Oxidation Mechanisms in the Presence of Fe(II)

The mechanisms of As(III) oxidation by δ-MnO_2 in the presence of Fe(II) are quite complicated, involving many simultaneous forward reactions and subsequent back reactions. Also, the mechanisms depend on the specific conditions, such as pH, or As(III) to Fe(II) ratio. Based on the stirred-flow experiments and XAS analysis, three key steps could be involved:

- 1^{st} Step: As(III) and Fe(II) are adsorbed onto the δ-MnO_2 surface where they are immediately oxidized into As(V) and Fe(III), respectively, and Mn(II) is released to solution. Competition for active sites on δ-MnO_2 exists between As(III) and Fe(II).

- 2nd Step: Fe(III) precipitates as ferrihydrite and goethite like Fe(III)-(hydr)oxides on thr δ-MnO_2 surface, causing surface passivation, which lowers the oxidation rates of both As(III) and Fe(II).
- 3rd Step: The newly formed ferrihydrite-like Fe(III)-(hydr)oxides effectively adsorb large amounts of As(III), As(V), Mn(II) or even Fe(II) from solution.

These steps shown above can occur simultaneously and other steps are also possible, such as As(V) and Mn(II) adsorption on the δ-MnO_2 surface.

3.4 Conclusions

The oxidation of As(III) to As(V) by Mn-oxides is an effective pathway to reduce As toxicity and mobility in the environment. The present study showed, in the presence of Fe(II), As(III) oxidation and As sorption by δ-MnO_2 was greatly affected, with the mechanisms depending largely on Fe(II) concentration. At low Fe(II) concentration, only As(V) was found to associate with the solid phase, while at high Fe(II) concentration, both As(III) and As(V) were sorbed on the solid phase. The formation of ferrihydrite and goethite were observed when Fe(II) was oxidized by δ-MnO_2. As adsorption on the newly formed Fe(III)-(hydr)oxides occurred via a bidentate binuclear corner-sharing complex. The Fe(III)-(hydr)oxides formed during Fe(II) oxidation were mainly composed of ferrihydrite and minor fractions of goethite and lepidocrocite. As As(III) and Fe(II) may coexist under varying conditions, a mechanistic understanding of the impact of Fe(II) on As(III) oxidation and sorption behavior is crucial in predicting As toxicity and mobility in the environment and in developing new remediation techniques for As contaminated soil and water.

REFERENCES

Ankudinov, A.L., and J.J. Rehr. 1997. Relativistic calculations of spin-dependent X-ray-absorption spectra. Phys. Rev. B 56: R1712.

Boland, D. D.; Collins, R. N.; Glover, C.; Waite, T. D. 2013. An in situ quick-EXAFS and redox potential study of the Fe(II)-catalysed transformation of ferrihydrite. Colloids Surf., 435: 2−8.

Boland, D.D., Collins, R.N., Miller, C.J., Glover, C.J., and Waite, D. 2014. Effect of Solution and Solid-Phase Conditions on the Fe(II)-Accelerated Transformation of Ferrihydrite to Lepidocrocite and Goethite. Environ. Sci. Technol., 48: 5477 -5485.

Burgos, W. D., Borch, T., Troyer, L. D., Luan, F., Larson, L. N., Brown, J. F., Lambson, J. and Shimizu, M. 2012. Schwertmannite and Fe oxides formed by biological low-pH Fe(II) oxidation versus abiotic neutralization: Impact on trace metal sequestration. Geochim. Cosmochim. Acta. 76: 29–44.

Cancès B., Juillot F., Morin G., Laperche V., Alvarez L., Proux O., Hazemann J. L., Brown, Jr., G. E. and Calas G. 2005. XAS evidence of As(V) association with iron oxyhydroxides in a contaminated soil at a former arsenical pesticide processing plant. Environ. Sci. Technol., 39: 9398–9405.

Carlson, L.; Bigham, J. M.; Schwertmann, U.; Kyek, A.; Wagner, F. 2002. Scavenging of As from mine drainage by schwertmannite and ferrihydrite: a comparison with synthetic analogues. Environ. Sci. Technol. 36: 1712 -1719.

Cornell, R. M. and Schwertmann, U. 2003. The Iron Oxides Structures, Properties, Reactions, Occurences and Uses. Wiley-VCH Verlag, Weinheim.

Farquhar, M. L., Charnock, J. M., Livens, F. R., and Vaughan, D. J. 2002. Mechanisms of arsenic uptake from aqueous solution by interaction with goethite, lepidocrocite, mackinawite, and pyrite: An X-ray absorption spectroscopy study. Env. Sci. Tech. 36: 1757-1762.

Fendorf, S., M.J. Eick, and P. Grossl. 1997. Arsenate and chromate retention mechanisms on goethite. 1. Surface structure. Environ. Sci. Technol. 31:315-320.

Foster, A.L., G.E. Brown, and G.A. Parks. 2003. X-ray absorption fine structure study of As(V) and Se(IV) sorption complexes on hydrous Mn oxides. Geochim. Cosmoch im. Ac. 67:1937 -1953.

Frankenberger, W.T. (ed.) 2002. Environmental Chemistry of Arsenic. Marcel Dekker. New York, NY. pp391.

He, Y. T., Hering, J. G. 2009. Enhancement of arsenic(III) sequestration by manganese oxides in the presence of iron(II), Water, Air, Soil Pollut. 203:359-368.

Hansel, C. M.; Benner, S. G.; Neiss, J.; Dohnalkova, A.; Kukkadapu, R. K.; Fendorf, S. 2003. Secondary mineralization pathways induced by dissimilatory iron reduction of ferrihydrite under advective flow. Geochim. Cosmochim. Acta, 67: 2977–2992.

Hansel, C. M.; Benner, S. G.; Nico, P.; Fendorf, S. 2004. Structural constraints of ferric (hydr)oxides on dissimilatory iron reduction and the fate of Fe(II). Geochim. Cosmochim. Acta, 68: 3217–3229.

Herbel, M. and Fendorf , S. 2006. Biogeochemical processes controlling the speciation and transport of arsenic within iron coated sands. Chem. Geol. 228: 16–32.

Hohmann, C., Morin, G., Ona-Nguema, G., Guigner, J.M., Brown G.E., Kappler, A. 2011. Molecular-level modes of As binding to Fe(III) (oxyhydr)oxides precipitated by the anaerobic nitrate-reducing Fe(II)-oxidizing Acidovorax sp. strain BoFeN1. Geochimica et Cosmochimica Acta 75: 4699–4712.

Jain, A., Raven K.P., Leoppert, R.H. 1999. Arsenite and arsenate adsorption on ferrihydrite: Surface charge reduction and net OH-release stoichiometry.Environ. Sci. Technol., 33: 1179–1184.

Jia, Y., Xu, L., Fang, Z., Demopoulos, G.P. 2006. Observation of Surface Precipitation of Arsenate on Ferrihydrite. Environ. Sci. Technol. 40: 3248-3253.

Kappler, A., and Straub, K. L. 2005. Geomicrobiological cycling of iron. Rev. Mineral. Geochem.59: 85–108.

Kukkadapu, R.K., Zachara, J.M., Fredrickson J.K., Smith, S.C., Dohnalkova, A.C., and Russell, C.K. 2003. Transformation of 2-line ferrihydrite to 6-line ferrihydrite under oxic and anoxic conditions. American Mineralogist, 88: 1903–1914.

Lafferty, B., M. Ginder-Vogel and D.L. Sparks. 2010 a. Arsenite oxidation by a poorly crystalline manganese-oxide 1. Stirred-flow experiments. Environ. Sci. Technol. 44:8460-8466.

Lafferty, B., M. Ginder-Vogel, M. Zhu, K.J.T. Livi and D.L. Sparks. 2010 b. Arsenite oxidation by a poorly crystalline manganese-oxide 2.Results from X-ray absorption spectroscopy and X-ray diffraction. Environ. Sci. Technol. 44:8467–8472.

Langmuir, D., Mahoney, J., MacDonald, A. and Rowson, J. 1999. Predicting arsenic concentrations in the porewaters of buried uranium mill tailings. Geochim. Cosmochim. Acta. 63: 3379–3394.

Mamtaz, R., Bache, D.H. 2001. Reduction of arsenic in groundwater by coprecipitation with iron, J. Water Supply Res. Technol. 50: 313–324.

Manceau A, Tamura N, Celestre RS, MacDowell AA, Geoffroy N, Sposito G, Padmore HA (2003) Molecular-scale speciation of Zn and Ni in soil ferromanganese nodules from loess soils of the Mississippi Basin. Environ. Sci. Technol. 37: 75-80.

Manning, B.A., Fendorf, S.E., Bostick, B., Suarez, D.L. 2002. Arsenic(III) oxidation and arsenic(V) adsorption reactions on synthetic birnessite. Environ. Sci. Technol. 36:976-981.

Michel, F. M., Ehm, L., Liu, G.; Han, W. Q., Antao, S. M., Chupas, P. J., Lee, P. L., Knorr, K., Eulert, H., Kim, J., Grey, C. P., Celestian, A. J., Gillow, J., Schoonen, M. A. A., Strongin, D. R., Parise, J, B. 2007. Similarities in 2- and 6-line ferrihydrite based on pair distribution function analysis of X-ray total scattering. Chem. Mater., 19(6): 1489−1496.

Mohan, D., Pittman, C. U. 2007. Arsenic removal from water/wastewater using adsorbents-a critical review, J. Hazard. Mater. 142:1-53.

Morin, G., Ona-Nguema, G., Wang, Y., Menguy, N., Juillot F., Proux, O., Guyot, F., Calas, G. and Brown, Jr., G. E. 2008. Extended X-ray absorption fine structure analysis of arsenite and arsenate adsorption on maghemite. Environ. Sci. Technol. 42: 2361–2366.

Newville, M. 2001. IFEFFIT : Interactive XAFS analysis and FEFF fitting. J. Synchrotron Radiat. 8: 322 -324.

Newville, M., B. Ravel, D. Haskel, J.J. Rehr, E.A. Stern, and Y. Yacoby. 1995. Analysis of multiple-scattering XAFS data using theoretical standards. Physica B: Condensed Matter 208-209:154-156.

Nickson, N. T., M cArthur, J. M., Ravenscroft, P., Burgess, W. G., Ahmed, K. M. 2000. Mechanism of arsenic release to groundwater, Bangladesh and West Bengal. Applied Geochemistry, 15: 403–413.

Nordstrom, D.K. 2002. Worldwide occurrences of arsenic in ground water. Science. 296: 2143- 2144.

Paktunc A. D., Foster A. and Laflamme J. 2003. Speciation and characterization of arsenic in Ketza River Mine tailings using X-ray absorption spectroscopy.Environ. Sci. Technol.37, 2067–2074.

Paktunc D., Foster A., Heald S. and Laflamme G. 2004. Speciation and characterization of arsenic in gold ores and cyanidation tailings using X-ray absorption spectroscopy. Geochim. Cosmochim. Acta68, 969–983.

Perez-Benito, J. F. 2002. Reduction of colloidal manganese dioxide by manganese(II). J. Colloid Interface Sci., 248(1), 130–135.

Rancourt, D. G., Fortin, D., Pichler, T., Thibault, P.-J., Lamarche, G., Morris, R. V. and Mercier, P. H. J. 2001. Mineralogy of a natural As-rich hydrous ferric oxide coprecipitate formed by mixing of hydrothermal fluid and seawater: implications regarding surface complexation and color banding in ferrihy-drite deposits.Am. Mineral. 86: 834–851

Schwertmann, U., and Cornell, R. M. 1991. Iron oxides in the Labora-tory: Preparation and Characterization. VCH Publishers. Wein-heim.

Sherman, D.M., and Randall, S.R. 2003. Surface complexation of arsenic (V) to iron (III) (hydr)oxides: Structural mechanism from ab initio molecular ge-ometries and EXAFS spectroscopy. Geochim. Cosmochim. Acta, 67: 4223–4230.

Swartz, C . H ., Blute, N. K., Badru zzman, B., Ali, A., Brabander, D., Jay, J. B. 2004. Mobility of arsenic in a Bangladesh aquifer: inferences from geochemical profiles, leaching data, and mineralogical characterization. Geochemical et Cosmochimica Acta, 68: 4539 – 4557.

Tournassat, C., Charlet, L., Bosbach, D. and Manceau, A. 2002. Arsenic(III) oxidation by birnessite and precipitation of man-ganese(II) arsenate. Environ. Sci. Technol. 36, 493–500.

Voegelin, A., Weber, F.A., Kretzschmar, R. 2007. Distribution and speciation of arsenic around roots in a contaminated riparian floodplain soil: Micro-XRF element mapping and EXAFS spectroscopy. Geochimica et Cosmochimica Acta. 71: 5804–5820.

Wang J. W., Bejan D. and Bunce N. J. 2003. Removal of arsenic from synthetic acid mine drainage by electrochemical pH adjustment and coprecipitation with iron hydroxide. Environ. Sci. Technol., 37: 4500–4506.

Wang, X., Li, W., Harrington, R., Liu, F., Parise, J.B., Feng, X., Sparks, D.L. 2013. Effect of Ferrihydrite Crystallite Size on Phosphate Adsorption Reactivity. Environ. Sci. Technol., 47: 10322−10331.

Wang, Y., Morin, G., Ona-Nguema, G., Menguy, N., Juillot, F., Aubry, E., Guyot, F., Calas, G. and Brown, Jr., G. E. 2008. Arsenite sorption at the magnetite-water interface during aqueous precipitation of magnetite. EXAFS evidence of a new surface complex. Geochim. Cosmochim. Acta72: 2573–2586.

Waychunas, G.A., B.A. Rea, C.C. Fuller, and J.A. Davis. 1993. Surface Chemistry of Ferrihydrite: Part 1. EXAFS Studies of the Geometry of Coprecipitated and Adsorbed Arsenate. Geochimica et Cosmochimica Acta 57:2251-2269.

Waychunas, G. A., Davis, J. A., and Fuller, C. C. 1995. Geometry of sorbed arsenate on ferrihydrite and crystalline FeOOH: Re-evalua-tion of EXAFS results and topological factors in predicting sorbates geometry, and evidence for monodentate complexes. Geochim. Cosmochim. Acta 59: 3655 –3661.

Waychunas, G. A., Trainor, T., Eng P., Catalano, J., Brown, G., Davis, J., Rogers, J. and Bargar, J. 2005. Surface complexation studied via combined grazing-incidence EXAFS and surface diffraction: arsenate on hematite (0001) and (1012). Anal. Bioanal. Chem. 383: 12–27.

Webb, S.M. 2005. SIXpack: a graphical user interface for XAS analysis using IFEFFIT. Physica Scripta T115:1011 -1014.

Webb, S. M.; Dick, G. J.; Bargar, J. R.; Tebo, B. M. 2005. Evidence for the presence of Mn(III) intermediates in the bacterial oxidation of Mn(II). Proc. Natl. Acad. Sci., 102(15), 5558–5563.

Yang, L.; Steefel, C. I.; Marcus, M. A.; Bargar, J. R. 2010. Kinetics of Fe(II)-catalyzed transformation of 6-line ferrihydrite under anaerobic flow conditions. Environ. Sci. Technol., 44(14): 5469−5475.

Chapter 4

DESORPTION OF ARSENIC FROM δ-MnO_2: STIRRED-FLOW EXPERIMENTS AND X-RAY ABSORPTION SPECTROSCOPY

ABSTRACT

Arsenic (As) mobility in the environment is greatly affected by its oxidation state and the degree to which it is sorbed on metal oxide surfaces. Manganese (Mn) and iron (Fe) oxides are ubiquitous solids in terrestrial systems and have high sorptive capacities for many trace metals, including arsenic. Although numerous studies have characterized the effects of As adsorption/desorption onto Fe and Mn oxides individually, the fate of arsenic within mixed systems representative of natural environments has not been completely resolved. In this study, As(III) is initially reacted with a poorly crystalline phyllomanganate (δ-MnO_2) in the presence of Fe(II), prior to desorption. This initial reaction results in the sorption of both As(III) and As(V) on mixed Fe/Mn-oxides surfaces. A desorption study was carried out using two environmentally significant ions, phosphate (PO_4^{3-}) and calcium (Ca^{2+}). Both a stirred-flow technique and X-ray absorption spectroscopy (XAS) analysis were used to investigate As desorption behavior. Results show that when As(III):Fe(II)=1:1 in the initial reaction, only As(V) was desorbed, agreeing with a previous study showing that As(III) is not associated with the Fe/Mn-oxides. When As(III):Fe(II)=1:10 in the initial reaction, both As(III) and As(V) can be desorbed from the Fe/Mn-oxide surface

and more As(III) is desorbed than As(V). Neither of the desorbents used in this study completely removes As(III) or As(V) from the Fe/Mn-oxides surface. However, the As desorption fraction decreases with increasing Fe(II) concentration in the initial reactions.

4.1 Introduction

Elevated levels of arsenic can be widely present in the environment as a result of mineral weathering and dissolution, geothermal activity, and numerous anthropogenic sources including mine wastes, coal ash, and arsenical pesticides, posing a severe health threat to millions of people worldwide (Smith et al., 1998; Manning et al., 1998; Mandal and Suzuki, 2002; Lafferty et al., 2011). In the environment, arsenic primarily exists in an organic form and in two oxidation states, As(III) and As(V), which together likely represent more than 99% of total arsenic in soils, sediments and waters (Ryu et al., 2002; Gao et al, 2013). Arsenate generally predominates in oxygenated waters, whereas arsenite can be prevalent in suboxic groundwater (Mohan and Pittman, 2007). The latter is considered more mobile and more toxic in natural environments (Zhu et al., 2009; Parikh et al., 2010). Below pH 9, As(III) appears predominately in its fully protonated form (H_3AsO_3), while at circumneutral pH values, As(V) occurs as a mixture of $H_2AsO_4^-$ and $HAsO_4^{2-}$ (Sadiq, 1997; Lafferty et al., 2011).

The mobility of arsenic in the environment is governed largely by its chemical speciation, as well as mineral-surface interactions (Manning et al., 1998; Lafferty et al., 2011). Adsorption or coprecipitation with metal oxides, particularly Fe-(hydr)oxides, is an important process controlling the fate and transport of arsenic in natural aquatic

systems due to their abundance in the environment and high affinity for arsenic species (Manning et al., 1998; Silva et al., 2012; Neupane et al., 2014). The molecular-scale adsorption mechanisms of arsenate and arsenite on a range of natural and synthetic minerals (e.g., metal oxides) have been extensively investigated using macroscopic and spectroscopic techniques including synchrotron X-ray absorption and FTIR spectroscopies (Sun and Doner, 1996; Fendorf et al., 1997; Raven et al., 1998; Goldberg and Johnston, 2001; Farquhar et al., 2002; Dixit and Hering, 2003). According to these studies, both arsenate and arsenite are strongly adsorbed on polyvalent metal (hydr)oxide surfaces, forming predominantly inner-sphere surface complexes by ligand exchange reactions resulting in either monodentate or binuclear bidentate complexes depending on surface loading and solution chemistry. Only a few prior studies reported that arsenite forms both inner-sphere and outer-sphere surface complexes on ferric (hydr)oxide surfaces (Goldberg and Johnston, 2001; Catalano et al., 2008).

Currently, there are three widely accepted mechanisms for arsenic release in sediments and soils: (1) oxidation of arsenic rich sulfide materials, (2) reductive dissolution of iron oxides and concurrent release of adsorbed arsenic, and (3) competitive adsorption/desorption (Luxton et al., 2008). Of these proposed mechanisms competitive adsorption/desorption has received the least amount of attention. Sorption/desorption is a dynamic process, which is determined by a number of geochemical factors, including pH, structural changes in the solid phases, and the presence of competing ions (Smith, 1999; Dong et al., 2012). The presence of other naturally occurring ions in waters may compete for sorption sites on the mineral surface and thereby affects the stability and mobility of adsorbed arsenic species

(Antelo, 2005; Dong et al., 2012; Gao et al., 2014). Previous research has indicated that individual anion species exhibit widely different affinities for mineral surface sites. For example, Goh and Lim (2005) reported that the capabilities of common anions to increase arsenic mobility in subsurface environments follows the order: phosphate > carbonate > sulfate ≈ chloride.

Phosphate (PO_4^{3-}) is one of the most common anions in groundwater, with concentrations ranging from 0 to 5 mg/L, owing to the use of phosphate fertilizers (Oinam et al., 2011). Phosphate is particularly effective at competing with arsenate for sorption sites due to their similarities in coordination geometry and geochemical behavior (Goh and Lim, 2005; Silva et al., 2012; Dong et al., 2012). Calcium is one of the dominant cations in both groundwater and soil solutions (Cowan et al., 1991). It has been reported that calcium (Ca^{2+}) can compete with many metals for sorption sites on soil mineral surfaces (Cowan et al., 1991; Ridley et al., 1999; Lafferty et al., 2011). Therefore, identifying the effects of phosphate and calcium on arsenic desorption is essential to understand the arsenic mobility in the environment.

In the previous study (Chapter 2 and 3), both As(III) and As(V) sorption on δ-MnO_2 increased in the presence of Fe(II), due to the formation of Fe(III)-(hydr)oxides. Although arsenic removal increases with increasing Fe(II) addition, the stability and mobility of the adsorbed arsenic remains unknown. The purpose of this study is to investigate the arsenic desorption behavior from δ-MnO_2 and the produced Fe(III)-(hydr)oxides. We aim to determine to what extent an anion (PO_4^{3-}), and a cation (Ca^{2+}), both of which are commonly found in the environment, are able to desorb As from δ-MnO_2 and the produced Fe(III)-(hydr)oxides.

4.2 Methods and Materials

4.2.1 Chemicals

All chemicals used in this study met or exceeded American Chemical Society standards. 18.2 MΩ deionized (DI) water was used for all solutions. $NaAsO_2$ and $FeSO_4 \cdot 7H_2O$ were used as sources of As(III) and Fe(II), respectively. As(III) stock solution (100 mmol/L) was stored at 4 ℃ and prepared every month. Fe(II) solution was freshly prepared every time in the glove box and the DI water used to make the Fe(II) solution was degased, using nitrogen gas, for 2 hours before use. Ca^{2+} and PO_4^{3-} desorptive solutions were made by dissolving certain amounts of NaH_2PO_4 and $CaCl_2$ in DI water, respectively.

4.2.2 Synthesis of Minerals

δ-MnO_2, a poorly-crystalline, phyllomanganate, was used in the studies presented here because of its high reactivity as well as its similarities to biogenic Mn-oxides (Villalobos et al., 2003). δ-MnO_2 is a form of hexagonal birnessite with a low degree of stacking of phyllomanganate sheets (Drits et al., 1997; Silvester et al., 1997). δ-MnO_2 was synthesized by drop wise addition of a 100 mL solution containing 11.29 g $Mn(NO_3)_2 \cdot 4H_2O$ to a 100 mL solution containing 2.4 g NaOH and 4.74 g KMnO4, corresponding to a final Mn(II):Mn(VII):OH ratio of 3:2:4 (Morgan and Stumm, 1964). After adding Mn(II) to the basic permanganate solution, the resulting suspension was stirred overnight (at least 12 hours) to allow complete conproportionation of Mn(II) and Mn(VII) to Mn(IV). Following synthesis, δ-MnO_2 was centrifuged at 10,000 RCF for 15 min, then the supernatant was removed and replaced with 18.2 MΩ deionized (DI) water. This wash step was repeated 6 times. Following washing, δ-MnO_2 was transferred to a polypropylene bottle, resuspended in

DI water, and stored at 4 ℃ prior to use in experiments. Experiments were conducted using δ-MnO_2 within a month of synthesis. Characterization of synthetic δ-MnO_2 is provided in Appendix A.

Two-line ferrihydrite was synthesized using a procedure adapted from Schwertmann and Cornell (1991). Ferric sulfate, $Fe_2(SO_4)_3$ $5H_2O$, was used as the source of the ferric ion. Briefly, the Fe(III) solution was prepared by dissolving $Fe_2(SO_4)_3$ $5H_2O$ in deionized water. The pH of the solution was raised to ~7.5 in about 5 min using a 1M NaOH solution and maintained at that pH for 1 h with the slurry vigorously agitated. The solid was washed five times with deionized water and then freeze dried.

Ferric arsenate ($FeAsO_4$ ·4-$7H_2O$) was synthesized using the method described by Jia et al. (2006). Briefly, a mixture of 0.02 M As(V) (Na_2HAsO_4 ·$7H_2O$) and 0.02 M Fe(III) ($Fe_2(SO_4)_3$ $5H_2O$) was adjusted from an initial pH 1.3 to pH 1.8 with 1M NaOH solution and maintained at that pH for 1 h. The solid product was then separated by filtration, washed with deionized water and freeze dried.

4.2.3 Stirred-flow Experiments

Stirred flow experiments were conducted using the same apparatus as described previously in Chapter 2 (Fig 2.1). The reactor is a modified version of the stirred-flow reactor described by Wielinga et al. (2001). The chamber volume is 12.0 mL. All stirred-flow reactions were conducted by pumping a solution of As(III) and Fe(II) in a 0.01 mol/L $NaNO_3$ background electrolyte buffered at a certain pH at a rate of 1.0 mL/min into a stirred-flow chamber containing 2.0 g/L δ-MnO_2. For reactions involving Fe(II), nitrogen gas was pumped into the solution to maintain anoxic conditions. All suspensions in the reaction chamber were mixed at 100 rpm via a

magnetic stir bar. Effluent solutions were filtered with a 0.22 μm pore size filter and then collected by a fraction collector. Effluent solutions which contained Fe(II) were immediately transferred into a glove box until analysis, and all other solutions were stored at 4 ºC in the dark until analysis. All stirred-flow experiments were conducted at least in duplicate.

In all desorption reactions, 2 g/L δ-MnO_2 was reacted with 100 μmol/L As(III) and 100 or 1000 μmol/L Fe(II) at pH 6 for 36 hours to ensure enough amounts of As(III) oxidation and As sorption on solid phase, followed immediately by reaction with a desorptive solution. Three desorptive solutions were used, including (1) 0.01 mol/L $NaNO_3$ background electrolyte alone, (2) 100 μmol/L calcium chloride in background electrolyte, and (3) 100 μmol/L sodium phosphate in background electrolyte. Prior to experiments, all desorptive solutions were adjusted to pH 6 with HCl and NaOH and pumped with nitrogen gas for 4 hours to maintain anoxic conditions. Background electrolyte was introduced into the stirred flow reactor (containing δ-MnO_2) for at least 2 hours at a rate of 1 mL/min prior to each experiment. In each reaction, As(III) oxidation was stopped after 36 hours by introducing the desorptive solution into the reactor, thus beginning the desorption phase of the reaction. Changing the influent solution from As(III) and Fe(II) solution to the desorbent solution took less than 5 seconds, and thus flow of solution into the reactor was effectively constant throughout each experiment (oxidation followed by desorption). A plot showing the full data, As(III) and Fe(II) oxidation followed by desorption from one experiment is presented in Figure 4.1.

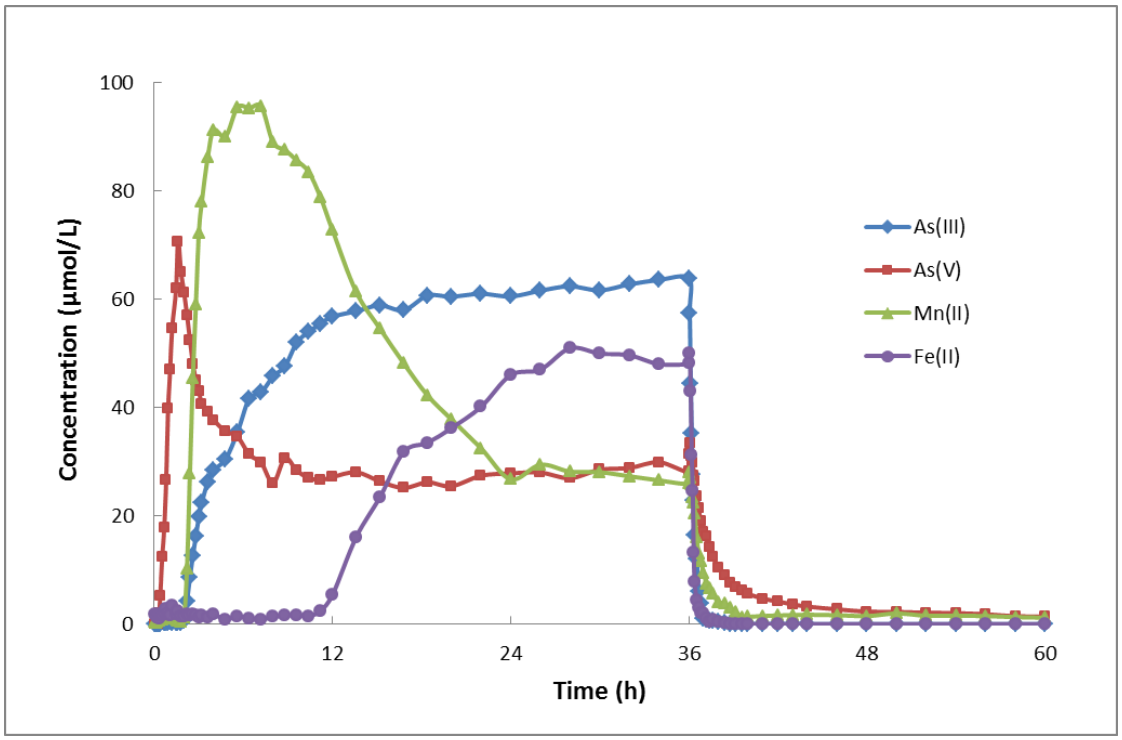

Figure 4.1 As(III), As(V), Mn(II) and Fe(II) concentrations from one replicate of 100 µmol/L As(III) oxidation by 2 g/L δ-MnO_2 in the presence of 100 µmol/L Fe(II) for 36 hours at pH 6, followed by desorption by 100 µmol/L sodium phosphate in a background electrolyte for another 24 hours, starting from 36 h to 60 h in the plot.

4.2.4 XAS Analysis

X-ray absorption spectroscopic analysis was performed on reacted δ-MnO_2 after 36 hours oxidation followed by 24 hours desorption. When the reaction was completed, the suspension in the reaction chamber was immediately filtered (0.22 µm) to remove any background electrolyte, and Mn(II), Fe(II) and As not bound to δ-MnO_2. After filtration, the residual wet paste was immediately covered with Kapton tape and stored under anoxic conditions for less than 3 days prior to spectroscopic analysis.

An As(V)-δ-MnO_2 sorption standard was prepared by reacting 100 μmol/L As(V) with 2 g/L δ-MnO_2 at pH 6 for 48 h in the same background electrolyte used in the stirred-flow reactions. As(V)- and As(III)-ferrihydrite sorption standards were prepared by reacting 100 μmol/L As(V) and 100 μmol/L As(III), respectively, with 2 g/L ferrihydrite at pH 6 for 48 h in the same background electrolyte used in the stirred-flow studies. An Fe(II)-δ-MnO_2 standard was prepared by reacting 100 μmol/L Fe(II) with 2 g/L δ-MnO_2 at pH 6 for 48 h in the same background electrolyte used in the stirred-flow studies. All standards were filtered, and the residual wet paste was immediately covered with Kapton tape and stored under anoxic conditions, for less than 3 days before spectroscopic analysis.

Extended X-ray absorption fine structure (EXAFS) and X-ray absorption near edge (XANES) spectroscopic data for As were collected at the National Synchrotron Light Source (Brookhaven National Laboratory) on beamline X-11A. The electron storage ring operates at 2.8 GeV with a current ranging from 300 to 150 mA. The monochromator consisted of two parallel Si-(111) crystals with a vertical entrance slit separation of 0.5 mm. As (11.9 keV) K-edge EXAFS spectra were collected. All samples were oriented at 45 °to the incident beam and a Lytle detector was used to collect As spectra in fluorescence mode. The monochromator angle was calibrated to the As(V) K-edge (11.874 keV) using diluted $Na_2HAs^VO_4$ as a standard (10% $Na_2HAs^VO_4$ with 90% boron nitride). This standard was monitored in transmission mode simultaneous to sample collection to check for potential shifts in their respective K-edges. Multiple scans were collected at room temperature for each sample to improve the signal-to-noise ratio for data analysis.

EXAFS and XANES spectroscopic data for Fe were collected at beamline 4-1 at the Stanford Synchrotron Radiation Lightsource (SSRL). The electron storage ring operates at 3.0 GeV with a current ranging from 100 to 90 mA. The monochromator consisted of two parallel Si-(220) crystals with a vertical entrance slit separation of 0.5 mm. Fe (7.1 keV) K-edge EXAFS spectra were collected in fluorescence mode. The monochromator crystals were detuned 40 % for Fe in I_0 to reject higher order harmonics. A 3-path length Mn filter was used, and Sollier slits were used for signal optimization and removal of elastically scattered radiation. The monochromator angle was calibrated to the Fe(0) K-edge (7.112 keV) using a Fe metal foil. This standard was monitored in transmission mode simultaneous to sample collection to check for potential shifts in their respective K-edges. Multiple scans were collected at room temperature for each sample to improve the signal-to-noise ratio for data analysis.

For data analysis, As K-edge EXAFS data were analyzed by shell-by-shell fitting of the Fourier transformed EXAFS spectra (k-range 3 to 13 $Å^{-1}$, r -range 0.8 to 4 Å) using the SixPACK (Webb, 2005) interface to IFEFFIT (Newville, 2001). The theoretical scattering paths were calculated using the FEFF 7.2 code (Ankudinov and Rehr, 1997). Flinkite ($Mn_3(OH)_4AsO_4$) was used as a structural model for As(V) sorbed on δ-MnO_2. Scorodite ($FeAsO_4 \cdot H_2O$) and tooeleite ($Fe_6(AsO_3)_4SO_4(OH)_4 \cdot 4H_2O$) were used as structural models for As(V) and As(III) sorbed on Fe-oxides (Morin et al., 2008; Wang et al., 2008). In the As EXAFS fitting, we considered As–O and As–Fe/Mn single scattering (SS) paths and one multiple scattering (MS) path (triangular As-O-O) within the AsO_4 tetrahedron or AsO_3 pyramid. The degeneracy of the As-O-O MS path was fixed to the theoretical value of 12 for As(V) and 6 for As(III).

Linear combination fitting (LCF) was performed on the Fe EXAFS spectra over the k-range of 3 to 12 $Å^{-1}$ using SixPACK's least square fitting module, which is a graphical interface for IFEFFIT's minimization function (Newville, 2001). A set of reference spectra were used for LCF, including 2-line ferrihydrite, goethite, lepidocrocite, hematite, magnetite and synthetic ferric arsenate. Both shell-by-shell fitting and linear combination fitting were optimized by minimizing reduced σ^2 (Newville et al., 1995).

4.2.5 Determination of Metal Concentrations

As(III) and As(V) were quantified by liquid chromatography inductively coupled plasma mass spectrometry (LC-ICP-MS). As(III) and As(V) were separated using a Phenomenex Prodigy 5 μm ODS-3 100 Å (150 x 4.6) column with a flow rate of 1 mL/min, using a 10 μm sample injection before quantification by LC-ICP-MS. The mobile phase consisted of 5% methanol in 5 mM tetra-butyl ammonium hydroxide, and the pH was adjusted to 5.9 using malonic acid (final concentration of about 3 mM). Arsenic species separated by LC were directly introduced via a nebulizer into an Agilent 7500ce inductively coupled plasma mass spectrometer operated in helium mode. Fe(II) concentration was determined by the ferrozine method (Stookey, 1970). In order to eliminate the interference of Fe(III) in Fe(II) measurements, 0.05 mol/L NaF was added to mask Fe(III) in Fe(II) determination. Total Fe was determined by reducing total Fe(III) to Fe(II) and then Fe(II) was measured by the ferrozine method without addition of NaF solution. The Fe(III) content in the liquid solution was obtained by difference. Mn, Ca, and P concentrations were quantified by inductively coupled plasma optical emission spectrometry (ICP-OES), where 5 mL of sample were acidified using 1% (w/v) nitric

acid mixed with 0.5% (w/v) hydrochloric acid. The amount of As sorbed/desorbed during the reaction was determined by calculating the difference between the mass of As (μmol) introduced into the reactor and the mass of As (μmol) removed from the reactor over time (more details please see Appendix B).

4.3 Results and Discussion

4.3.1 As(III) Oxidation and Sorption

All desorption experiments in this study are preceded by reaction of 100 μmol/L As(III) oxidation by 2 g/L δ-MnO_2 in the presence of either 100 or 1000 μmol/L Fe(II) for 36 hours at pH 6. Two Fe(II) concentrations were used in order to investigate As mobility under different As(III) to Fe(II) ratios, 1 to 1 and 1 to 10, in the initial oxidation reactions. To better understand the desorption process, we summarize As(III) oxidation and sorption behaviors from the results of stirred-flow experiments and spectroscopic analysis (Chapter 2 and 3). This initial reaction among As(III), Fe(II) and δ-MnO_2 involves three key steps: (1) As(III) and Fe(II) are adsorbed onto the δ-MnO_2 surface where they are immediately oxidized into As(V) and Fe(III), respectively, and Mn(II) is released to solution. Competition for active sites on δ-MnO_2 exists between As(III) and Fe(II); (2) Fe(III) precipitates as ferrihydrite and goethite like Fe(III)-(hydr)oxides on the δ-MnO_2 surface, causing surface passivation, which lowers the oxidation rates of both As(III) and Fe(II); and (3) the remaining As(III), As(V), Mn(II) and Fe(II) are partially adsorbed onto the produced Fe(III)-(hydr)oxides. Also, some As(V) and Mn(II) can be adsorbed on δ-the MnO_2 surface. The oxidation of As(III) and Fe(II) proceedes in two distinct phases, a fast oxidation phase during the initial few hours followed by a slow oxidation phase

due to the surface passivation of δ-MnO_2. After 24 hours, the reaction reaches a steady state phase, where concentrations of all metals in solution stay constant. Therefore, 36 hours after reaction was chosen as the starting point for our desorption study (Fig. 4.1).

4.3.2 As(III) Desorption

When the As(III) to Fe(II) ratio is 1 to 1 in the initial reaction, As(III) concentration in solution follows the dilution curve very well, no matter what desorptive was used (Fig. 4.2). This suggests that no As(III) was desorbed from the solid phase using any of the three desorptives, which agrees with previous findings in Chapter 3 that no As(III) is adsorbed on the solid phase during As(III) oxidation by δ-MnO_2 in the presence of Fe(II) when the As(III) to Fe(II) ratio is 1 to 1. Besides, As K-edge XANES analysis also proves that no As(III) is found to be associated with the solid phase after 24 hours of desorption (Fig. 4.4 a).

When the As(III) to Fe(II) ratio was 1 to 10 in the initial reaction, As(III) was found to be desorbed from the solid phase (Fig. 4.3). Among the three desorptives, PO_4^{3-} desorbed the most As(III), 20.56 μmol, followed by Ca^{2+}, which desorbed 16.55 μmol As(III), and the background electrolyte (BE) desorbed the least As(III), 13.52 μmol (Table 4.1). This trend was also supported by the As XANES spectra (Fig. 4.4 a), where the As(III) peak intensity decreased in the order of BE > Ca > P. In spite of the desorptive, As(III) desorption was greater than As(V) desorption (Table 4.1), which can be ascribed: (1) in the presence of high Fe(II) concentrations, most of the As(III) is adsorbed in the unoxidized form on the produced Fe(III)-(hydr)oxides, since a large amount of Fe(II) competes with As(III) for the limited amount of δ-MnO_2; and (2) although As(III) can adsorb to a greater extent on iron oxides than As(V) (Raven et al., 1998; Dixit and Hering, 2003; Herbel and Fendorf, 2006), a substantial portion of

As(III) is bound in weak complexes (Goldberg and Johnston, 2001; Catalano et al., 2007), leading to extensive desorption upon a change in solute conditions (Ying et al., 2012). Although a large amount of As(III) is desorbed from the solid phases, some As(III) remained on the solids after 24 hours of desorption, since the As(III) peak was observed in the XANES spectra (Fig. 4.4 a). Also, from EXAFS fitting results in Table 4.2, the relatively longer As-O distance (> 1.69 Å) and lower coordination number (< 4) are both indications of the presence of As(III) in the solids after desorption.

Table 4.1 The amount (μmol) of As(III), As(V), Fe(II) and Mn(II) desorbed by Ca^{2+}, PO_4^{3-}, and background electrolyte (BE) for 24 hours after 100 μmol/L As(III) oxidation by 2 g/L δ-MnO_2 in the presence of either 100 or 1000 μmol/L Fe(II) for 36 hours at pH 6.

Metals	Desorption Amount (μmol)					
	As(III):Fe(II)=1:1			As(III):Fe(II)=1:10		
	BE	Ca^{2+}	PO_4^{3-}	BE	Ca^{2+}	PO_4^{3-}
As(III)	-	-	-	13.52	16.55	20.56
As(V)	2.40	3.12	8.98	4.70	6.32	14.53
Mn(II)	4.45	8.53	4.07	11.91	21.78	12.76
Fe(II)	-	-	-	9.19	13.27	9.70
% of As desorbed	11.8%	15.4%	44.3%	11.1%	14.0%	21.4%

Note: The total As sorbed (As(III) and As(V)) calculated from previous stirred-flow experiments are 20.26 μmol and 163.63 μmol for reaction of 100 μmol/L As(III) oxidation by 2 g/L δ-MnO_2 in the presence of either 100 or 1000 μmol/L Fe(II), respectively. The percent of As desorbed is calculated as the quantity of As desorbed divided by the quantity of As sorbed.

4.3.3 As(V) Desorption

Desorption of As(V) from the solid phase was observed for both initial reactions, with either As(III):Fe(II)=1:1 or 1:10 (Fig. 4.2 and 4.3). For all three desorptivrd, more As(V) was desorbed using an initial reaction with As(III):Fe(II)=1:10 (Table 4.1), for more Fe(III)-(hydr)oxides are formed in initial reaction with As(III):Fe(II)=1:10 so that more As(V) is adsorbed to the solids. Similar to As(III) desorption, PO_4^{3-} desorbs the most amount of As(V), about 2 to 4 times as the amounts desorbed by Ca^{2+} or the background electrolyte (Table 4.1). Due to similarities in acid dissociation constants and coordination geometry, phosphate (pK_{a1}=2.1, pK_{a2}=7.2 and pK_{a3}=12.3) behaves much like arsenate (pK_{a1}=2.2, pK_{a2}=6.9 and pK_{a3}=11.4) (Silva et al., 2012). It has been reported that phosphate could desorb arsenate more readily and more efficiently from metal oxide minerals, compared to other ions such as carbonate, silicate, calcium, magnesium, potassium and sodium etc. (Luxton et al., 2008; Lafferty et al., 2011; Silva et al., 2012; Neupane et al., 2014). As a percentage of total As, 44.3 % of the sorbed As can be desorbed by PO_4^{3-} when the As(III):Fe(II)=1:1 in the initial reaction, while only 21.4 % of the sorbed As can be desorbed by PO_4^{3-} when the As(III):Fe(II)=1:10 in the initial reaction. A desorption study by Lafferty et al. (2011) showed that roughly 67% of the sorbed As was mobilized from the δ-MnO_2 surface after 24 hours of desorption by PO_4^{3-}. Compared with the As desorption fractions in the current study, more As tends to be sequestrated on the solid phase in the presence of Fe(II)/Fe(III)-(hydr)oxides and the fraction of desorbed As decreases as the Fe(II) to As(III) ratio increases. This indicates that As sorbed on the Fe(III)-(hydr)oxides surface is less mobile than As sorbed on the δ-MnO_2 surface.

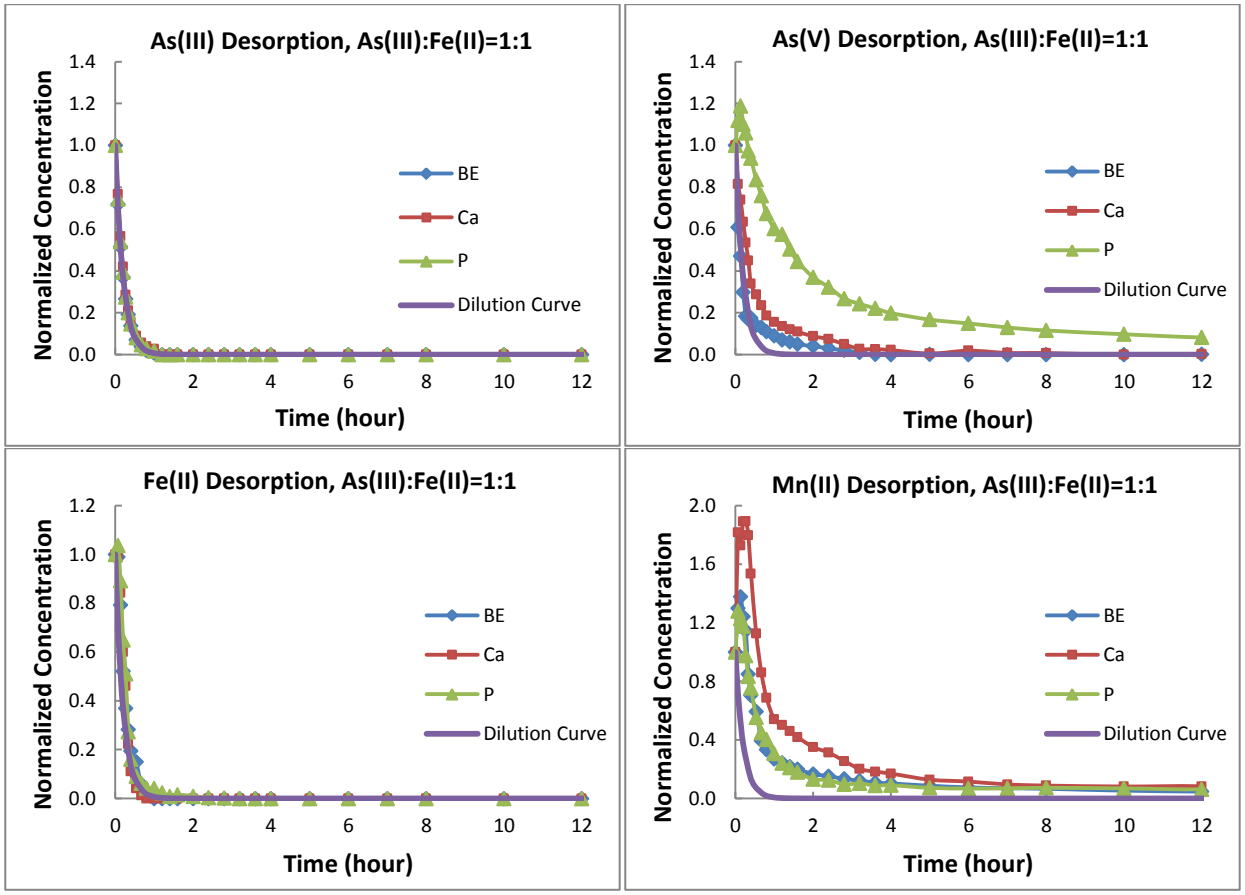

Figure 4.2 As(III), As(V), Fe(II) and Mn(II) desorbed by Ca^{2+}, PO_4^{3-}, and background electrolyte (BE) after 100 μmol/L As(III) oxidation by 2 g/L δ-MnO_2 in the presence of 100 μmol/L Fe(II) for 36 hours at pH 6. The data points on each graph are normalized by the initial concentration at the beginning of desorption. As(III) oxidation data prior to desorption are not shown and data shown are the first 12 h of 24 h desorption experiments.

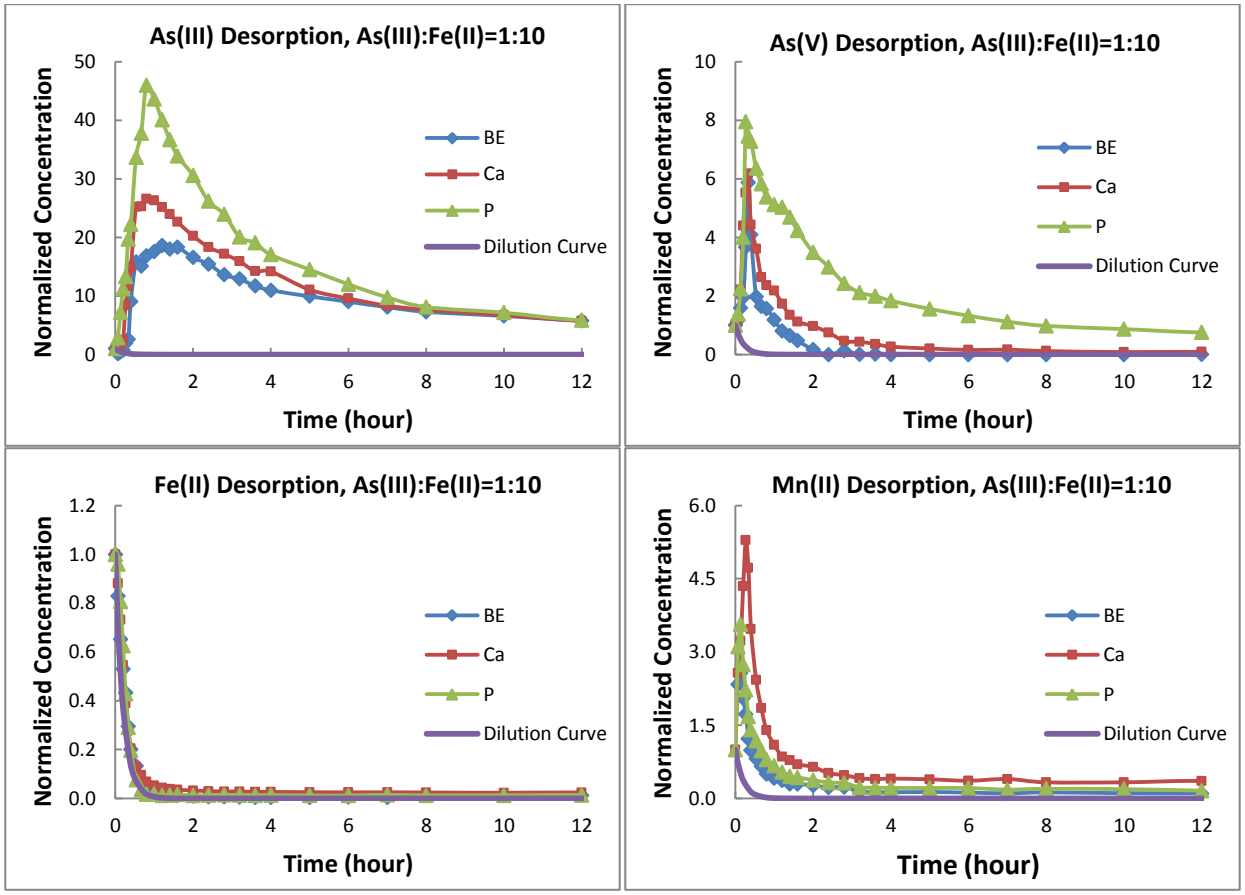

Figure 4.3 As(III), As(V), Fe(II) and Mn(II) desorbed by Ca^{2+}, PO_4^{3-}, and background electrolyte (BE) after 100 µmol/L As(III) oxidation by 2 g/L δ-MnO_2 in the presence of 1000 µmol/L Fe(II) for 36 hours at pH 6. The data points on each graph are normalized by the initial concentration at the beginning of desorption. As(III) oxidation data prior to desorption are not shown and data shown are the first 12 h of 24 h desorption experiments.

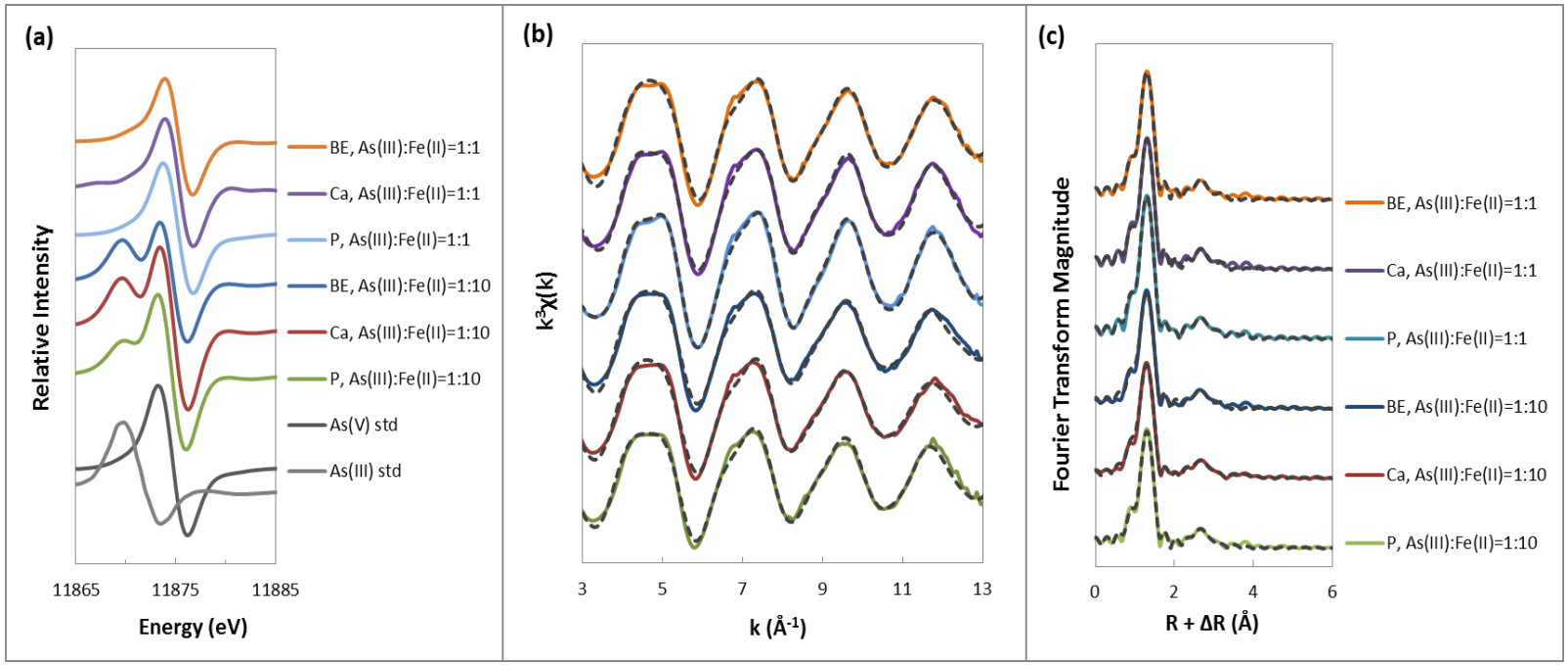

Figure 4.4 (a) Arsenic K-edge derivative XANES; (b) As K-edge EXAFS; and (c) Fourier transformed EXAFS of desorption by Ca^{2+}, PO_4^{3-}, and background electrolyte (BE) for 24 hours after 100 µmol/L As(III) oxidation by 2 g/L δ-MnO_2 in the presence of either 100 or 1000 µmol/L Fe(II) for 36 hours at pH 6. XAS data are presented as solid lines, and fits are presented as dashed lines.

Table 4.2 Structural parameters derived from shell-by-shell fits to k^3-weighted As EXAFS data of 100 μmol/L As(III) oxidation by 2 g/L δ-MnO_2 in the presence of either 100 or 1000 μmol/L Fe(II) for 36 hours at pH 6, and then desorbed by Ca^{2+}, PO_4^{3-}, and background electrolyte (BE) for 24 hours. Fitting parameters for sorption standards of As(V) on δ-MnO_2, As(III) and As(V) on ferrihydrite (Fh), as well as a standard of a synthetic ferric arsenate precipitate was also provided.

Sample	Desorbent	As-O			As-O-O			As-Mn/Fe			ΔE_o	S_o^2	R factor
		CN	R	σ^2	CN	R	σ^2	CN	R	σ^2			
As(III):Fe(II)=1:1	BE	4.00	1.69	0.003	12	3.12	0.007	1.92	3.32	0.011	5.88	0.97	0.0118
	Ca^{2+}	3.99	1.69	0.003	12	3.12	0.008	1.90	3.32	0.011	5.57	0.95	0.0133
	PO_4^{3-}	4.03	1.69	0.003	12	3.11	0.011	1.35	3.33	0.007	5.72	0.91	0.0112
As(III):Fe(II)=1:10	BE	3.55	1.71	0.004	12	3.11	0.008	1.92	3.32	0.009	4.68	0.92	0.0159
	Ca^{2+}	3.69	1.71	0.004	12	3.12	0.012	1.98	3.32	0.011	3.82	0.91	0.0163
	PO_4^{3-}	3.84	1.71	0.003	12	3.12	0.007	1.34	3.31	0.009	4.08	0.92	0.0162
Standards	As(V)-δ-MnO_2	3.97	1.69	0.002	12	3.08	0.005	0.52	3.21	0.005	6.44	0.97	0.0167
	As(V)-Fh	4.55	1.69	0.002	12	3.09	0.010	0.92	3.29	0.006	5.30	0.91	0.0097
	As(III)-Fh	2.96	1.79	0.004	6	3.20	0.007	1.05	3.35	0.006	9.05	0.91	0.0146
	Ferric Arsenate	4.38	1.69	0.002	12	3.11	0.003	1.79	3.33	0.003	6.33	0.98	0.0086

Note: CN, coordination number, uncertainty for As-O is ±0.1-0.47, for As-Mn/Fe is ±0.18-0.54, $CN_{As\text{-}O\text{-}O}$ is fixed to 12; R(Å), interatomic distance, uncertainty for As-O is ±0.002-0.003, for As-Mn/Fe is ±0.01-0.03; σ^2, Debye-Waller factor, uncertainty for As-O is ±0.001-0.002, for As-Mn/Fe is ±0.001-0.013; ΔE_0 (eV), difference between experimentally determined threshold energy and the FEFF calculated threshold energy, uncertainty is ±0.3-2.1; S_0^2, amplitude reduction factor, uncertainty is ±0.02-0.15; R factor, goodness of fit, $R=\sum(\text{data-fit})^2/\sum\text{data}^2$.

Shell-by-shell fits of the As EXAFS spectra of solids after 24 hours desorption showed that only one second As-Fe/Mn shell was found between 3.31 Å and 3.33 Å, with coordination number about 2. These distances and coordination numbers are in good agreement with a As bidentate binuclear corner-sharing complex on Fe oxides (Fendorf et al., 1997; Waychunas et al., 1993; Manning et al., 2002; Manceau et al., 2003) as well as a As(V)-Fe(III) precipitate (e.g. ferric arsenate), suggesting that the un-desorbed As is either in a precipitate phase or in the form of a bidentate binuclear complex on Fe(III)-(hydr)oxides. A previous study by Sherman and Randall (2003) using density functional theory calculations showed the bidentate binuclear complex was more favored energetically and more stable than the monodentate complex. It was also observed that As in monodentate complexes with iron oxides was more readily desorbed compared with that in bidentate complexes, which was due to the weaker binding strength of the Fe-As bond in the monodentate complexes (Grossl et al., 1997). Both of these also explains why the bidentate binuclear complex is the dominate species after desorption.

4.3.4 Mn(II) Desorption

Desorption of Mn(II) from the solid phase was observed in both initial reactions, with either As(III):Fe(II)=1:1 or 1:10 (Fig. 4.2 and 4.3). For all three desorptives, more Mn(II) was desorbed from an initial reaction with As(III):Fe(II)=1:10 than the other one (Table 4.1), since more δ-MnO_2 is reduced in the presence of higher Fe(II) concentration, resulting in more Mn(II) adsorbed to the solids. Of the three desorptives used in this study, Ca^{2+} is expected to react with sorption sites on Fe/Mn-oxides most similar to Mn(II). It has been reported that Ca^{2+} can compete with many transition metals for sorption sites on metal oxides surfaces

(Cowan et al., 1991; Ridley et al., 1999; Lafferty et al., 2011). Lafferty et al. (2011) postulated that Ca^{2+} could bind in triple corner sharing complexes at the vacancy sites of δ-MnO_2, which is the primary location of Mn(II) sorption on δ-MnO_2. Similar to previous studies, we found that Ca2+ desorbed the most Mn(II), twice as much as the amount desorbed by PO43- or the background electrolyte for both initial reactions with either As(III):Fe(II)=1:1 or 1:10 (Table 4.1).

4.3.5 Fe(II) Desorption and Fe(III)-(hydr)oxides after Desorption

When the As(III) to Fe(II) ratio is 1 to 1 in the initial reaction, the Fe(II) concentration in solution followed the dilution curve very well, no matter what desorptive was used (Fig. 4.2). This suggests that no Fe(II) is desorbed from the solid phase using any of the three desorptives, which agrees with our previous finding in Chapter 3 that no Fe(II) is adsorbed on the solid phase during As(III) oxidation by δ-MnO_2 in the presence of Fe(II) when the As(III) to Fe(II) ratio is 1 to 1. Besides, Fe K-edge XANES analysis also proved that no Fe(II) was found to be associated with the solid phases after 24 hours of desorption (Fig. 4.5 a). When the As(III) to Fe(II) ratio was 1 to 10 in the initial reaction, Fe(II) was desorbed from the solid phase (Fig. 4.3). Similar to Mn(II) desorption, Ca^{2+} desorbed the largest amount of Fe(II), 13.27 μmol, since Ca^{2+} reaction with sorption sites on Fe/Mn-oxides was most similar to Fe(II). PO_4^{3-} and the background electrolyte desorbed almost equal amounts of Fe(II), 9.7 and 9.19 μmol, respectively (Table 4.1). For all three desorptives, Fe(II) peaks were observed in the Fe XANES spectra (Fig 4.5 a), meaning that there were still amounts of Fe(II) associated with the solid phases after 24 hours of desorption.

Fe K-edge EXAFS spectra of the solid phases after 24 hours desorption were also analyzed by linear combination fitting in order to investigate the composition of

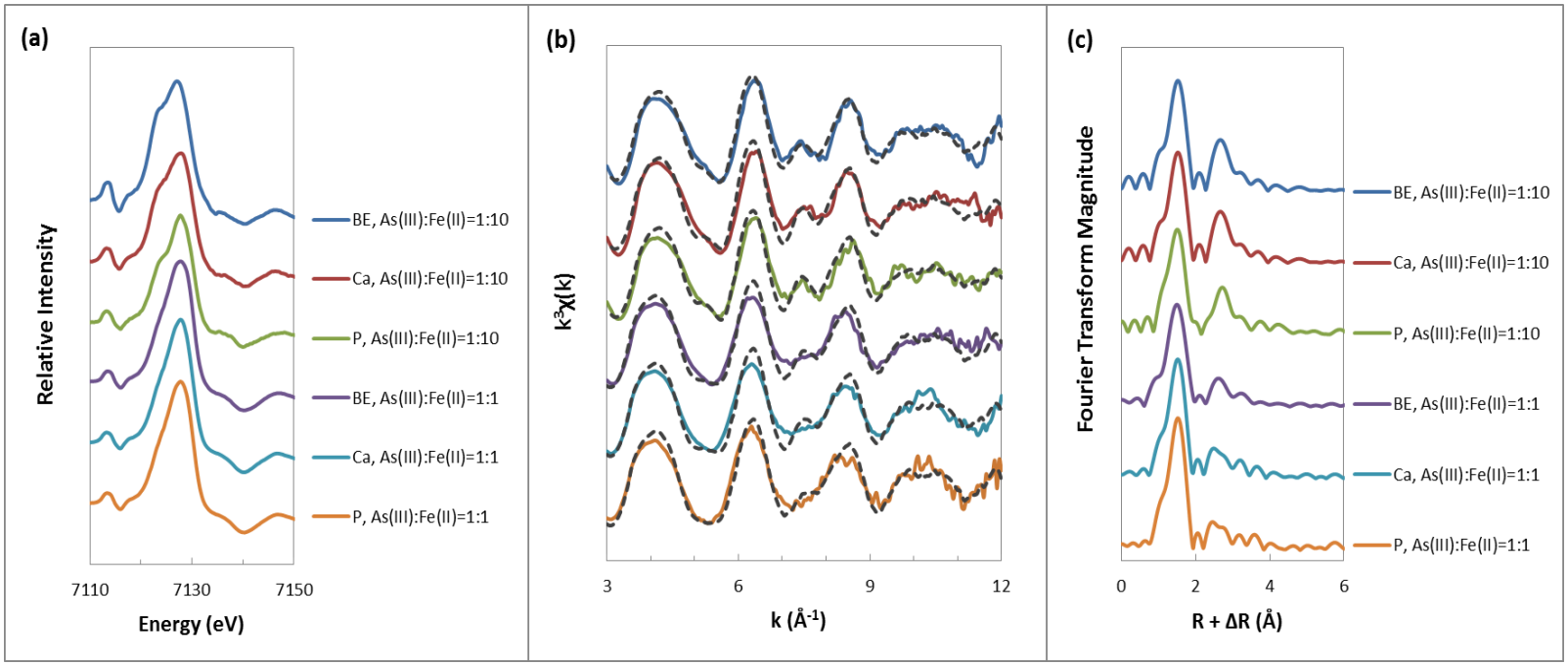

Figure 4.5 (a) Fe K-edge derivative XANES; (b) Fe K-edge EXAFS; and (c) Fourier transformed EXAFS of desorption by Ca^{2+}, PO_4^{3-}, and background electrolyte (BE) for 24 hours after 100 μmol/L As(III) oxidation by 2 g/L δ-MnO_2 in the presence of either 100 or 1000 μmol/L Fe(II) for 36 hours at pH 6. XAS data are presented as solid lines, and fits are presented as dashed lines.

Table 4.3 Mineralogical composition of Fe(III)-(hydr)oxides derived from linear combination fits to k^3-weighted Fe EXAFS data of 100 μmol/L As(III) oxidation by 2 g/L δ-MnO_2 in the presence of either 100 or 1000 μmol/L Fe(II) for 36 hours at pH 6, and then desorbed by Ca^{2+}, PO_4^{3-}, and background electrolyte (BE) for 24 hours.

Sample	Desorbent	Standards				R factor
		Ferric Arsenate	Ferrihydrite	Goethite	Lepidocrocite	
As(III):Fe(II)=1:1	BE	51.6 ± 2.8 %	42.3 ± 3.2 %	6.1 ± 0.9 %	-	0.0789
	Ca^{2+}	43.7 ± 4.1 %	46.8 ± 2.3 %	5.3 ± 2.0 %	4.2 ± 0.9 %	0.0714
	PO_4^{3-}	41.2 ± 2.1 %	47.3 ± 1.8 %	7.0 ± 1.4 %	4.5 ± 0.5 %	0.0593
As(III):Fe(II)=1:10	BE	23.1 ± 1.1 %	60.3 ± 4.3 %	8.3 ± 0.7 %	8.3 ± 1.3 %	0.0452
	Ca^{2+}	21.3 ± 1.7 %	58.1 ± 2.8 %	10.7 ± 0.9 %	9.9 ± 1.2 %	0.0507
	PO_4^{3-}	16.3 ± 1.3 %	60.8 ± 3.5 %	17.1 ± 1.6 %	5.8 ± 0.4 %	0.0463

Note: R factor, goodness of fit, $R=\sum(data-fit)^2/\sum data^2$.

the Fe(III)-(hydr)oxides. The fitting results are shown in Table 4.3 and data fits are plotted in Figure 4.5 b. The mineralogical composition of the solids before desorption was presented in Chapter 3 (Table 3.3). Four major Fe(III)-(hydr)oxides were found in the solids after desorption, including ferric arsenate, ferrihydrite, goethite and lepidocrocite, which are the same as our previous results. For the initial reaction with As(III):Fe(II)=1:1, the ferric arsenate fraction decreased from 56.1 % before desorption to 41.2 ~ 51.6 % after desorption, while the fractions of ferrihydrite, goethite and lepidocrocite increased slightly. This indicates that the As associated with Fe(III) (hydr)oxides during the initial reaction was not immobile and could be partially dissolved during the desorption reaction, resulting in the release of As. For the initial reaction with As(III):Fe(II)=1:10, the fraction of each Fe(III)-(hydr)oxide does not change much after desorption.

4.4 Conclusions

The mobility of As in the environment is governed largely by its chemical speciation, as well as mineral-surface interactions. As adsorbs to a wide range of minerals, including Fe, Al and Mn oxides. The current study examined the competitive sorption/desorption between As and two environmental significant ions (Ca^{2+} and PO_4^{3-}) from a mixed Fe/Mn-oxides surface. This study showed that As can be desorbed from the Fe/Mn-oxides surface, to some extent, under all conditions studied. Even the background electrolyte (Na^{+}) was able to desorb As to some degree, indicating that a portion of As sorbed on Fe/Mn-oxides is potentially quite mobile in the environment. More As(III) was desorbed than As(V), due to the weaker binding of As(III) with Fe/Mn-oxides. Although some sorbed As can be desorbed from the Fe/Mn-oxides surface, there is still a certain amount of As that was not desorbed under any of the conditions studied. Thus, if As comes in contact with Mn and Fe oxides in nature, these minerals could potentially decrease As availability and mobility by oxidation of As(III) and sorption of both As(III) and As(V). This study emphasizes the importance of understanding competitive effects of co-existing ions when predicting As mobility in the environment.

REFERENCES

Ankudinov, A.L., and J.J. Rehr. 1997. Relativistic calculations of spin-dependent X-ray-absorption spectra. Phys. Rev., B 56: R1712.

Antelo, J., Avena, M., Fiol, S., Lopez, R., Arce, F., 2005. Effects of pH and ionic strength on the adsorption of phosphate and arsenate at the goethite-water interface. Journal of Colloid and Interface Science, 285: 476–486.

Catalano, J.G., Park, C., Fenter, P., Zhang, Z., 2008. Simultaneous inner- and outersphere arsenate adsorption on corundum and hematite. Geochimica et Cosmochimica Acta, 59: 3647–3653.

Catalano J. G., Zhang Z., Park C., Fenter P. and Bedzyk M. J., 2007. Bridging arsenate surface complexes on the hematite (012) surface. Geochimica et Cosmochimica Acta, 71(8): 1883–1897.

Cowan, C.E., Zachara, J.M., and Resch, C.T., 1991. Cadmium Adsorption on Iron Oxides in the Presence of Alkaline-Earth Elements. Environmental Science and Technology, 25: 437–466.

Dong, H., Guan, X., and Irene, M.C.L., 2012. Fate of As(V)-treated nano zero-valent iron: Determination of arsenic desorption potential under varying environmental conditions by phosphate extraction. Water Research, 46: 4071–4080.

Dixit, S., and J.G. Hering. 2003. Comparison of arsenic(V) and arsenic(III) sorption onto iron oxide minerals: Implications for arsenic mobility. Environmental Science and Technology, 37: 4182-4189.

Drits, V.A., E. Silvester, A.I. Gorshkov, and A. Manceau. 1997. Structure of synthetic monoclinic Na -rich birnessite and hexagonal birnessite. 1. Results from X – ray diffraction and selected-area electron diffraction. American Mineralogist, 82: 946 -961.

Farquhar, M. L., Charnock, J. M., Livens, F. R., and Vaughan, D. J. 2002. Mechanisms of arsenic uptake from aqueous solution by interaction with goethite, lepidocrocite, mackinawite, and pyrite: An X-ray absorption spectroscopy study. Environmental Science and Technology, 36: 1757-1762.

Fendorf, S., M.J. Eick, and P. Grossl. 1997. Arsenate and chromate retention mechanisms on goethite. 1. Surface structure. Environmental Science and Technology, 31:315-320.

Gao, X., Root, R., Farrell, J., Ela, W. and Chorover, J., 2013. Effect of silicic acid on arsenate and arsenite retention mechanisms on 6-L ferrihydrite: A spectroscopic and batch adsorption approach. Applied Geochemistry, 38: 110–120.

Goh, K.H., Lim, T.T., 2005. Arsenic fractionation in a fine soil fraction and influence of various anions on its mobility in the subsurface environment. Applied Geochemistry, 20: 229–239.

Goldberg, S., and Johnston, C.T. 2001. Mechanisms of arsenic adsorption on amorphous oxides evaluated using macroscopic measurements, vibrational spectroscopy, and surface complexation modeling. J. Colloid Interf. Sci., 234: 204–216.

Grossl, P.R., Eick, M., Sparks, D.L., Ainsworth, C.C., 1997. Arsenate and chromate retention mechanisms on goethite. 2. Kinetic evaluation using a pressure-jump relaxation technique. Environmental Science and Technology, 31: 321–326.

Herbel, M. and Fendorf , S. 2006. Biogeochemical processes controlling the speciation and transport of arsenic within iron coated sands. Chem. Geol. 228: 16–32.

Jia, Y., Xu, L., Fang, Z., Demopoulos, G.P. 2006. Observation of Surface Precipitation of Arsenate on Ferrihydrite. Environ. Sci. Technol. 40: 3248-3253.

Lafferty, B., M. Ginder-Vogel and D.L. Sparks. 2011. Arsenite oxidation by a poorly crystalline manganese-oxide 3. Arsenic and manganese desorption. Environmental Science and Technology, 45(12): 9218–9223.

Luxton, T.P., Eick., M.J., and Rimstidt, D.J., 2008. The role of silicate in the adsorption/desorption of arsenite on goethite. Chemical Geology, 252: 125–135.

Mandal, B.K., and K.T. Suzuki. 2002. Arsenic Round the World: a review. Talanta. 58:201-235.

Manning, B.A., Fendorf, S.E., and Goldberg, S., 1998. Surface Structures and Stability of Arsenic(III) on Goethite: Spectroscopic Evidence for Inner-Sphere Complexes. Environmental Science and Technology, 32: 2383–2388.

Manning, B.A., Fendorf, S.E., Bostick, B., Suarez, D.L. 2002. Arsenic(III) oxidation and arsenic(V) adsorption reactions on synthetic birnessite. Environ. Sci. Technol. 36:976-981.

Mohan, D., Pittman, C. U. 2007. Arsenic removal from water/wastewater using adsorbents-a critical review, J. Hazard. Mater. 142:1-53.

Morgan, J.J., and W. Stumm. 1964. Colloid-chemical properties of manganese dioxide. J. Colloid Sci. 19:347-359.

Morin, G., Ona-Nguema, G., Wang, Y., Menguy, N., Juillot F., Proux, O., Guyot, F., Calas, G. and Brown, Jr., G. E. 2008. Extended X-ray absorption fine structure analysis of arsenite and arsenate adsorption on maghemite. Environ. Sci. Technol. 42: 2361–2366.

Neupane, G., Donahoe, R.J., and Arai, Y., 2014. Kinetics of competitive adsorption/desorption of arsenate and phosphate at the ferrihydrite-water interface. Chemical Geology, 368: 31–38.

Newville, M. 2001. IFEFFIT : Interactive XAFS analysis and FEFF fitting. J. Synchrotron Radiat. 8: 322 -324.

Newville, M., B. Ravel, D. Haskel, J.J. Rehr, E.A. Stern, and Y. Yacoby. 1995. Analysis of multiple-scattering XAFS data using theoretical standards. Physica B: Condensed Matter 208-209:154-156.

Oinam, J.D., Ramanathan, A.L., Linda, A., Singh, G., 2011. A study of arsenic, iron and other dissolved ion variations in the groundwater of Bishnupur District, Manipur, India. Environmental Earth Sciences, 62: 1183–1195.

Parikh, S.J., B. J. Lafferty, T. G. Meade and D.L. Sparks. 2010. Evaluating environmental influences on AsIII oxidation kinetics by a poorly crystalline Mn-oxide. Environ. Sci. Technol. 44: 3772-3778.

Raven, K.P., A. Jain, and R.H. Loeppert. 1998. Arsenite and arsenate adsorption on ferrihydrite: kinetics, equilibrium, and adsorption envelopes. Environ. Sci. Technol. 32: 344-349.

Ridley, M.K., Machesky, M.L., Wesolowski, D.J., and Palmer, D.A., 1999. Calcium adsorption at the rutile-water interface: A potentiometric study in NaCl media to 250 ℃. Geochimica et Cosmochimica Acta, 63: 3087–3096.

Ryu, J.H., Gao, S.D., Dahlgren, R.A., Zierenberg, R.A., 2002. Arsenic distribution, speciation and solubility in shallow groundwater of Owens Dry Lake, California. Geochimica et Cosmochimica Acta, 66: 2981–2994.

Sadiq, M. 1997. Arsenic chemistry in soils: An overview of thermodynamic predictions and field observations. Water Air And Soil Pollution 93: 117-136.

Schwertmann, U., and Cornell, R. M. 1991. Iron oxides in the Labora-tory: Preparation and Characterization. VCH Publishers. Wein-heim.

Sherman, D.M., and Randall, S.R. 2003. Surface complexation of arsenic (V) to iron (III) (hydr)oxides: Structural mechanism from ab initio molecular ge-ometries and EXAFS spectroscopy. Geochim. Cosmochim. Acta, 67: 4223–4230.

Silva, J., Vargas de Mello, J.W., Gasperon, M., and Abrahao, W.A.P., 2012. Effects of Competing Anions and Iron Bioreduction on Arsenic Desorption. Water Air and Soil Pollution, 223: 5707–5717.

Silvester, E., A. Manceau, and V.A. Drits. 1997. Structure of synthetic monoclinic Na-rich birnessite and hexagonal birnessite. 2. Results from chemical studies and EXAFS spectroscopy. Am. Mineral. 82: 962-978.

Smith, E., R. Naidu, and A.M. Alston. 1998. Arsenic in the Soil Environment: A Review. Advances in Agronomy 64:149-195. Academic Press, San Diego, CA.

Smith, K.S., 1999. Metal sorption on mineral surfaces: an overview with examples relating to mineral deposits. In: Plumlee, G.S., Logsdon, M.J. (Eds.), The Environmental Geochemistry of Mineral Deposits. Part A: Processes, Techniques, and Health Issues. Reviews in Economic Geology,vol. 6A. Society of Economic Geologists, pp. 161–182.

Stookey, L.L. 1970. Ferrozine – a new spectrophotometric reagent for iron. Anal. Chem. 42: 779–781.

Sun, X., and Doner, H.E. 1996. An investigation of arsenate and arsenite bonding structures on goethite by FTIR.Soil Sci., 161: 865–872.

Villalobos, M., B. Toner, J. Bargar, and G. Sposito. 2003. Characterization of the manganese oxide produced by Pseudomonas putida strain MnB1. Geochim. Cosmochim. Acta 67:2649 -2662.

Wang, Y., Morin, G., Ona-Nguema, G., Menguy, N., Juillot, F., Aubry, E., Guyot, F., Calas, G. and Brown, Jr., G. E. 2008. Arsenite sorption at the magnetite-water interface during aqueous precipitation of magnetite. EXAFS evidence of a new surface complex. Geochim. Cosmochim. Acta72: 2573–2586.

Waychunas, G.A., B.A. Rea, C.C. Fuller, and J.A. Davis. 1993. Surface Chemistry of Ferrihydrite: Part 1. EXAFS Studies of the Geometry of Coprecipitated and Adsorbed Arsenate. Geochimica et Cosmochimica Acta 57: 2251-2269.

Webb, S.M. 2005. SIXpack: a graphical user interface for XAS analysis using IFEFFIT. Physica Scripta T115: 1011 -1014.

Wielinga, B., M.M. Mizuba, C.M. Hansel, and S. Fendorf. 2001. Iron promoted reduction of chromat e by dissimilatory iron reducing bacteria. Environ. Sci. Technol. 35: 522-527.

Ying, S.C., Kocar, B.D., and Fendorf, S., 2012. Oxidation and competitive retention of arsenic between iron- and manganese oxides. Geochimica et Cosmochimica Acta, 96: 294–303.

Zhu, M., K. W. Paul, J. D. Kubicki and D.L. Sparks. 2009. Quantum chemical study of arsenic (III, V) adsorption on Mn-oxides: Implications for arsenic(III) oxidation. Environ. Sci. Technol. 43: 6655–6661.

Appendix A

Characterization of δ-MnO_2

The following characteristics of synthetic δ-MnO_2 were conducted by Brandon Lafferty in previous publications (Lafferty et al., 2010 a and b). The average oxidation state of Mn in the δ-MnO_2 structure used in these experiments was determined, by oxalate titration (Villalobos et al., 2003), to be 3.95. The point of zero charge (PZC) of δ-MnO_2 is 1.85 using the prolonged salt titration method (PST) appropriate for Mn-oxides as outlined by Tan et al. (2008). X-ray diffraction (XRD) confirmed that the only product of the synthesis was poorly -crystalline δ-MnO_2. The surface area of δ-MnO_2 was 273.5 m^2, using BET analysis in which air-dried δ-MnO_2 was purged with a dry He atmosphere at room temperature (~25 ^oC) for 16 hours to remove as much water as possible without heating the mineral. An average δ-MnO_2 particle size of 450 nm was determined by dynamic light scattering (Zetasizer Nano Series, Malvern Instruments Ltd). High-resolution transmission electron microscopy (HRTEM) further showed that δ-MnO_2 had few small crystalline domains surrounded by poorly-crystalline (i.e. TEM amorphous) material, all of which were aggregated together into larger particles that varied in size (Figure A.1).

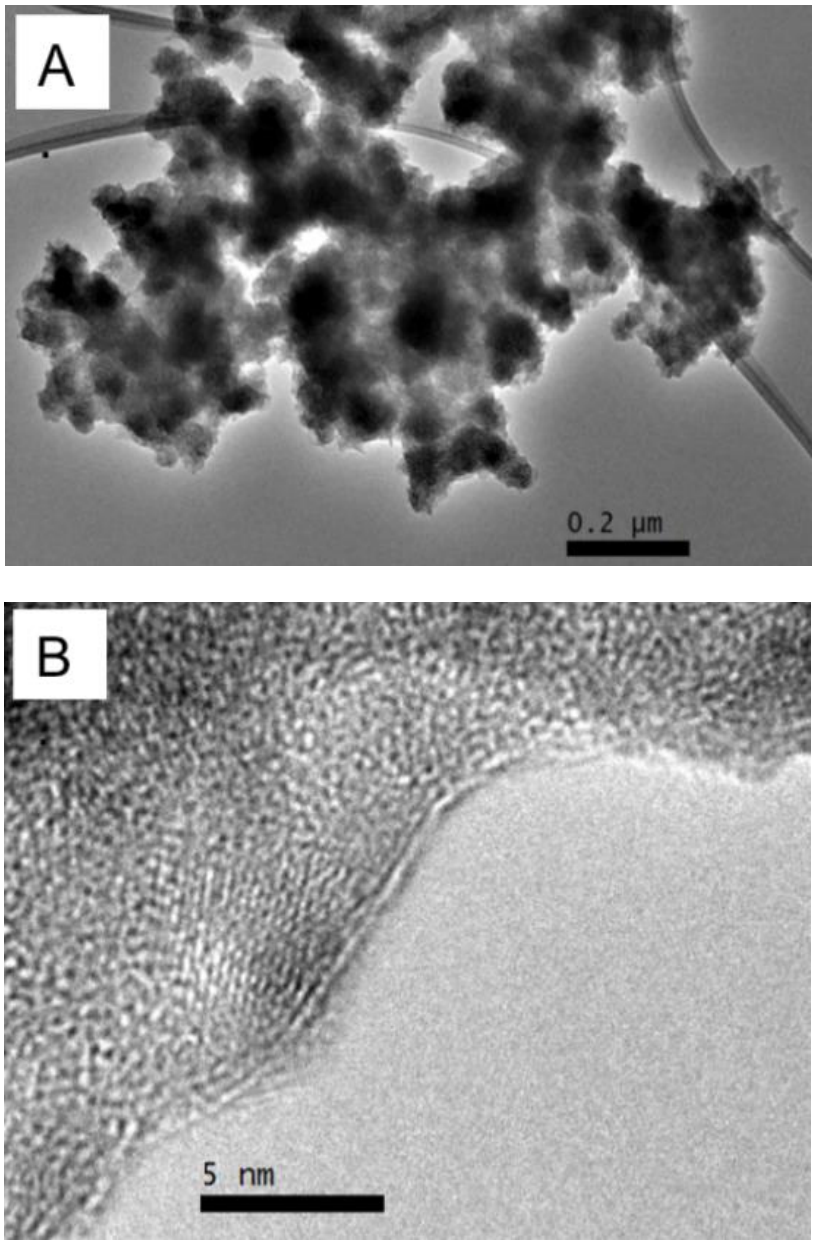

Figure A.6 Transmission electron micrographs of synthetic δ-MnO_2.

Appendix B

Arsenic Sorption Calculation

The flow rate used for all stirred-flow reactions in this study was 1 mL/min, and the concentration of reactants when each reaction started (i.e. t=0) was zero. Thus, when a reactant was introduced into the stirred –flow reactor, a certain time was required before the reactant concentration in the reactor reached equilibrium (i.e. concentration of a reactant entering the reactor equaled the concentration of that same reactant leaving the reactor, assuming no retention of that reactant in the stirred-flow reactor). For example, in this study, when 100 μmol/L As(III) was introduced to the stirred-flow reactor (chamber volume = 12 ml), about 1.1 hours was required for the concentration of total As flowing out of the reactor to equal 100 μmol/L (assuming no As sorption).

In order to calculate the amount of As sorbed during stirred-flow reactions, a dilution curve was calculated for each experiment, representing the amount of As expected in the reactor effluent over time. Equation A1 was used to calculate dilution curves (Bar-Tal et al., 1990), where Cout is the concentration of As leaving the reactor (mol/m3), Cin is the concentration of As introduced into the reactor (mol/m3), and t is time (min). The variable q in equation A1 represents the flow rate (m3/min) divided by the volume of the reactor (m3), in the experiments conducted for this research, q= 0.083

$$C_{out} = C_{in} [1 - \exp (- q t)] \quad (A1)$$

In order to calculate the amount of As sorbed/desorbed during stirred flow reactions, the integral of the area between the dilution curve and the curve representing the total amount of As removed from the reactor (solid line and dots, respectively, in Figure A.2 and Figure A.3) was determined.

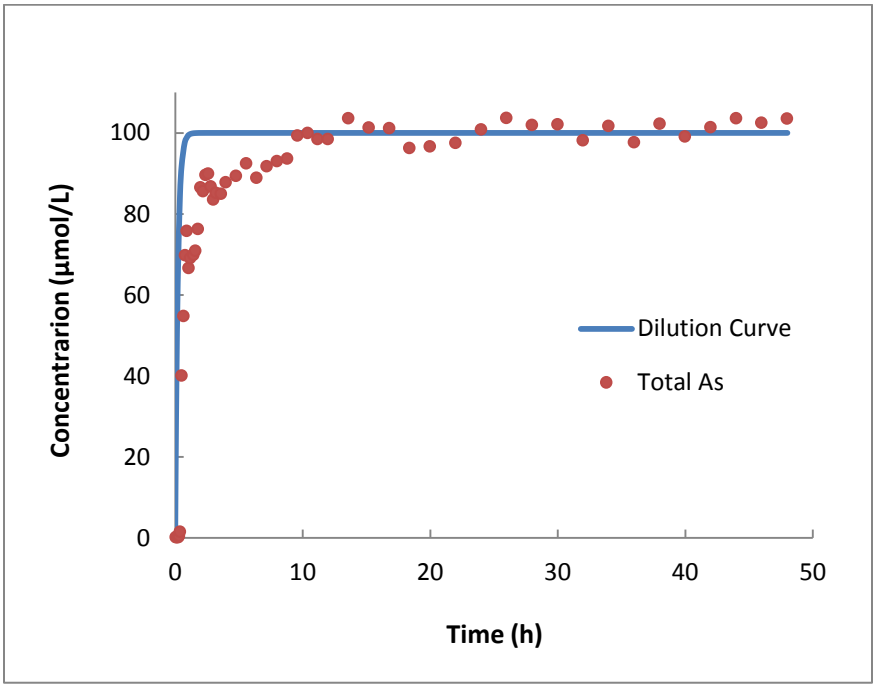

Figure A.7 The concentration (µmol/L) of As in the effluent of a stirred-flow experiment reacting 2 g/L δ-MnO_2 with 100 µmol/L As(III) flowing at 1 mL/min for 48 hours. Also shown is the calculated dilution curve representing the concentration (µmol/L) of As expected in stirred-flow reactor effluent if no sorption occurs.

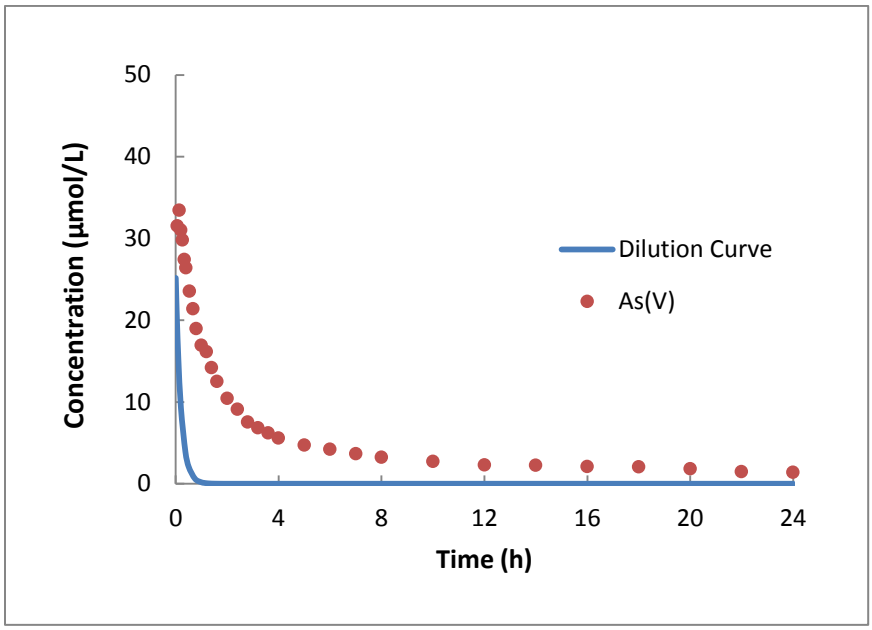

Figure A.8 The concentration (µmol/L) of As(V) in the effluent of a stirred-flow experiment reacting 2 g/L δ-MnO_2 with 100 µmol/L As(III) and 100 µmol/L Fe(II) flowing at 1 mL/min for 36 hours, prior to desorption by background electrolyte for 24 hours (only desorption part is shown). Also shown is the calculated dilution curve representing the concentration (µmol/L) of As(V) expected in stirred-flow reactor effluent if no desorption occurs.

Appendix C

Characterization of Ferric Arsenate

Ferric arsenate ($FeAsO_4 \cdot 4\text{-}7H_2O$) used in this study was synthesized using the method described by Jia et al. (2006). Ferric arsenate is a precursor to scorodite ($FeAsO_4 \cdot 2H_2O$) formation. Terms such as amorphous scorodite, poorly crystalline scorodite and poorly crystalline ferric arsenate were used to describe ferric arsenate in previous publications (Demopoulos et al., 1995; Langmuir et al., 1999, 2006; Jia et al., 2006). Natural occurrences of ferric arsenate-like compounds were reported from a sea-floor hydrothermal vent (Rancourt et al., 2001), acid mine drain-age precipitates (Carlson et al., 2002), and mine tailings (Langmuir et al., 1999; Paktunc et al., 2003).

The As K-edge EXAFS spectrum of synthesized ferric arsenate is shown in Figure A.4. A characteristic feature of the ferric arsenate precipitates is the presence of a subtle double-hump feature at about 4 Å and 5 Å of the broadened first oscillation, which is analogous to that of the amorphous ferric arsenate observed in gold mine tailings (Paktunc et al., 2003, 2004). Furthermore, a subtle oscillation feature present in scorodite at about 10.5 Å does not exist in ferric arsenate, which is similar to that observed in the ferric arsenate reported by Paktunc et al. (2003). Shell-by-shell fitting of this synthetic ferric arsenate (Table 4.1) gives an As-Fe distance at 3.33 Å with a coordination number of 1.79, which is in good agreement with previous studies that reported the As-Fe distance of ferric arsenate is from 3.30 Å to 3.33 Å and the coordination number varies from 1.8 to 2.8 (Paktunc et al., 2003, 2008; Chen et al., 2009). The binding structure of ferric arsenate is similar to samples of As sorbed on

Fe-oxides and a scorodite mineral. However, the As-Fe distance for the adsorption sample is often shorter (3.25 Å to 3.30 Å), while the As-Fe distance for crystalline scorodite is longer (3.33 Å to 3.36 Å) and with much higher coordination numbers of about 4 (Paktunc et al., 2008; Chen et al., 2009).

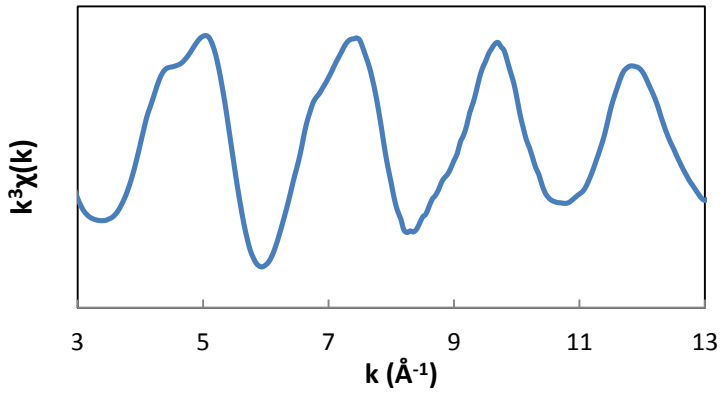

Figure A.9 As K-edge EXAFS spectrum of synthesized ferric arsenate.

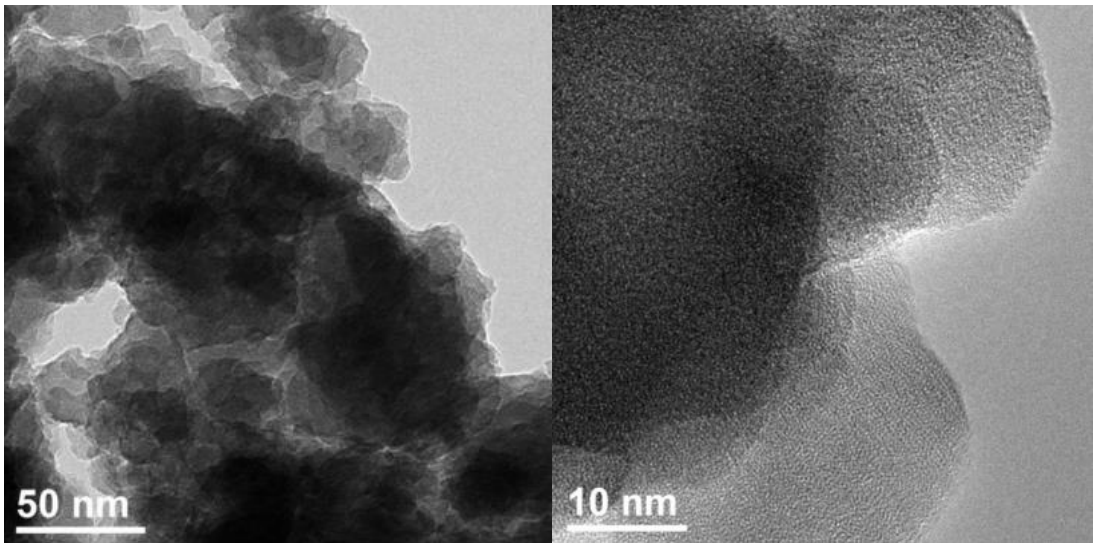

Figure A.10 Transmission electron micrographs of synthetic ferric arsenate.

Transmission electron microscopy (TEM) (Figure A.5) further shows this synthetic ferric arsenate is quite amorphous. Particles in the ferric arsenate have irregular shapes with somewhat rounded outlines. These particles appear to aggregate into clusters varying in size from about 10 to 100 nm.

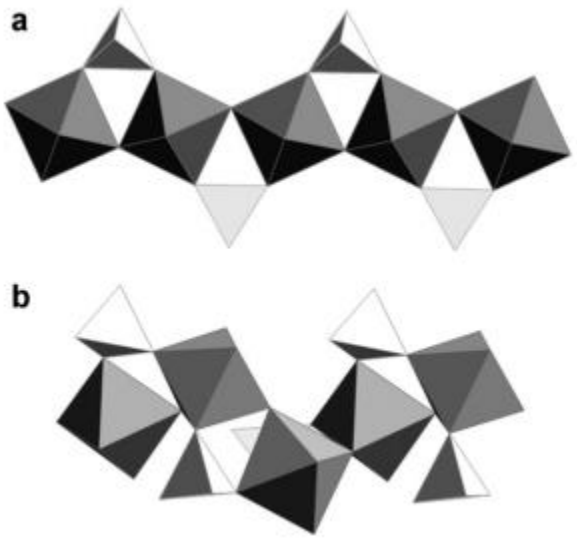

Figure A.11 Structural models envisioned for ferric arsenate. (a) A single chain formed by corner linkage of FeO_6 octahedra and AsO_4 tetrahedra; (b) A single chain composed of FeO_6 octahedra and AsO_4 tetrahedra (Paktunc et al., 2008).

A postulated ferric arsenate structure by Paktunc et al. (2008) is shown in Figure A.6, which is analogous to the butlerite ($FeSO_4(OH) \cdot 2H_2O$) structure.

REFERENCES

Bar-Tal, A., S. Feigenbaum, D.L. Sparks, and J.D. Pesek. 1990. Analyses of adsorption kinetics using a stirred-flow chamber: I. Theory and critical tests. Soil Sci. Soc. Am. J. 54: 1273-1278.

Carlson, L.; Bigham, J. M.; Schwertmann, U.; Kyek, A.; Wagner, F. 2002. Scavenging of As from mine drainage by schwertmannite and ferrihydrite: a comparison with synthetic analogues. Environ. Sci. Technol. 36: 1712 -1719.

Chen, N., Jiang, D. T., Cutler, J., Kotzer, T., Jia, Y. F., Demopoulos, G. P. and Rowson, J. W. 2009. Structural characterization of poorly-crystalline scorodite, iron(III)-arsenate co-precipitates and uranium mill neutralized raffinate solids using X-ray absorption fine structure spectroscopy. Geochim. Cosmochim. Acta 73: 3260–3276.

Lafferty, B., M. Ginder-Vogel and D.L. Sparks. 2010 a. Arsenite oxidation by a poorly crystalline manganese-oxide 1. Stirred-flow experiments. Environ. Sci. Technol. 44: 8460-8466.

Lafferty, B., M. Ginder-Vogel, M. Zhu, K.J.T. Livi and D.L. Sparks. 2010 b. Arsenite oxidation by a poorly crystalline manganese-oxide 2.Results from X-ray absorption spectroscopy and X-ray diffraction. Environ. Sci. Technol. 44: 8467–8472.

Langmuir, D., Mahoney, J., MacDonald, A. and Rowson, J. 1999. Predicting arsenic concentrations in the porewaters of buried uranium mill tailings. Geochim. Cosmochim. Acta. 63: 3379–3394.

Paktunc A. D., Foster A. and Laflamme J. 2003. Speciation and characterization of arsenic in Ketza River Mine tailings using X-ray absorption spectroscopy.Environ. Sci. Technol.37, 2067–2074.

Paktunc D., Foster A., Heald S. and Laflamme G. 2004. Speciation and characterization of arsenic in gold ores and cyanidation tailings using X-ray absorption spectroscopy. Geochim. Cosmochim. Acta68, 969–983.

Paktunc, D., Dutrizac J., and Gertsman, V. 2008. Synthesis and phase transformations involving scorodite, ferric arsenate and arsenical ferrihydrite: implications for arsenic mobility. Geo-chim. Cosmochim. Acta72: 2649–2672.

Rancourt, D. G., Fortin, D., Pichler, T., Thibault, P. J., Lamarche, G., Morris, R. V. and Mercier, P. H. J. 2001. Mineralogy of a natural As-rich hydrous ferric oxide

coprecipitate formed by mixing of hydrothermal fluid and seawater: implications regarding surface complexation and color banding in ferrihy-drite deposits.Am. Mineral. 86: 834–851.

Tan, W. F., S. J. Lu, F. Liu, X.-H. Feng, J.-Z. He, and L.K. Koopal. 2008. Determination of the point-of-zero charge of manganese oxides with different methods including an improved salt titration method. Soil Sci. 173: 277-286.

Villalobos, M., B. Toner, J. Bargar, and G. Sposito. 2003. Characterization of the manganese oxide produced by Pseudomonas putida strain MnB1. Geochim. Cosmochim. Acta 67: 2649 -2662.